The Hong Kong Polytechnic University

School of Optometry

The characterization of retinal electrical signals of the *in-vitro* and *in-vivo* porcine eye

– a novel large mammalian eye model

Ng Yiu-Fai

A thesis submitted in partial fulfillment of the requirements for the Degree of Doctor of Philosophy

August 2008

CERTIFICATE OF ORIGINALITY

I hereby declare that this thesis is my own work and that, to the best of my knowledge and belief, it reproduces no material previously published or written, nor material that has been accepted for the award of any other degree or diploma, except where due acknowledgement has been made in the text.

_____ *(Signed)*

_____Ng Yiu-Fai_____ *(Name of student)*

ABSTRACT

Introduction:

A convenient and easily available experimental eye model would facilitate studies to understand the physiology and pathophysiology of the complex retina.

In the animal kingdom, primate eyes are most similar to human eyes. However, there are ethical and legal issues in using primates for research studies. Thus, it is essential to develop an alternative animal model for eye research.

In terms of structure and physiology, the porcine eye is a good alternative to the non-human primate as a model for eye research. Although the photoreceptor distribution of the porcine retina is different from that of the primate, many retinal characteristics of the pig are similar to that of human. In this study, we investigate the characteristics of retinal electrical activity in the porcine eye using multifocal electroretinography (mfERG) to determine the suitability of this model for future eye research in different aspects, including *in-vivo* and *in-vitro* conditions as well as normal and abnormal conditions.

Objectives:

- To study the cellular origins of the porcine mfERG *in-vivo* by use of pharmacological agents blocking specific retinal pathways.
- To identify alterations of the porcine mfERG *in-vivo* by use of a transgenic pig model with known retinal re-wiring.
- To study the cellular origins of the porcine mfERG *in-vitro* by use of pharmacological agents blocking specific retinal pathways.
- To identify the alterations of the porcine mfERG *in-vitro* by use of anesthetics and variations of the culture environment.

The findings from this study will enhance our understanding of the characteristics of retinal electrical signals of the *in-vivo* and *in-vitro* porcine eyes.

Methods:

There were three experiments in this study.

In Experiment 1, the mfERG was recorded from normal (wild type) porcine eye to characterize the cellular origins of the porcine mfERG by injection of pharmacological agents known to block specific retinal pathways.

In Experiment 2, the mfERG was recorded from the transgenic pig (Tg) with retinitis pigmentosa (RP). The mfERG from the transgenic pig was compared with the mfERG obtained from Experiment 1 to characterize the alteration of retinal signal pathway at an early stage of RP.

In Experiment 3, the mfERG was recorded from isolated perfused pig eye to assess the properties of retinal components *in-vitro*. The cellular origins of mfERG *in-vitro* were characterized by injection of the same pharmacological agents used in Experiment 1. The effect of anesthesia on the mfERG was also assessed.

Results:

From Experiment 1, the cellular origins of the porcine mfERG were found to be similar to that of the primate. The cellular origins of the first order kernel (K1) and the first slice of the second order kernel (K2.1) porcine mfERG appear to be both the inner and outer retina. In K1 mfERG, the n1 involve responses of cone photoreceptors and OFF-bipolar cells. The leading edge of p1 was dominated by ON-bipolar cell depolarization. The rear edge of p1, n2 and p2 was dominated by ON-bipolar

activities and shaped by the activities of OFF-bipolar cells and retinal cells with NMDAr and voltage gated sodium channels other than ganglion cells. The p3 was mainly inner retinal activities. In Experiment 2, the alteration in porcine mfERG associated with neural re-wiring in the degenerating porcine RP model (six-week P347L transgenic pig (Tg)) was demonstrated. The signal alterations in the Tg pigs involved both outer and inner retinal responses. In particular, the early components of the inner retinal contribution were obviously altered in Tg mfERG; the inner retinal components at about 24 and 40ms appeared to be inverted. The differences in the estimates of OFF-bipolar cell pathway contributions were minimal. There was no change of cone cell responses in Tg mfERG. In Experiment 3, the functional cellular components of porcine mfERG *in-vitro* were demonstrated by use of pharmacological agents as in Experiment 1. A close relationship between inner retinal activity and effect of commonly used anesthesia was found. Isoflurane and propofol caused influence on mfERG resembled the inner retinal activities sensitive to TTX+NMDA application.

Conclusions:

The porcine eye could be a good alternative to primate eye for studies of retinal physiology. Experiments 1 and 3 showed the possibilities of obtaining useful mfERG information from the porcine model, and the similarity of cellular origins of mfERG between pig and primate. Experiment 2 and 3 illustrated a good example of using porcine mfERG *in-vivo* and *in-vitro* for experiments that may not be easily performed in primates.

TABLE OF CONTENTS

CERTIFICATE OF ORIGINALITY ---------- II

ABSTRACT ---------- III

Introduction ---------- III
Objectives ---------- IV
Methods ---------- IV
Results ---------- V
Conclusions ---------- VII

TABLE OF CONTENTS ---------- VIII

PUBLICATION ARISING FROM THE THESIS ---------- XII

CONFERENCE PRESENTATION ---------- XII

ACKNOWLEDGEMENTS ---------- XIII

LIST OF FIGURES, TABLES, EQUATION & ABBREVIATIONS - XV

List of Figures ---------- XV
List of Tables ---------- XX
List of Equation ---------- XXII
Abbreviations ---------- XXII

PART I – INTRODUCTION & LITERATURE REVIEW ---------- 1

Chapter 1 – Introduction ---------- 2

Chapter 2 – Examples of Animal Model for Eye Research ---------- 3

2. Animal eyes ---------- 3
2.1. Non-human primate ---------- 4
2.1.1. Examples in eye research ---------- 4
2.2. Pig ---------- 5
2.2.1. Eyeball ---------- 6
2.2.2. Retina ---------- 6
2.2.3. Examples in eye research ---------- 8
2.2.4. Porcine electroretinogram ---------- 9
2.2.5. Pig eye as a good candidate for retinal research -------- 10
2.3. Other animals ---------- 11

Chapter 3 – *In-vitro* retinal models ---------- 12

3. Retinal studies: *in-vivo* and *in-vitro* ---------- 12
   3.1. Different types of *in-vitro* models ----------12
      3.1.1. Cultured retina ----------13
      3.1.2. Whole eye perfusion ----------14

Chapter 4 - Fundamentals of Retinal Structure and Function ----------16

4. Retinal structures ---------- 16
   4.1. Photoreceptors ---------- 17
   4.2. Bipolar cells ----------20
      4.2.1. Cone ON-bipolar cells ----------20
      4.2.2. Cone OFF-bipolar cells ---------- 21
      4.2.3. Rod bipolar cells ---------- 22
      4.2.4. Transient and sustained bipolar cells ---------- 23
   4.3. Amacrine cells ----------25
   4.4. Reciprocal feedback to bipolar cells ----------25
      4.4.1. AII amacrine cells ----------26
   4.5. Ganglion cells ----------27
   4.6. Retinal pigment epithelium (RPE) ----------30

Chapter 5 – Signal Transmission in Retina ----------31

5. Signal transmission in vertical pathways of retina: neurotransmitters and receptors ----------31
   5.1. Principle neurotransmitter in retina: glutamate ---------- 32
      5.1.1. Metabotropic receptors – mGlu6R ---------- 34
         5.1.1.1.APB (2-amino-4-phosphonobutyric acid) receptors ---------- 36
      5.1.2. Ionotropic receptors ----------36
         5.1.2.1.NMDA receptors ---------- 37
         5.1.2.2.Non-NMDA receptors ---------- 38
            5.1.2.2.1. KA receptors ---------- 39
            5.1.2.2.2. AMPA receptors ---------- 39
            5.1.2.2.3. PDA ((±)-cis-2,3-piperidinedicarboxylic acid) ----------40
   5.2. Signal propagation ---------- 41
      5.2.1. TTX (tetrodotoxin) ----------41

Chapter 6 – Fundamentals of Electroretinogram ---------- 43

6. Electroretinography ---------- 43
   6.1. Flash ERG ----------45
      6.1.1. a-wave ----------47
      6.1.2. b-wave ----------48
      6.1.3. c-wave ----------49
   6.2. Multifocal electroretinogram (mfERG) ---------- 49

Chapter 7 – Factors Affecting the Multifocal Electroretinogram -------55

7. Factors affecting the retinal physiology of *in-vivo* and *in-vitro* models
   ---------- 55
   7.1. Retinal disorders/diseases ----------56
   7.2. Anesthesia ----------58
      7.2.1. Isoflurane ----------59
      7.2.2. Ketamine ---------- 61
      7.2.3. Propofol ---------- 62
   7.3. Parameters affecting retina physiology: in *in-vitro* studies ----63

Chapter 8 – Purpose of Investigation ----------64

PART II – EXPERIMENTS ----------66

Chapter 9. Experiment I - Pharmacologically defined components of the normal porcine multifocal ----------67

   9.1 Abstract ---------- 67
   9.2 Introduction ---------- 69
   9.3 Method ---------- 71
   9.4 Results ---------- 78
   9.5 Discussion ---------- 88

Chapter 10. Experiment II - Multifocal Electroretinogram in Rhodopsin P347L Transgenic Pigs ----------98

   10.1 Abstract ----------98
   10.2 Introduction ----------101
   10.3 Method ---------- 103
   10.4 Results ----------112
   10.5 Discussion ----------119

Chapter 11. Experiment III - The characteristics of multifocal electroretinogram in isolated perfused porcine eye ---------- 127

11.1 Abstract ---------- 128
11.2 Introduction ---------- 129
11.3 Method ---------- 131
11.4 Results ---------- 141
11.5 Discussion ---------- 146

Chapter 12. Discussion and Conclusions ---------- 154

APPENDICES ---------- 163

A - Multifocal electroretinograph (mfERG) in isolated porcine eye: the effects of temperature and flow rate ---------- 163

A.1 Introduction ---------- 163
A.2 Method ---------- 166
A.3 Results ---------- 170
A.4 Discussion ---------- 172

B - Morphological investigation of isolated, perfused porcine eyes --- 174

B.1 Introduction ---------- 174
B.2 Method ---------- 174
B.3 Results ---------- 177
B.4 Discussion ---------- 178

REFERENCE ---------- 179

PUBLICATION ARISING FROM THE THESIS

1) Ng Y.F., Chan H.H.L., Chu P.H.W., Siu A.W., To C.H., Beale B.A., Gilger B.C., Wong F. (2008). Pharmacologically defined components of the normal porcine multifocal ERG. *Doc Ophthalmol, 116:165-176.*

2) Ng Y.F., Chan H.H.L., Chu P.H.W., To C.H., Beale B.A., Gilger B.C., Petters R.M., Wong F. (2008). Multifocal Electroretinogram in Rhodopsin P347L Transgenic Pigs. *Invest Ophthalmol Vis Sci, 49:2208-2215.*

3) Ng Y.F., Chan H.H.L., To C.H., Yap, M. (2008). The characteristics of multifocal electroretinogram in isolated perfused porcine eye. *Doc Ophthalmol, 117:205-14.*

CONFERENCE PRESENTATION

1) Ng Y.F., Chan H.H.L., To C.H., Shahidulla M. (2003) In-vitro Multifocal ERG Measurement of Perfused Pig Eye. *XXXXI ISCEV Conference. Nagoya. Japan. Poster Presentation.*

2) Ng Y.F., Chan H.H.L., Shahidullah M., To C.H., Yap M.K. (2004). Effect of Allopurinol on mfERG of In-vitro Arterially Perfused Pig Eye. *Academy' 04 Global-Pacific Rim, Honolulu, Hawaii. Poster Presentation.*

3) Ng Y.F., Shahidullah M., Chan H.H.L., To C.H., Yap M.K.. Allopurinol and Hypothermia Can Revive Ischemic Pig Eye for mfERG Study. *ARVO 2005 Annual meeting, Fort Lauderdale, Florida, USA. Poster Presentation.*

4) Ng Y.F., Chan H.H.L., Chu P.H., Beale B.A., Gilger B.C., Wong F., Retinal Origins and Nonlinear Characteristics of the Porcine Multifocal ERG. *ARVO 2007 Annual meeting, Fort Lauderdale, Florida, USA. Poster Presentation.*

ACKNOWLEDGEMENTS

Over the five years of this study, I have received kindness and support from many people in the School of Optometry. I especially want to thank my chief supervisor, Dr. Henry Chan, who guided me how to undertake a research project and how to write a thesis. In additions, he showed greatest empathy and encouragement to me in this study. Furthermore, I thank him for supporting me to attend several international conferences, which broadened my view of future research direction. I am also grateful to my co-supervisor, Prof. Chi-Ho To, who initiated my interest on research work since his supervision on my final year project in the undergraduate study. I am especially indebted to Prof. Maurice Yap, who gave me many useful comments on my research planning, and Prof. Brian Brown, who gave me many helpful suggestions on my research studies and my thesis. I would also want to thank Dr. Mohammad Shahidullah and Dr. Gena Leung for helping me to master the dissection technique for perfused eye and the histological experiment skill in this study.

For that and more I owe them a huge debt of gratitude. All of them have not only been generous with their time but have helped me to a better understanding of research methodology. Last, I am grateful to my dear wife for her love and support over the

years. I am also grateful to my twin brother who provided financial and spiritual support to my family during my studies.

LIST OF FIGURES, TABLES, EQUATION & ABBREVIATIONS

List of Figures

Chapter 4

Figure 4.1. Highly schematic rod and cone pathways in the mammalian retina (Sharpe and Stockman, 1999).

Chapter 5

Figure 5.1.1. L-glutamate

Figure 5.1.2. Glutamate receptors on cone pathway neurons.

Figure 5.1.1.1. Classifications of metabotropic glutamate receptors.

Figure 5.1.2. Ionotropic glutamate receptors

Figure 5.2.1. Pufferfish

Chapter 6

Figure 6. Schematic presentation of extracellular current (*i*) triggered by luminous stimulus.

Figure 6.1. ERG waveform of biphasic retinal electrical potential variation following a flash stimulus.

Figure 6.2. (A) 103 non-scaled hexagonal stimulation array of mfERG. **(B)** Averaged

first order kernel response of mfERG. **(C)** 103 response traces of mfERG. **(D)** Three dimensional presentation of mfERG response amplitude.

Chapter 7

Figure 7.2.1. Isoflurane

Figure 7.2.2. Ketamine

Figure 7.2.3. Propofol

Chapter 9

Figure 9.1. (A) 103 non-scaled hexagonal stimulus pattern of mfERG. **(B)** 1st order trace array of mfERG under propofol anesthesia from Pig #6.

Figure 9.2. (A) First-order kernel (K1) waveform and second-order kernel first slice (K2.1) waveform of averaged mfERG from all porcine eyes under propofol anesthesia. **(B)** The K1 and K2.1 waveforms of averaged mfERG of both eyes from the same pig (Pig #3) under propofol and isoflurane anesthesia.

Figure 9.3. (A) K1 waveforms of averaged mfERG under effect of NMDA, TTX and TTX+NMDA with isoflurane anesthesia. **(B)** K2.1 waveforms of averaged mfERG under effect of NMDA, TTX and TTX+NMDA with isoflurane anesthesia.

Figure 9.4. (A) K1 waveforms of averaged mfERG under effect of APB, PDA and

APB+PDA with pre-administration of TTX+NMDA and isoflurane anesthesia. **(B)** K2.1 waveforms of averaged mfERG under effect of APB, PDA and APB+PDA with pre-administration of TTX+NMDA and isoflurane anesthesia.

Chapter 10

Figure 10.1. (A) 1st order trace array of mfERG under propofol anesthesia from Tg Pig#2 right eye and WT Pig #4 right eye. **(B)** 103 non-scaled hexagonal stimulus pattern of mfERG. **(C)** First-order kernel (K1) waveform of averaged mfERG from right eye of WT Pig#4 under propofol anesthesia.

Figure 10.2. First-order kernel (K1) waveform of averaged mfERG from both eyes of WT Pig#4 and Tg Pig#2 under propofol **(A)** and isoflurane **(B)** anesthesia.

Figure 10.3. (A) First-order kernel (K1) waveform of mfERG from WT Pig#4 (blue traces) and Tg Pig#2 (red traces) after TTX, NMDA, PDA and APB administration under isoflurane anesthesia. **(B)** The estimates of difference between the K1 waveforms of averaged mfERG of all Tg and WT porcine eyes.

Figure 10.4. The averaged estimates of inner retinal response from both eyes of WT Pig#4 and Tg Pig#2.

Chapter 11

Figure 11.1 (A) Electrodes configuration of the perfused eye. **(B)** The K1 mfERG trace array after 90 minutes perfusion from eye (#2007-06-08e1). **(C)** Time line depicturing the time of mfERG recording and intravitreal injections.

Figure 11.2. K1 waveform of averaged mfERG from all perfused porcine eyes after 90 minutes of perfusion without pharmacological agent administrations.

Figure 11.3. (A) Averaged K1 waveforms of mfERG responses at 150 minutes after pharmacological administration (ie. 240 minutes after perfusion). **(B)** Estimates of TTX, NMDA, TTX+NMDA sensitive elements of the K1 mfERG responses.

Figure 11.4. (A) Averaged K1 waveforms of mfERG responses at 150 minutes after PDA, APB and APB+PDA administration with co-administration of TTX+NMDA (ie. 240 minutes after perfusion). **(B)** Estimates of APB and PDA sensitive elements of the K1 mfERG responses at 150 minutes after pharmacological administrations (ie. 240 minutes after perfusion).

Figure 11.5. (A) Averaged K1 waveforms of mfERG responses at 150 minutes after ISO and propofol administration (ie. 240 minutes after perfusion). **(B)** Estimates of ISO and propofol sensitive elements of the K1 mfERG responses at 150 minutes after pharmacological administrations (ie. 240 minutes after perfusion).

Appendix - A

Figure A1. Time line depicturing the time of mfERG recording.

Appendix – B

Figure B1. Porcine retinal paraffin blocks preparation.

Figure B2. Porcine retinal section prepared after five hours of perfusion.

Figure B3. Mean thickness (um) with SEM of retina layers after enucleation (control), after five hours with perfusion (perfused) and without perfusion (non-perfused).

List of Tables

Chapter 5

Table 5.1. Glutamate receptors on cone pathway neurons.

Chapter 9

Table 9.1. Mean of amplitude (nV/degree^2) with SEM of mfERG features of the 1st order kernel and 1st slice of 2nd order kernel traces at optic streak.

Table 9.2. Mean of implicit time (ms) with SEM of mfERG features of the 1st order kernel and 1st slice of 2nd order kernel traces at optic streak.

Chapter 10

Table 10.1. Mean of amplitude (nV/degree^2) of 1st order kernel traces with SEM of mfERG at optic streak.

Table 10.2. Mean of implicit time (ms) of 1st order kernel traces with SEM of mfERG at optic streak.

Table 10.3. Mean of amplitude (nV/degree^2) of 1st order kernel traces with SEM of inner retinal elements at optic streak.

Table 10.4. Mean of implicit time (ms) of 1st order kernel traces with SEM of inner retinal elements at optic streak.

Chapter 11

Table 11.1. Mean of implicit time (ms) with SEM of first-order kernel mfERG features at optic streak.

Table 11.2. Mean of percentage amplitude with SEM of mfERG first-order kernel traces at optic streak.

Appendix - A

Table A1A. Mean of implicit time (ms) with SEM of first-order kernel mfERG features at optic streak after 90 minutes of perfusion with different temperatures.

Table A1B. Mean of amplitude (nV/degree^2) with SEM of first-order kernel mfERG features at optic streak after 90 minutes of perfusion with different temperatures.

Table A1C. Mean of implicit time (ms) with SEM of first-order kernel mfERG features at optic streak after 240 minutes of perfusion with different temperatures.

Table A1D. Mean of amplitude (nV/degree^2) with SEM of first-order kernel mfERG features at optic streak after 240 minutes of perfusion with different temperatures.

List of Equation

Chapter 11

Equation 11.1. Percentage amplitude calculation.

Abbreviations

AMPA	α-amino-3-hydroxy-5-methylisoxazole-4- propionic acid
ANOVA	Analysis of variance
APB	L-2-amino-4-phosphonobutyric acid
ARMD	Age-related macular degeneration
cGMP	Cyclic-GMP
CNQX	6-cyano-7-nitroquinoxaline-2,3-dione
CNS	Central nervous system
CRT	Cathode-ray tube
D-AP5	D-2-amino-5-phosphonopentanoate
ERG	Electroretinogram
GABA	Gamma-aminobutyric acid
GABAa	Gamma-aminobutyric acid alpha
GABAr	Gamma-aminobutyric acid receptor
H&E	Haematoxylin and eosin
iGluR	Ionotropic glutamate receptor
IPL	Inner plexiform layer
ISO	Isoflurane
IV	Intra-vascular injection
Lox/-	Retinoblastoma gene
MBC	Minimum blood concentration
mfERG	Multifocal electroretinogram
mGluR	Metabotropic glutamate receptor
mGlu1R	Metabotropic glutamate receptor – type1
mGlu2R	Metabotropic glutamate receptor – type 2
mGlu3R	Metabotropic glutamate receptor – type 3
mGlu4R	Metabotropic glutamate receptor – type 4
mGlu5R	Metabotropic glutamate receptor – type 5
mGlu6R	Metabotropic glutamate receptor – type 6
mGlu7R	Metabotropic glutamate receptor – type 7
mGlu8R	Metabotropic glutamate receptor – type 8
MIC	Minimum aveolar concentration
NMDA	N-methyl-D-aspartic acid
NMDAr	N-methyl-D-aspartic acid receptor
K1	First order kernel
K2.1	First slice of the second order kernel
KA	Kainic acid

OLM	Outer limiting membrane
ONL	Outer nuclear layer
OPL	Outer plexiform layer
PDA	cis-2,3 piperidine dicarboxylic acid
PDE	Phosphodiesterase
PERG	Pattern electroretinogram
POS	Photoreceptor outer segment
RP	Retinitis pigmentosa
RPE	Retinal pigment epithelium
SEM	Standard Error of Mean
Tg	Transgenic
TTX	Tetrodotoxin
WT	Wild type

PART I – INTRODUCTION &

LITERATURE REVIEW

Chapter 1 - Introduction

If there is an eye model having retinal physiology comparable to human and being highly accessible, the pace of eye research would move faster than at present.

Many retinal diseases are not fully understood and extensive investigations are necessary to understand the physiology and pathophysiology of the complex retina. Therefore, a convenient and easily available experimental model is necessary.

In the animal kingdom, non-human primates, such as monkey and gorilla, are most similar to humans in terms of genetic and physiology. However, there are ethical issues in using non-human primates in the experiments with invasive procedures. In many countries, it is illegal to perform experiments on non-human primates and thus, it is essential to develop an alternative animal model for eye research.

In terms of structure and physiology, the pig is a good model to substitute the non-human primate and the porcine eye is a good alternative as a model for eye research. Although the photoreceptor distribution of porcine retina is different from that of humans and other primates, many retinal characteristics of the pig is similar to that of

humans. In this study, I plan to investigate the characteristics of retinal electrical activity in porcine eye using multifocal electroretinograms (mfERG) and to examine the suitability of this eye model for future eye research in different aspects, including *in-vivo* and *in-vitro* conditions, under normal and abnormal conditions.

Chapter 2 – Examples of Animal Models for Eye Research

2. Animal eyes

Different animals have been used for the research in ocular physiology. The selection of different animals is usually according to the nature of experiments. For some experiments, the growth rate of animals is crucial for data collection, such as growth of the eyeball and the progress of myopia. Rats, rabbit and chicken are commonly selected for this purpose. In contrast, sometimes, the similarity of physiology between animals and humans is important for extrapolation of the experimental result for future clinical applications. Thus, the size, structure and physiology of animal eyes are main concerns for the selection of animal. Relatively large animals, such as monkey, dog, cat, pig and ox, are mostly selected for this reason. For all different animal models, there are advantages and disadvantages comparing to non-human

primates which are generally accepted as the best animal model.

2.1. Non-human primates

Non-human primates are genetically most similar to humans. The physiology and body structure are very close to those of humans. However, the availability of non-human primates is low and there are ethical issues involved in the of conduct invasive procedures on these animals. In some countries, it is even illegal to use non-human primates for experiments. Thus, other large mammalian models are essential alternatives to non-human primates for research studies.

2.1.1. Examples in eye research

Non-human primates are close to humans in terms of retinal structure and physiology. Thus, non-human primates are the best alternative to humans in retinal physiology research. The light-evoked retinal electrical response of non-human primates is similar to that of humans (Hare and Ton, 2002; Hood et al., 2002). The physiological changes in the retina associated with different retinopathies, such as glaucoma (Raz et al., 2002), diabetics (Johnson et al., 2005) and retinal detachment (Hamasaki et al.,

1969), can be examined by use of non-human primate models. However, due to the close relationship between humans and non-human primates, the use of non-human primates in research has many restrictions.

2.2. Pig

Apart from non-human primates, the pig is better than other animals as a model for the study of retinal physiology. It is phylo-genetically close to humans and more available than the monkey. There are many similarities between pig and human, such as eyeball size, dietary habits, digestive physiology, kidney structure and function, pulmonary physiology, coronary artery distribution, haemo-dynamics and aptitude for obesity (Cooper, 1992; Niekrasz et al., 1992). In addition, breeding of the pig is easier than that of non-human primates. The pig is genetically amenable to simulation of different diseases (Petters, 1994; Petters et al., 1997). All these factors have raised interest in employing porcine organs for xenotransplantation (Cooper, 1992). In addition, porcine corneal stroma induces no hyperacute rejection but only mild cellular rejection in corneal transplantation in cynomolgus monkeys (Amano et al., 2003); this factor makes porcine tissue a recent focus of corneal research as well.

2.2.1. Eyeball

The pig eye resembles that of the human eyeball because of similarities in dimension, structure and vasculature, although the porcine eyeball has no central retinal artery (see below). Its scleral thickness is very similar to that of the human eye (Olsen et al., 2002). The blood filling pattern of the choriocapillaris also resembles the pattern in humans (De Schaepdrijver et al., 1992).

2.2.2. Retina

The retinal vasculature of the pig has numerous characteristics in common with the human retina, such as vascular bed and blood vessels size. As with humans, porcine retina is trilaminar holangiotic (vascular) in nature (Simoens et al., 1992). The major retinal blood vessels of the porcine retina lie superficially on the nerve fiber layer, similar to that of human retina. The blood vessels of porcine retina are branches of chorioretinal arteries and veins that enter the eyeball at the peri-papillary region. In human retina, however, the retinal arteries originate from central retinal artery at the center of optic nerve head. The optic streak of the porcine retina has no major blood vessels but, in contrast to the central fovea of human retina, it is not completely

avascular (Simoens et al., 1992).

Even though the photoreceptor distribution of porcine retina is different from that of humans, the structure and function of porcine retina are very similar to those of human retina. Porcine retina has no fovea but a band like structure called the optic streak or visual streak (Gerke Jr et al., 1995; Hendrickson and Hicks, 2002) and the cone density gradually decreases and tapers towards the peripheral and inferior retina as the rod to cone ratio increases (Hendrickson and Hicks, 2002). The porcine cone density is approximately 35,000 to 40,000 mm^{-2} (Hendrickson and Hicks, 2002) at the optic streak, which resembles the human cone density within 5° of the fovea.

The photoreceptor mosaic of the pig is generally similar to that of the primate (Chandler et al., 1999). Microscopically, both pig eye and human eye process with similar microglial (astrocyte) cells in the retina (Ruiz-Ederra et al., 2003) and the porcine retina contains a rich network of microglial cells. The normal porcine retina is devoid of lymphocytes, monocytes, and granulocytes. The distribution of immunocompetent cells in the porcine retina largely resembles that observed in the human retina (Yang et al., 2002). The porcine eye is classified as an arrhythmic eye, which is appropriate to diurnal life (Neitz and Jacobs, 1989). As with humans, the

porcine eye has no tapetum lucidum (Ollivier et al., 2004), and it cannot reflect light to enhance photoreceptor sensitivity.

The most important reason that porcine retina is judged to be similar to the human retina is because of its physiology. Apart from the presence of rod cells, there are two classes of cone cells which give the pig dichromatic color vision. According to Neitz & Jacobs (1989), Klopfer in 1966 measured the spectral sensitivity in the pig eye: the dark adapted peak is at 515nm while the light adapted peaks are at 465nm and 550-575nm (the average cone pigment absorption peak at 556nm). In addition, among common domestic animals, such as pig, sheep, ox, dog and horse, the pig visual acuity was predicted to be the best (Hebel, 1976) because of the highest ganglion cell density.

2.2.3. Examples in eye research

Different parts of pig eye have been used for different research. For example, the anterior segment of porcine eye was used for the studies in corneal xenotransplantation (Bohnke et al., 1999), artificial tears efficacy (Choy et al., 2006) and aqueous humor dynamics (Shahidullah et al., 2005a; Kong et al., 2006; Vaajanen

et al., 2007) and the posterior segment of porcine eye was used for studying neuro-excitotoxicity (Wehrwein et al., 2004), glaucoma (Ruiz-Ederra et al., 2005), age related macular degeneration (ARMD) and retinal transplantation (Engelsberg and Ghosh, 2007). Porcine eye is believed to be a good animal model for studying trans-scleral drug delivery, because the scleral thickness is similar to that of humans (Olsen et al., 2002). Recently, apart from normal pig, studies employing P347L rhodopsin transgenic pigs as a model for investigation of retinitis pigmentosa have been reported (Li et al., 1998; Banin et al., 1999; Peng et al., 2000).

2.2.4. Porcine electroretinogram

The flash electroretinogram (ERG) from porcine eye was firstly documented by Hanna and Lachapelle (1995). They demonstrated the flash ERG of newborn piglets (at 1-5 days of age). The ERG waveform of the pig is very similar to that of humans under similar conditions (Rosolen et al., 2004); it demonstrates a well-demarcated i-wave which is a feature separated from the a-b wave complex by approximately 20ms. It is claimed that this originates at the level of ganglion cells or more distally (Rosolen et al., 2004). The i-wave of the porcine ERG is reduced when glaucoma is simulated by increase of intra-ocular pressure (Rosolen et al., 2003).

Recently, porcine mfERG data have been published (Lalonde et al., 2006); an optic nerve section sensitive component from the porcine mfERG has been identified but there is no detailed information about the other response components contributed from the rest of retinal cells or pathways. In order to compare the characteristics of porcine retinal electrical signals to that of non-human primates and humans, more understanding of the cellular origins of porcine retinal electrical responses is needed.

2.2.5. Pig eye as a good candidate for retinal research

Besides the close physiology and anatomical structure between human eye and pig eye, there are advantages of choosing porcine eye for research. First, the breeding of pigs is easier than breeding of primates, so that pig eyes are readily available. Second, alternative pig eye models are available, for example, the RP transgenic pig (Peng et al., 2000) which is a genetically engineered pig model. Such a model is more feasible in the pig than the primate. In addition, for *in-vitro* experiments, there is an abundant supply of fresh porcine eye from slaughterhouses. Thus, the usage of porcine eye *in-vivo* and *in-vitro* in retinal research can overcome certain obstacles in primate experiments, such as the availability of normal and diseased animals and current

stringent ethical issues.

2.3. Other animals

Eyes of rat, mouse, cat, dog and ox are also widely used in research. They all share certain advantages of using pig eyes for research, such as the availability of eyes. However, they also have some drawbacks. Rodents are nocturnal animals without tapetum in the retina (Ollivier et al., 2004), and they have low percentage of cones (Nixon et al., 2001). Unlike human and pig, there is a distal tapetal layer in dog, cat and ox to increase the sensitivity to light (Ollivier et al., 2004). The tapetum alters the diffusion kinetics of pharmacological agents (Olsen et al., 2002). In rabbit, the retina is merangiotic, or almost avascular, and that adds extra difficulty in comparing experimental results to those from human retina. In terms of ERG waveform, the b-waves and photopic i-waves of monkeys, pigs, dogs and cats are similar to those of humans; however, the b-waves and i-waves of rodents are different from those of humans (Rosolen et al., 2004). Thus of the animals considered, eye of the pig would be the preferred alternatives to the primate eye in the study of electroretinography.

Chapter 3 – *In-vitro* retinal models

3. Retinal studies: *in-vivo* and *in-vitro*

Although the study of retina *in-vivo* provides us an intact retinal network and physiology, there are still some practical disadvantages. General anesthetics are essential in animal experiments *in-vivo*. Anesthetics affect retinal physiology and signal transmission. In addition, the metabolism of animals also affects drug delivery to the retina. *In-vivo* animal models may limit the dosage and type of drugs which can be used due to toxicity issues. Thus, the studies of the retina *in-vitro* are used to overcome these limitations although retinal physiology and structures may be impaired to greater or lesser degree.

3.1. Different types of *in-vitro* models

According to previous studies (Niemeyer, 1973a; Ames and Nesbett, 1981), functional properties of the retina can be maintained *in-vitro*. Currently, there have been two major types of technique used to study *in-vitro* retina: cultured isolated retina and isolated whole eye perfusion.

3.1.1. Cultured retina

According to Niemeyer (1975), Kuchler and his co-workers studied the survival rate of incubated eyes in a moist chamber in 1956. Retinal function was monitored using the ERG. The elicited light response of the incubated frog eyes could be obtained in pure oxygen gas phase condition. There are several advantages of using cultured retina for physiological experiments. This technique allows simple and direct drug delivery to retina. Because there is no diffusion across the vitreous, the pharmacological response of the retina can be directly observed. Alteration of extracellular conditions may be brought about by simple exchange of culture media.

Although cultured and superfused retinal models have been widely used (Ames and Nesbett, 1981; Quinones-Hinojosa et al., 1999) and rabbit retinal responses could be monitored for as long as 8 hours, the neural network of the retina and the retinal topography are disturbed. In addition, the extracellular environment has been altered and, hence, the physiological condition and the electrical activity of the cultured retina are believed not to be totally comparable to conditions *in-vivo*.

3.1.2. Whole eye perfusion

Perfused mammalian eyes were once a popular tool for the study of ocular physiology. The earliest *in-vitro* arterially perfused mammalian eye models were proposed by Gouras & Hoff (1970). Perfused eye models were used in the studies of aqueous humor formation (AHF) (Kishida et al., 1985; Millar et al., 1997; Shahidullah and Wilson, 1999; Shahidullah et al., 2005a), flash ERG (Imaizumi et al., 1972; Hoff and Gouras, 1973; Niemeyer, 1973a, b, 1975; Cringle et al., 1986; Thoreson and Purple, 1989), retinal tolerance to ischemia (Nicholls and Attwell, 1990; Tseng et al., 1990; Block and Schwarz, 1998) and ocular pharmacology (Tseng et al., 1989; Peachey et al., 1993).

There are certain advantages of the perfused eye model over the isolated retinal model. The retinal environment is minimally disturbed and the blood-retinal barrier is preserved. Moreover, the retinal network is relatively intact, even though the optic nerve is cut. Most importantly, the eyeball architecture is preserved. Thus, the physiology of the perfused eye should be closer to *in-vivo* eye model.

There are different arterially perfusion eye models from different mammals, such as

rabbit (Ames and Nesbett, 1981), cat (Niemeyer, 1981), dog (Cringle et al., 1986) and ox (Shahidullah et al., 2005b). Retinal tolerance to ischemia in the cat eye was studied using an *in-vitro* perfusion method (Hoff and Gouras, 1973). Niemeyer (1973a; 1973b) then developed his own perfused cat eye model and successfully recorded intracellular retinal responses using micro-electrodes. Retina of *in-vitro* mammalian eyes was employed as a substitute for *in-vivo* retina. Due to the high density of complex neural and glial cells and the ease of manipulation and functional assessment, *in-vitro* mammalian retinas were widely used in the studies of retinal physiology and pharmacology, for neural protection and for neural toxicity screening. In the past, *in-vitro* perfused mammalian retina was mainly employed in studies of treatment of retinal ischemia for central retinal artery occlusion (CRAO) and stroke. Arterially perfused cat eye was employed to study reperfusion injury by use of the xanthine oxidase blocker, allopurinol (Peachey et al., 1993). Dog eye was also employed in studies of retinal function, physiology, metabolism, pharmacology and tolerance to ischemia. Seaman et al. (1965) perfused bovine eye with blood perfusate to test the viability of their perfusion model. Tazawa & Seaman (1972) perfused bovine eyes to study effects of anoxia and hypothermia on retinal physiology. Imaizumi et al. (1974) conducted a perfusion experiment by incorporating fluorinated compounds into the perfusate to increase oxygen carrying capacity of the perfusate.

The perfused bovine eye models had been employed for acute retinal toxicity screening (Tseng et al., 1989) and study of mitochondria in the post-ischemic retina (Tseng et al., 1990). These studies showed that perfused mammalian eyes would be feasible alternatives to *in-vivo* animal eyes for retinal physiology studies.

Chapter 4 - Fundamentals of Retinal Structure and Function

4. Retinal structures

The retina is a laminated structure on the inner surface of the eyeball, adjacent to the choroid. It can be subdivided into ten layers which are arranged in the following manner from the outermost location to the innermost location: retinal pigment epithelium (RPE), photoreceptor outer segment layer (POS), outer limiting membrane (OLM), outer nuclear layer (ONL), outer plexiform layer (OPL), inner nuclear layer (INL), inner plexiform layer (IPL), ganglion cell layer (GCL), nerve fiber layer (NFL) and inner limiting membrane (ILM).

Light rays pass through the inner layers to reach the POS, where light is transformed into an electrochemical signal. The axons of photoreceptors synapse in the OPL with

the process of bipolar cells and horizontal cells, whose cell bodies are located at the INL. The bipolar cells transmit signal to amacrine cells and ganglion cells. The horizontal cells serve for lateral communication among the photoreceptors where their axons are connected. The amacrine cells providing feedback and lateral interaction within the retina connect to bipolar cells and ganglion cells. The ganglion cell axons form the retinal nerve fiber and exit at the posterior scleral foramen as the optic nerve.

4.1. Photoreceptors

Photoreceptors are cells differentiated for capturing photons and transforming light energy into visual signals. There are two types of photoreceptors: rod cells for scotopic vision and cone cells for photopic vision. The original classification was based on their appearance under light microscopy. Rods and cones contact specific types of bipolar cells. The cone cells are mainly located in the fovea. There are 4 to 5 million cone cells, which are mainly for spatial and trichromatic vision in the photopic environment. The rod cells distribution is minimal foveally and peaks at about 15 deg eccentricity, and then falls off to the periphery. There are 78 to 107 million rod cells in human retina (Curcio et al., 1990).

Figure 4.1. Highly schematic rod and cone pathways in the mammalian retina (Sharpe and Stockman, 1999). The retina is a complex neural tissue with multiple circuits or channels for transmitting visual signals from photoreceptors to the ON- and OFF-ganglion cells. The numbered red circles highlight six rod-signal transmission: (1) rod–rod bipolar metabotropic (sign-inverting) glutamatergic synapse; (2) rod bipolar–AII amacrine cell (sign-conserving) glutamatergic synapse; (3) AII–ON cone bipolar (sign-conserving) electrical gap junction; (4) AII–OFF cone bipolar (sign-inverting) glycinergic synapse; (5) rod–cone (sign-conserving) electrical gap junction (once each for the ON and OFF pathways); and (6) rod–OFF cone bipolar ionotropic (sign-conserving) glutamatergic synapse. Only the parasol ON (light green) and OFF (beige) pathways, which transmit the rod signals, are shown. Diagram courtesy of Sharpe and Stockman (1999).

The photoreceptors extend across the POS, OLM and ONL. The outer segment of photoreceptor is the site for phototransduction, which converts light energy into an electrical signal. Both rod and cone cells are composed internally of a stack of membranous discs. There are visual pigments on these discs, which absorb photons and trigger the phototransduction. The discs are shed from the photoreceptor every day and are engulfed by RPE cells for recycling of the visual pigments. The visual pigment in rod cell discs is called rhodopsin, which consists of opsin and retinal. Opsin is a bundle of seven transmembrane helices binding retinal. Retinal is vitamin A derived photoreactive chromophore.

In darkness or the condition below their absolute threshold, the photoreceptors continuously release glutamate to bipolar cells. When the photoreceptors are excited by light, the glutamate secretion reduces. This dynamic variation of glutamate secretion according to the amount of photons received is the first step of signal processing of the visual system (Sharpe and Stockman, 1999). Cone cells transmit information to cone ON- and OFF-bipolar cells. Rod cells mainly transmit information to rod bipolar cells and recently have been suspected to communicate with cone OFF-bipolar cells in some rodents (Sharpe and Stockman, 1999) (Figure 4.1).

4.2. Bipolar cells

The bipolar cell is a type of neuron with two extensions. Bipolar cells are located between photoreceptors and ganglion cells. They selectively connect with either rod cells or cone cells to form the first synaptic connection of the visual pathway. Basically, there are two classes of bipolar cells: ON- and OFF-bipolar cells. For the rod-bipolar connection, there is normally a single, depolarizing ON-bipolar cell. For the cone-bipolar connection, there are both ON- and OFF-bipolar classes. The depolarizing (ON-) and hyperpolarizing (OFF-) bipolar cells depolarize and hyperpolarize in response to light stimulation. Both form specific ON- and OFF-synaptic pathways with ganglion cells and they react differently to the neurotransmitter released by the photoreceptors (Nelson and Kolb, 1983). In addition, the bipolar cells can be further classified as transient and sustained bipolar cells (Ichinose et al., 2005).

4.2.1. Cone ON-bipolar cells

Cone ON-bipolar cells respond to light by depolarization. They invaginate in the ribbon synapses of cone pedicles (Wassle and Boycott, 1991) to form sign-inverting

glutamatergic synapses (Sharpe and Stockman, 1999). The ON-bipolar cells are driven by a type of metabotropic glutamate receptors generally named mGlu6R. When the glutamate supply from cone cells is reduced, after triggered by light, the ON-bipolar cells depolarize via stimulation of the mGlu6R receptor (Vardi and Morigiwa, 1997) and G-protein cascade (Dhingra et al., 2001). The mGlu6R receptor is thought to trigger a second messenger cascade involving Galphao, G-protein, transducin molecules, to act on voltage gated Ca^{2+} channels (Dhingra et al., 2000). The mGlu6Rs bind selectively with glutamate agonist APB, and are insensitive to AMPA-kainate ligands. The application of APB selectively hyperpolarizes ON-bipolar cell and suppresses the light-responses of ON-bipolar cells (Slaughter and Miller, 1981). In addition to cone photopic signal input, the cone ON-bipolar cells also mediate the scotopic rod visual signal conducted by the gap junction connection with AII amacrine cells (Sharpe and Stockman, 1999) (Figure 4.1).

4.2.2. Cone OFF-bipolar cells

Cone OFF-bipolar cells respond to light by hyperpolarization. They have basal flat contacts with cone pedicles (Boycott and Wassle, 1991) to form sign-conserving glutamatergic synapses (Sharpe and Stockman, 1999). The OFF-bipolar cells are

driven by ionotropic glutamate receptors (iGluR). There are two types of iGluR: NMDA receptors and non-NMDA receptors. The OFF-bipolar response are mainly driven by the non-NMDA, kainic acid-preferring receptors, which are blocked by PDA ((+/-)cis-2,3-piperidine dicarboxylic acid) (Dvorak, 1984). Although NMDA receptor subunits have been identified (Pourcho et al., 2001) in the outer retina, OFF bipolar cells have never been observed to utilize NMDA receptors in the generation of light responses. In addition to cone response input, the cone OFF-bipolar cells receive scotopic rod visual information via activation of sign-inverting glycinergic synapse between AII amacrine cells and OFF-bipolar cells. Recently, new evidence (Sharpe and Stockman, 1999) of rod-OFF-bipolar cells with sign-conserving ionotropic glutamatergic synapses has been reported (Figure 4.1).

4.2.3. Rod bipolar cells

Rod bipolar cells respond to light by depolarization. Each rod bipolar cell contacts 15 to 30 rod spherules to form sign-inverting synapses. Unlike cone bipolar cells, they do not have direct contact with ganglion cells. They pass the visual information via AII amacrine cells and cone bipolar cells to ganglion cells (Sharpe and Stockman, 1999). Firstly, they pass the visual information to AII amacrine cells (Figure 4.1) by sign-

conserving glutamatergic synapses. Then the AII amacrine cells transmit the information to cone ON-bipolar cells by gap junctions and to cone OFF-bipolar cells by sign-inverting glycinergic synapses. The visual information is finally passed to ganglion cells. Similar to cone ON-bipolar cells, rod bipolar cells expressing mGlu6R receptors form invaginating contacts with photoreceptors (Dhingra et al., 2000). Since the mGlu6R receptor is thought to trigger a second messenger cascade involving Galphao G-protein, transducin molecules, to act on voltage gated Ca^{2+} channels, the rod-bipolar cells are believed to be ON-type in nature (Dhingra et al., 2000).

4.2.4. Transient and sustained bipolar cells

Besides the ON- and OFF-classification of bipolar cells, bipolar cells can also be divided into transient and sustained based on their recovery from desensitization. Transient bipolar cells recover quickly from desensitization and sustained bipolar cells slowly from desensitization. The streaming of visual information into transient and sustained characteristics at the bipolar cell level is believed to form part of the origin of transient and sustained ganglion cell responses. The molecular mechanism of the transient and sustained light response characteristics are not understood, but it is suspected to be the consequence of processing of visual information via the different

glutamate receptors of the bipolar cells. These receptors re-sensitize at different rates after exposure to glutamate. They emphasize different temporal characteristics of the transient and sustained visual signal. Generally, the ionotropic receptors mediate faster and more sustained transmission of signal than metabotropic receptors (Saito et al., 1981; DeVries, 2000). Non-NMDA receptors mediate responses faster than NMDA receptors. KA receptors mediate sustained signals, while AMPA receptors transfer transient signals (DeVries, 2000).

Although retinal bipolar cells usually do not fire action potentials, but propagate electrical signals passively along the dendrites (Lukasiewicz, 2005), voltage-dependent sodium current has been reported in a subset of retinal bipolar cells of rat (Pan and Hu, 2000) and goldfish (Zenisek et al., 2001). Tetrodotoxin (TTX) has been reported to reduce but not to totally remove the transient ON-bipolar cell light response (Ichinose et al., 2005). In contrast, the sustained ON-bipolar cell response and the photoreceptor input to bipolar cells were not affected (Ichinose et al., 2005). Thus, the voltage-dependent sodium current contributes to fast response of the transient ON-bipolar cells.

4.3. Amacrine cells

Amacrine cells are local circuit interneurons. There are at least 25 different amacrine cell types in the monkey and human retina. They differ from ganglion cells, which possess long axons for long distance signal transmission. Amacrine cells have short or even no axons that interact merely with their neighbor cells. They are synaptically active in the IPL. The types of amacrine cells are often distinguished by the size of their dendritic fields, such as narrow-field (30-150um), small-field (150-300 um), medium-field (300-500 um) and wide-field (>500 um) (Kolb et al., 1981) and the location of their stratifications. They have different connections within the retinal circuit and play different roles in creating and modifying the retinal physiological output. Generally, amacrine cells provide feedback, lateral interaction and modulation of retinal response characteristics.

4.4. Reciprocal feedback to bipolar cells

Amacrine cell synapses are frequently seen to be reciprocal to bipolar input; amacrine cells synaptically contact with proximal bipolar cell input synapses. Amacrine cells are sensitive to both AMPA and NMDA excitation. The AMPA receptors mediate fast

transient response of amacrine cells. The NMDA receptors mediate a delayed (10ms) sustained AMPA response dependent response, which cannot be eliminated by TTX (Vigh and von Gersdorff, 2005). Thus, AMPA receptors are believed to be close to the glutamate release sites of bipolar cells and NMDA receptors are farther away (extrasynaptic) (Vigh and von Gersdorff, 2005). These duplex channels of glutamate sensitive currents favor translation of the temporal characteristics of signals from bipolar cells to amacrine cells. Most amacrine cells are inhibitory in nature, releasing inhibitory neurotransmitters, GABA (gamma-aminobutyric acid) or glycine, after excitation by the aforementioned duplex glutamate signals. The GABAergic amacrine cells, in particular, typically make reciprocal synapses with bipolar cells and tune the bipolar cell output (Vigh and von Gersdorff, 2005) to match the dynamic range of ganglion cells.

4.4.1. AII amacrine cells

Among different types of amacrine cells, there is a unique type of amacrine cells, named AII amacrine cells, conducting the rod visual signal to cone bipolar pathways. They mediate predominantly the vertical flow of information of the inner retina, rather than any lateral interaction. They transmit and amplify both rod and cone

driven signals within the ON- and OFF-retinal pathways to the inner retina. They contact rod bipolar cells by sign conserving glutamatergic synapses. They also connect to cone ON-bipolar cells with gap junction and cone OFF-bipolar cells with sign inverted glycinergic synapses.

The AII amacrine cells play the role of intermediary between retinal ON- and OFF-pathways in both photopic and scotopic vision. In the photopic state, light stimulation reduces glutamate release from cone cells and the AII amacrine cells mediate the inhibition of the OFF-pathway according to ON-pathway information. In scotopic conditions, light stimulation reduces glutamate release from rod cells and causes rod bipolar cells to depolarize and excite the AII amacrine cells via the sign conserving glutamatergic synapse. Then AII amacrine cells depolarize cone ON-bipolar cells (by gap junctions) and hyperpolarize cone OFF-bipolar cells (by sign inverting glycinergic synapses). As a result, in scotopic conditions, the AII amacrine cells transfer the rod vision information to the cone ON-pathway and mediate the inhibition of the OFF-pathway. In both cone and rod vision, during light stimulation, the AII amacrine cells are depolarized and the OFF-pathway signals are inhibited (Sharpe and Stockman, 1999). This approach serves to enhance the signal to noise ratio of visual information passing to the inner retina. However, there is a lack of information about

the physiology and role of the AII amacrine cells if both rod bipolar and cone ON-bipolar cells depolarized together, such as in mesopic condition.

4.5. Ganglion cells

The ganglion cells are the retinal neurons which synapse with the bipolar cells and amacrine cells. Most of the axons of ganglion cells exit the eyeball at the optic disc, form the optic nerve and terminate at the lateral geniculate nuclei (LGN), while a fraction of ganglion cells pass to the superior colliculus and the pretectal nucleus in the mid-brain. As with amacrine cells, the classification of ganglion cells is usually based on their dendritic morphologies. In cats, the common ganglion cell types are alpha (large dendritic field) and beta cells (small dendritic field). In the human retina, the common ganglion cell types are the midget ganglion cells and the parasol ganglion cells. The midget ganglion cells are also called P cells because of their projection to the parvocellular layers in LGN, and the parasol ganglion cells are called M cells because of their projection to the magnocellular layers of the LGN. The human P and M cells are believed to be equivalent to cat beta and alpha ganglion cells respectively.

The ON- and OFF-ganglion cells synapse with bipolar cells and amacrine cells at different strata of the IPL. In simple terms, the strata are divided into stratum “a”, which is relatively outer IPL, and stratum “b”, which is relatively inner IPL. The interactions between OFF-ganglion cells and the basal-contacting cone OFF-bipolar cells occur strictly in stratum “a”, and the interactions between ON-ganglion cells and the cone ON-bipolar cells occur strictly in stratum “b”.

In general, retinal ganglion cells respond to most of the excitatory and inhibitory neurotransmitters. Physiological evidence suggests that both NMDA and non-NMDA receptors are present in ganglion cells. In primate retina the transmission from bipolar cells to ganglion cells may be predominantly mediated by non-NMDA receptors (Cohen and Miller, 1994). The blockage of the AMPA receptor by CNQX largely suppresses the light response of ganglion cells (Jacoby and Wu, 2001). The NMDA mediated current has a pre-requisite of excitatory current triggered by other excitatory neurotransmitters and it is suspected to play a role in modulating the sensitivity of the ganglion cells. This is because the blockage of NMDA receptors in ganglion cells results in more sustained light response instead of response suppression (Cohen and Miller, 1994). In addition to ionotropic glutamate receptor agonists, extracellular acetylcholine is the excitatory neurotransmitter of retinal ganglion cells (Cohen et al.,

1994). However, inhibitory neurotransmitters, such as GABA and glycine, can trigger inhibitory currents in ganglion cells (Cohen et al., 1994; Yang, 2004).

4.6. Retinal pigment epithelium (RPE)

The cell biology of the RPE has been reviewed by Thumann and Hinton (2001). The RPE cells are situated between the choroid and the neural retina. They are arranged in a tight hexagonal pattern as a monolayer of highly specialized pigmented cells. The RPE cell density decreases from the fovea to the peripheral retina. The existence of RPE cells is critical to the function and viability of the photoreceptors. They participate in phagocytosis of photoreceptor outer segment discs, metabolism of retinol, formation of the blood-retinal barrier, interaction with light by melanin, extracellular matrix synthesis, ions and regulation of the transport of metabolites. The major end-product of phagocytosis of photoreceptor outer segment discs is lipofuscin granules, which accumulate in the RPE cytoplasm and then are removed by the choroidal circulation.

Chapter 5 – Signal Transmission in the Retina

5. Signal transmission in vertical pathways of retina: neurotransmitters and receptors

Visual signal or information conduction through the retina involves communications among cells and signal propagation along neurons. Basically, there are different types of communication among cells facilitated by various structures such as gap junctions, electrical synapses and chemical synapses, using neurotransmitters. Cation channels open when presynaptic neurons being stimulated, and cations influx into the axon terminal. Consequently, a cascade of events is triggered to release neurotransmitters. Then neurotransmitters diffuse across the synaptic cleft and bind to receptors on the postsynaptic membrane to allow signal propagation.

Different techniques, such as autoradiography, immunocytochemistry and molecular biology, are widely used to identify the presence and location of various neurotransmitter receptors in retinal neurons. Consequently, use of agonists and antagonists of those receptors can be used to investigate the physiology of different retinal neurons. The following sections will discuss the use of agonists and antagonists for studying the physiology of retinal neurons along vertical pathways.

5.1. Principle neurotransmitter in the retina: glutamate

In the retina, the principle neurotransmitter in vertical pathways is the excitatory amino acid, glutamate (Figure 5.1.1). It contributes to the excitation of second neurons at all level of synaptic connection in the retina. Similar to the brain, there are two glutamate sensitive channels for signal processing in the retina. They are metabotropic and ionotropic channels. There are wide varieties of metabotropic receptors (mGluR) and ionotropic receptors (iGluR). Although they both influence the membrane permeability of ions upon glutamate activation, they mediate the ion channels in different ways. The mGluR activation couples with ion channels opening and some cellular function of neurons indirectly by influencing intracellular second messenger cascades (Sladeczek et al., 1992). The iGluR gates the membrane ion channels directly upon activation (Sheardown et al., 1993). The existence of different glutamate receptors on cone pathway was summarized in Table 5.1 and Figure 5.1.2. In OPL, the mGluR and iGluR are present in ON- and OFF-bipolar cells specifically (Marc et al., 2007). In contrast, in IPL, both mGluR and iGluR are present in ON- and OFF-ganglion cells (Cohen and Miller, 1994).

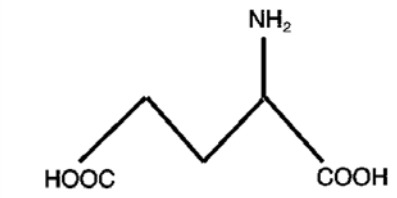

Figure 5.1.1. L-glutamate

	Glutamate		
	iGluR		mGluR
	NMDA	Non-NMDA (AMPA / KA)	
Horizontal cells	- (NMDA insensitive)	+ (PDA sensitive)	+ (APB insensitive)
ON-bipolar cells	- (NMDA insensitive)	+ (PDA insensitive) (CNQX insensitive)	+ (APB sensitive)
OFF-bipolar cells	- (NMDA insensitive)	+ (PDA sensitive) (AMPA insensitive)	+ (APB insensitive)
Amacrine cells	+ (NMDA sensitive)	+ (PDA sensitive)	+ (AII: APB insensitive)
Ganglion cells	+ (NMDA sensitive)	+ (PDA sensitive)	+

Table 5.1. Glutamate receptors on cone pathway neurons. The "+" sign indicates the presence of histological evidence of those receptors. The "–" sign indicates the lack of histological evidence of those receptors. The bracketed text indicates the sensitivity of light current to those corresponding pharmacological agents. The grayed color text indicates positive sensitivity to those corresponding pharmacological agents. (The information in table is a brief summary from the work of Yang(2004) and Shen and

his co-workers(2006).)

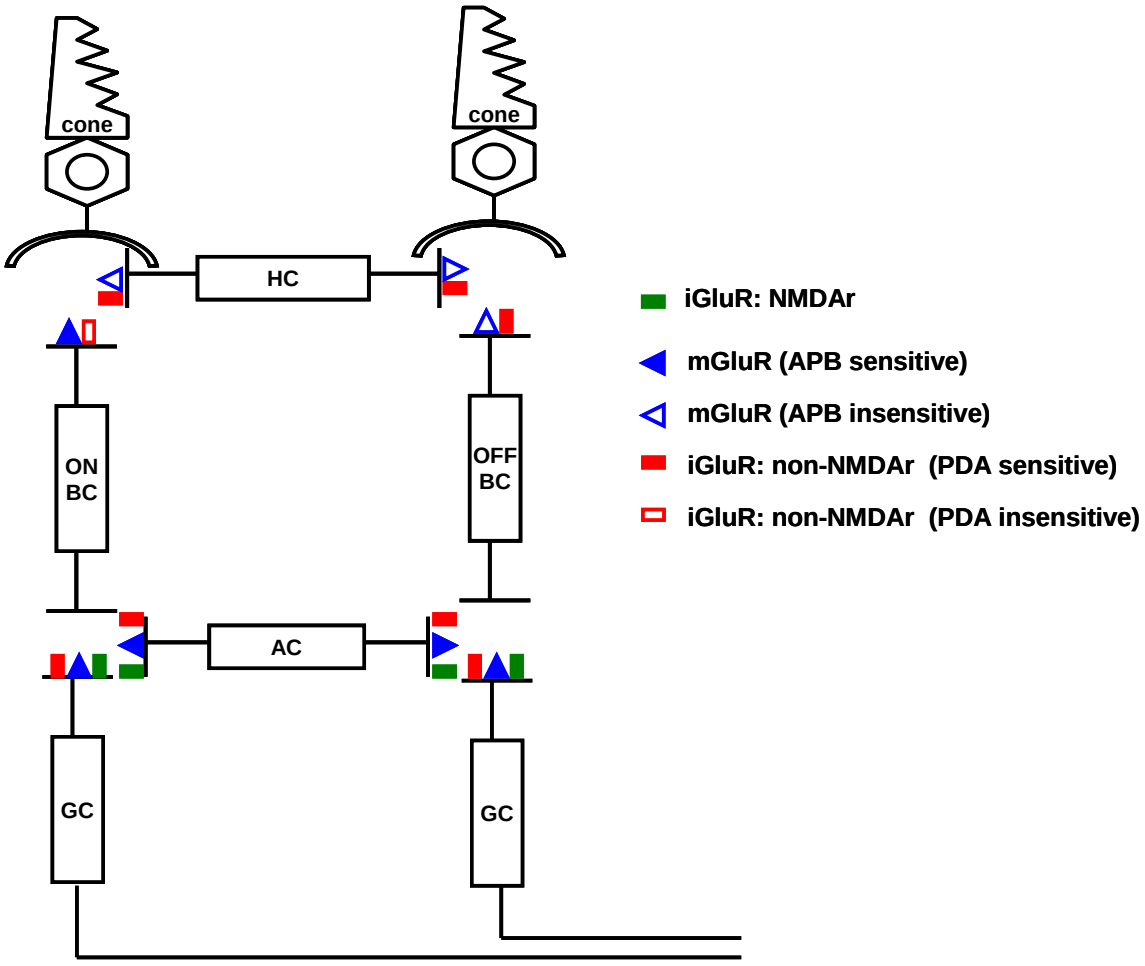

Figure 5.1.2. Glutamate receptors on cone pathway neurons. (The information in figure is a brief summary from the work of Yang(2004) and Shen and his co-workers(2006).)

5.1.1. Metabotropic receptors – mGlu6R

Unlike ionotropic receptors with their direct linked ion channels, metabotropic receptors couple to ion channels through secondary messenger and G-protein

pathways (Sladeczek et al., 1992). Metabotropic receptors form a large family of glutamate receptors. There are eight sub-types of mGluR (Figure 5.1.1). They are further classified into three groups: 1, 2, and 3, based on their structural homology, agonist selectivity, and their associated second messenger cascades. In brief, group 1 mGluR (mGlu1R and mGlu5R) couples with the hydrolysis of fatty acids and the release of calcium from internal stores. Their activation may enhance the excitability of post-synaptic neurons. Group 2 mGluR (mGlu2R and mGlu3R) and group 3 mGluR (mGlu4R, mGlu6R, mGlu7R and mGlu8R) are inhibitory; only the mGlu6R (APB receptor) is widely distributed among the mGluR family.

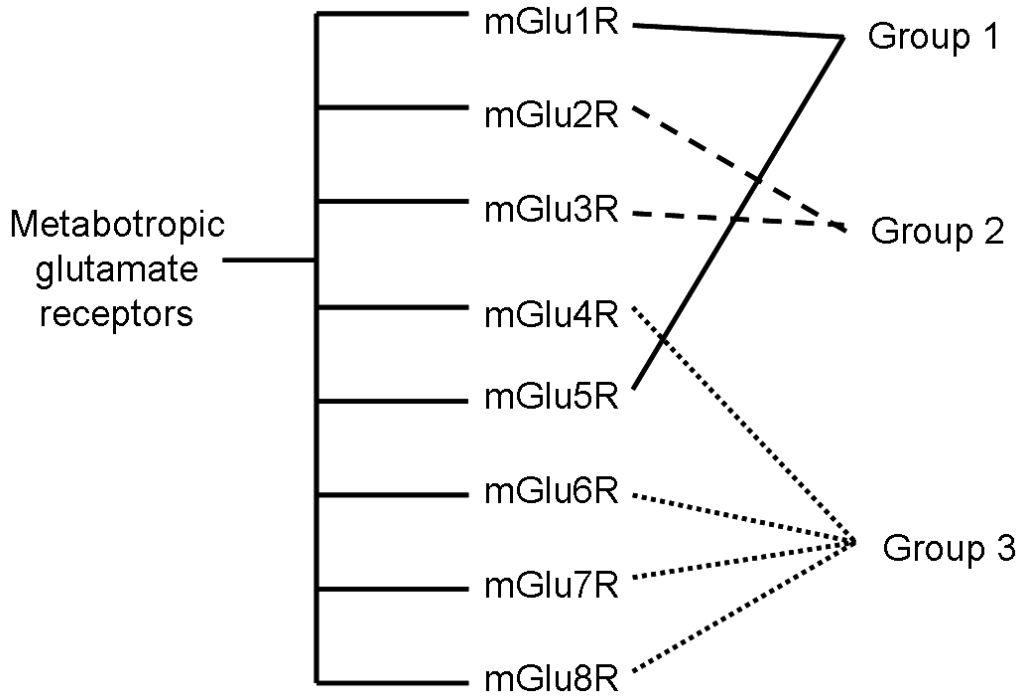

Figure 5.1.1.1. Classifications of metabotropic glutamate receptors.

5.1.1.1.APB (2-amino-4-phosphonobutyric acid) receptors

APB (2-amino-4-phosphonobutyric acid, also known as L-AP4) receptor (mGlu6R) is a key receptor in photoreceptor signaling for ON-pathways in the retina. It is expressed in dendritic tips of all ON-bipolar cells (rod and cone driven) (Marc et al., 2007). In contrast to iGluR, glutamate binding to APB receptors results in reduced membrane permeability to cations due to closure of cGMP-gated non-selective cation channels (Nawy and Jahr, 1990). APB selectively blocks the ON-pathway signal propagation of the retina. It inhibits glutamate release of ON-bipolar cells at the pre-synaptic dendritic membrane. In turn, it results in a lack of signal input to ON-ganglion cells and ON-amacrine cells from the ON-bipolar cells.

5.1.2. Ionotropic receptors

Unlike metabotropic receptors without directly linked ion channels, ionotropic glutamate receptors (iGluR) gate ion channels by forming complexes with them. They mediate fast excitatory synaptic transmission between neurons. There are two types of receptors in the family of iGuRs. They are NMDA and non-NMDA receptors (Figure

5.1.2).

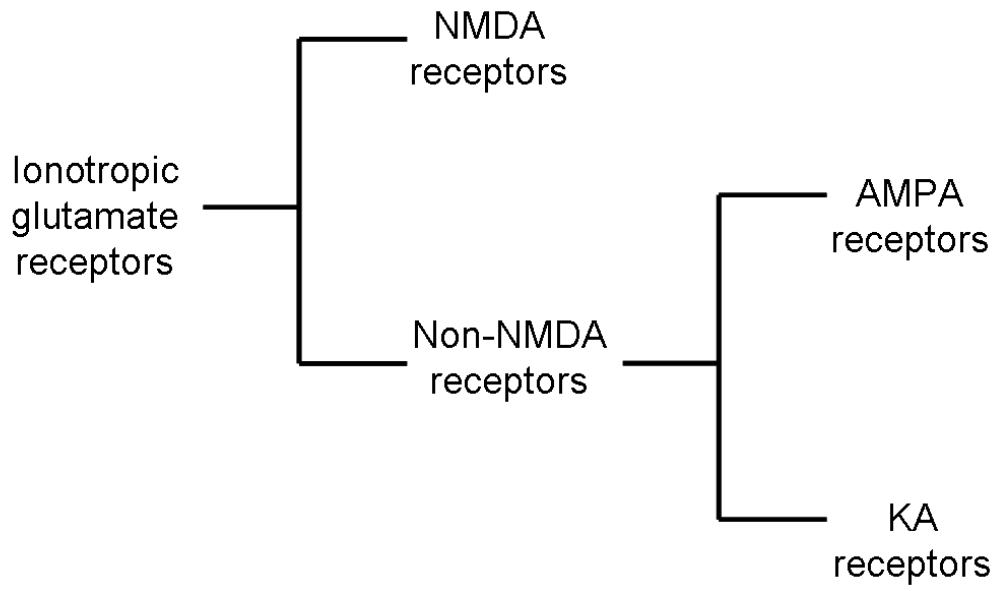

Figure 5.1.2. Ionotropic glutamate receptors

5.1.2.1.NMDA receptors

NMDA receptors bind glutamate and glutamate analogue NMDA (N-methyl-D-aspartate). Upon ligands binding, different from non-NMDA receptors, NMDA receptors open non-selective cation channels with higher permeability to calcium than to sodium and potassium ions. In mammals, NMDA receptors are not associated with ON-bipolar cells (Fletcher et al., 2000), and physiologically, there is no NMDA response in ON- and OFF-bipolar cells and photoreceptors (Shen et al., 2006). Retinal ganglion cells and some amacrine cells express functional NMDA receptors in

addition to non-NMDA receptors (Cohen and Miller, 1994; Vigh and von Gersdorff, 2005). Currents mediated by these two types of iGluR can be distinguished pharmacologically since the NMDA mediated current has slower kinetics than non-NMDA mediated current. The non-NMDA receptor antagonist, CNQX (6-cyano-7-nitroquinoxaline-2, 3-dione), which inhibits a transient component of the amacrine cell response and NMDA receptor antagonist, D-AP5 (D-2-amino-5-phosphonopentanoate), inhibits a sustained component of the amacrine cell response (Vigh and von Gersdorff, 2005). Thus, NMDA receptors and non-NMDA receptors contribute differently to the signal processing in inner retina.

5.1.2.2.Non-NMDA receptors

Non-NMDA ionotropic receptors bind glutamate but not the glutamate analogue NMDA. Upon ligand binding, non-NMDA receptors with higher permeability to sodium and potassium ions than to calcium ions open non-selective cation ion channels. As they mediate current with faster kinetics, they are believed to mediate fast responses in the central nervous system (CNS) including the retina. The non-NMDA receptors can be further divided into two sub-types: KA (kainate) receptors and AMPA (α-amino-3-hydroxy-5-methylisoxazole-4- propionic acid) receptors

(Figure 5.1.2), and the kinetics of their ligand-gated currents are different. The KA receptor mediated current desensitizes slowly, while the AMPA receptor mediated current desensitizes rapidly. CNQX (6-cyano-7-nitroquinoxaline-2,3-dione) is a competitive antagonist of both AMPA receptors and KA receptors.

5.1.2.2.1. KA receptors

KA (kainate) receptors which are non-NMDA ionotropic glutamate receptors, bind glutamate and kainate. The excitatory properties of KA receptors are mediated by activating post-synaptic neurons and inhibiting GABA (an inhibitory neurotransmitter) released from the pre-synaptic neurons (Huettner, 2003).

5.1.2.2.2. AMPA receptors

AMPA (α-amino-3-hydroxy-5-methylisoxazole-4-propionic acid, formerly known as quisqualate) receptors bind glutamate and AMPA. They are non-NMDA ionotropic glutamate receptors mediated fast synaptic transmission in CNS including retina.

5.1.2.2.3. PDA ((±)-cis-2,3-piperidinedicarboxylic acid)

PDA ((±)-cis-2,3-piperidinedicarboxylic acid) was proposed by Slaughter and Miller (1983) as an excitatory amino acid antagonist to block light response of OFF-bipolar cells and horizontal cells. Although PDA is less specific than APB, there is no reduction of light response of ON-bipolar cells in high PDA concentrations and the synaptic release from cone cells is unchanged. The conductive resistance of OFF-bipolar cell membrane is increased by PDA application. Slaughter and Miller (1983) reported that PDA caused reversible hyperpolarization of mudpuppy OFF-bipolar cells. For maximum inhibition of OFF-bipolar cell light response, 6-10uM PDA is needed, but 5-10% of OFF-bipolar cell light response was reported to be left (Slaughter and Miller, 1983).

5.2. Signal propagation

After the excitation of post-synaptic membrane receptors, which couple with ion channels directly or indirectly, the post-synaptic neurons depolarize. In the resting state, a potential between extracellular space and cytoplasm is intracellular negative. The potential difference is caused by imbalance of ions distributions inside and outside neurons. When the depolarization of neurons exceeds their membrane potential threshold, they fire one or more action potentials as graded responses to light in retina. The action potential is a rapid voltage change from negative to positive polarity and then vice versa which permits rapid, long distance propagation of electrical current along the membrane of neurons. The process of action potential propagation involves contribution of voltage-dependent cation channels.

5.2.1. TTX (tetrodotoxin)

TTX (tetrodotoxin) is a potent neurotoxin with no known antidote at this moment. TTX blocks action potentials in neurons by binding the extracellular pore openings of voltage-gated sodium channels on neuronal membranes. It is named tetrodotoxin because of its natural presence in Tetradontiformes, an order of fish including

pufferfish (Figure 5.2.1). Although TTX is processed by Tetradontiformes, it actually is a product of certain bacteria. Due to its potency in blocking the action potentials in CNS, TTX is a valuable agent for silencing neural activity in the inner retina.

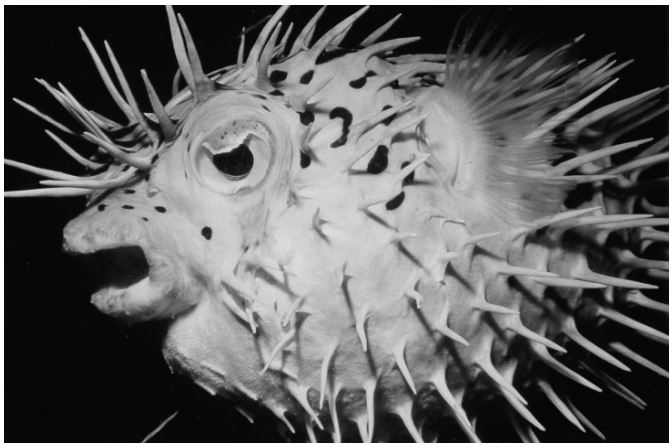

Figure 5.2.1. Pufferfish.

Chapter 6 – Fundamentals of Electroretinogram

6. Electroretinography

Electroretinography (ERG) is an objective recording of electric potential changes in retina after stimulation by light. Electroretinogram is the record obtained by electroretinography. Electroretinograph is an instrument for measuring the retinal electrical response to light (also abbreviated ERG conventionally).

ERG involves electrical activity of different retinal cells. According to Fishman (2001), ERG was first identified by a Swedish physiologist Alarik Frithiof Holmgren in recordings from a frog eye. Since then, retinal electrical activity has been studied using animals including monkeys (Lutjen-Drecoll et al., 1977), cat (Frishman and Steinberg, 1990), rabbit (Xin and Bloomfield, 1999) and rat (Ball and Petry, 2000), and recently pig (Banin et al., 1999).

The electrical basis of ERG recordings is conceptually similar to measuring the voltage across an array of batteries. The retinal activities triggered by luminous stimulus are recorded with an extracellular “active” electrode positioned either on

cornea, in vitreous or at difference strata of retina. The recording of electrical activities is feasible when electrical currents spread along extracellular matrix with electrical resistance. Simply speaking, the photoreceptors are arranged nearly in radial or emanated from the optical nodule point of the vertebrate eyeball. Consequently, the propagations of electrical current along the retinal pathways generate electrical potential differences across the retina (Figure 6). Then the potential difference variation across time can be recorded by ERG.

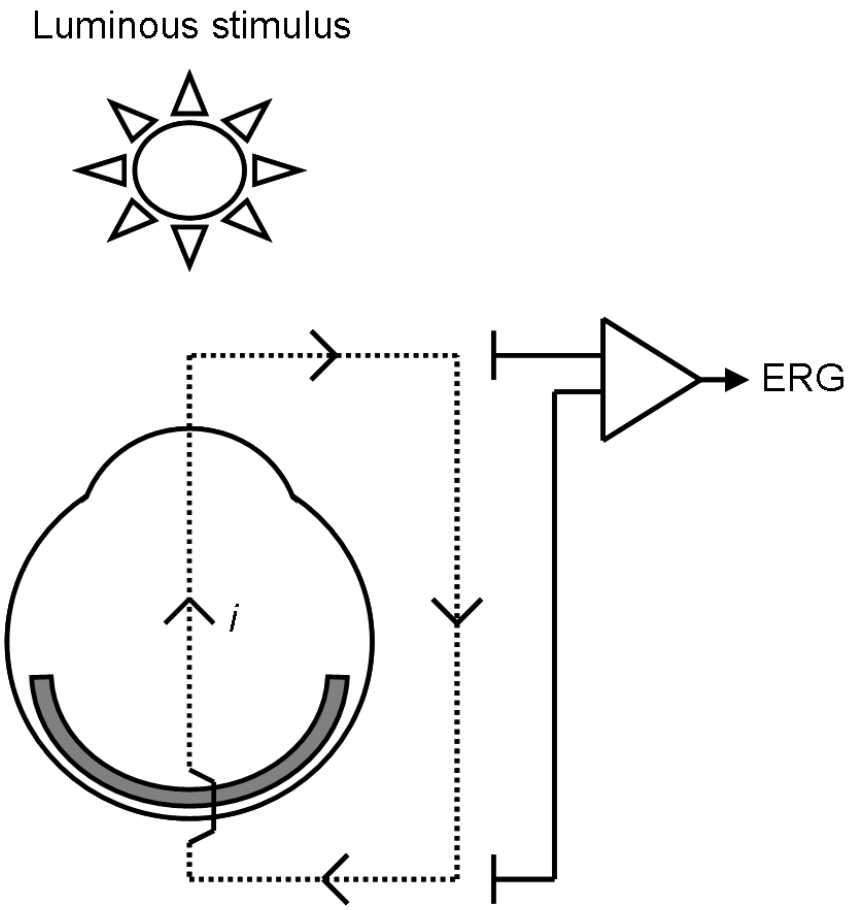

Figure 6. Schematic presentation of extracellular current (*i*) triggered by luminous stimulus. There is a local current within the retina (black line). The current leaves retina via vitreous and cornea and returns back to retina through choroid and retinal pigment epithelium (dotted line). ERG recording in human is measuring the potential difference along the extracellular current (*i*) (dotted line).

6.1. Flash ERG

The flash (full-field) ERG is a mass electrical response of retina to luminous stimulation. It is commonly used to assess the (normal or abnormal) status of the retina in human and animals. The basic method of recording the ERG is by stimulating the eye with a bright light source such as a flash (Figure 6). The flash triggers a biphasic electrical potential change (a-wave and b-wave) relative to the potential at cornea (Figure 6.1). The a-wave is an initial negative deflection, followed by a subsequent positive component called b-wave. The b-wave is then followed by a prolonged positive component known as c-wave. Conventionally, there are two measuring parameters in the ERG: amplitudes (baseline to negative peak amplitude of a-wave and peak-to-peak amplitude of b-wave) and implicit time (from stimulus onset to peaks of a-wave and b-wave).

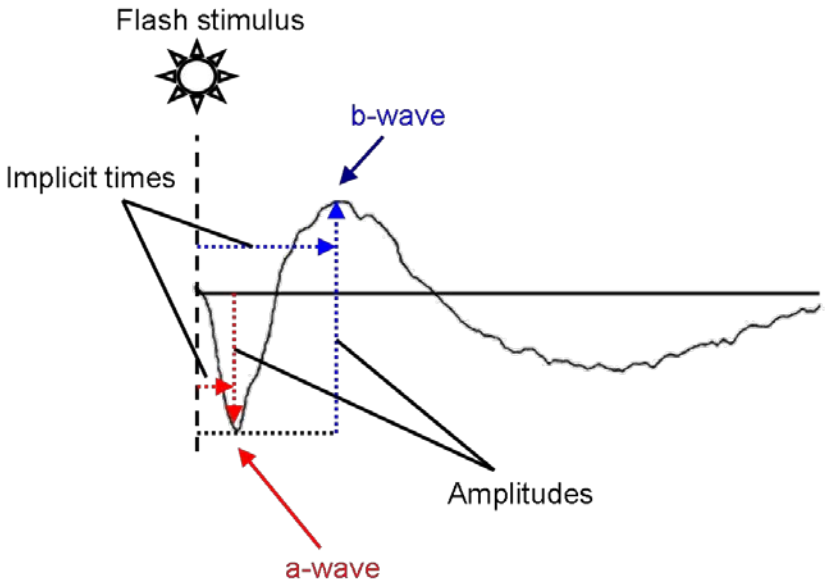

Figure 6.1. ERG waveform of biphasic retinal electrical potential variation following a flash stimulus. The vertical arrows show the amplitudes of a-wave (red) and b-wave (blue). The horizontal arrows show the implicit times of a-wave (red) and b-wave (blue).

Based on the information obtained by *in-vitro* ERG in animals, the cellular origins of *in-vivo* ERG are also identified. The ERG measurement *in-vivo* including clinical applications, usually measures the corneal potential changes elicited by light stimulation. It involves positioning of three fundamental electrodes (active, reference and ground) on the area of interest. Usually the active electrode is placed at the corneal surface. The reference attaches the skin close to the outer canthus or location of posterior eyeball. The active and reference electrodes are used to measure the potential difference across the eyeball from anterior to posterior pole. The ground electrode is placed at skin distal to the eyeball and susceptible to minimal muscular activity. The ERG signals are amplified, averaged and filtered to enhance the signal to

noise ratio for interpretation.

6.1.1. a-wave

The a-wave is an early corneal negative component of the ERG. In vertebrate retinas, there is a continuous flow of Na^+ ions from the extracellular space into the outer segment of the photoreceptors in the dark. It causes depolarization of the photoreceptor membrane. At the inner segment, there is a K^+ flow to complete the current loop. This current flow occurred in darkness is called “dark-current”. The low Na^+ concentration and high K^+ concentration balance in intracellular space is maintained by Na^+/K^+ pump.

Under light stimulation, visual pigment in photoreceptor outer segments absorbs photons and initiates a sequence of bio-chemical events, called phototransduction, which causes hyperpolarization of photoreceptors. Employing rod as an example, the activated visual pigment (rhodopsin) triggers a protein (transducin or G-protein) to activate an enzyme, cGMP phosphodiesterase (PDE), which facilitates the reduction of photoreceptor cGMP level. The low cGMP level causes the closure of sodium ion channels, which is normally permeable to sodium ion in darkness. As a result, the

sodium ion influx into photoreceptor is inhibited and then the dark current ceases. The decrease in intracellular Na^+ concentration makes the intracellular electrical potential more negative. The corneal negative a-wave is due to this light-induced hyperpolarization.

6.1.2. b-wave

After the occurrence of corneal negative a-wave, the photoreceptor potential is cut off by the corneal positive contribution from the ON-bipolar cells. This corneal positive potential is called b-wave which was previously thought to be contributed by Műller cells. The hyperpolarization of photoreceptors causes the depolarization and hyperpolarization of ON- and OFF-bipolar cells, respectively. The bipolar cell depolarization increases extracellular potassium ion level in the OPL. This elevated potassium ion level, in turn, triggers depolarization of Műller cells, amacrine cells and ganglion cells, and then potassium ion level rises in the IPL. However, recent studies (Tian and Slaughter, 1995; Hanitzsch et al., 1996) suggested that the b-wave was mainly contributed by ON-bipolar cells activity, but not the potassium sensitive Műller cells. They found that the APB-suppressed ON-bipolar cell activity was correlated to the decrease of b-wave amplitude. The $MgCl_2$ blockage of b-wave

occurred with the K^+ concentration raise, thus the blockage of b-wave was independent to the K^+ concentration.

6.1.3. c-wave

The c-wave is a corneal positive component following the b-wave. According to Fishman (2001), the c-wave is the algebraic summation of a corneal positive component from RPE and a corneal negative component from Műller cell activities. As the extracellular K^+ around outer segment of photoreceptor cell decreases following light stimulation, standing potential between the apical and basal surfaces of RPE changes. Light flash, thus, induces a transient hyperpolarization at the apical surface of RPE cells and Műller cells.

6.2. Multifocal electroretinogram (mfERG)

Although the *in-vitro* flash ERG renders us opportunities to study the retinal physiology, it conventionally cannot provide any topographical information of retina easily. The assessment of inner retinal activities (ganglion cells and amacrine cells activities) is even more difficult. Thus, there are demands of different types of

modified flash ERG to facilitate the monitoring of local retinal physiology and reveal the electrical activities of inner retina.

Traditional focal ERG is an extension or a derivative of full-field ERG (Birch, 2001). The only difference is the stimulus size. Theoretically, repeated assessment of focal ERG at different retinal areas can produce topographical retinal information. However, due to time factor, the assessment is usually limited to several retinal regions. Thus an innovative solution to record simultaneously from multiple retinal areas is necessary. In early 1990s, Dr. Erich Sutter (Sutter and Tran, 1992) developed a new system, multifocal ERG (mfERG), to solve this problem. It is called VERIS^{TM} (Visual Evoked Response Imaging System).

Multifocal electroretinography (mfERG) (Sutter and Tran, 1992) is a procedure for recording the local electroretinogram (ERG) from different retinal regions over a short period using multi-input stimulation (Marmor et al., 2003). The resulting high resolution functional map of the retina (Hood, 2000) is regarded as a powerful tool for detecting abnormalities of retinal function and understanding different potentially blinding diseases of the retina (Hood, 2000), including glaucoma (Chan and Brown,

1999), diabetic retinopathy (Onozu and Yamamoto, 2003), macular degeneration (Jurklies et al., 2002) and etc.

The most obvious difference between conventional flash ERG and mfERG is the methods of retinal stimulation. The mfERG stimulus is presented with different stimulus pattern arrays, such as 103, 61 and 31 hexagon arrays on a computer monitor (Figure 6.2A). In general, the hexagonal elements of the array are usually scaled with eccentricity, in order to achieve approximately equal signal-to-noise ratio across the field in human subjects. However, depending on the protocol, the hexagonal array can also be changed into non-scaled with eccentricity and it is commonly used in animal study. During the stimulating period, there are about 50% of elements being at high luminance (white) and the other 50% being at low luminance (dark). The stimulation rate is the number of display changes per second that is a multiple of the frame rate of the video monitor (stimulator). In order to facilitate the cross-correlation, each element is governed by the same pseudo-random sequence of stimulation, called “maximum-length sequence” or “m-sequence”. For each stimulus location, the m-sequence is lagged by different amount and the responses associated with these elements are effectively uncorrelated to each other. Consequently, each element triggers a localized retinal response, which contributes to retinal topographical

information over the whole stimulated area.

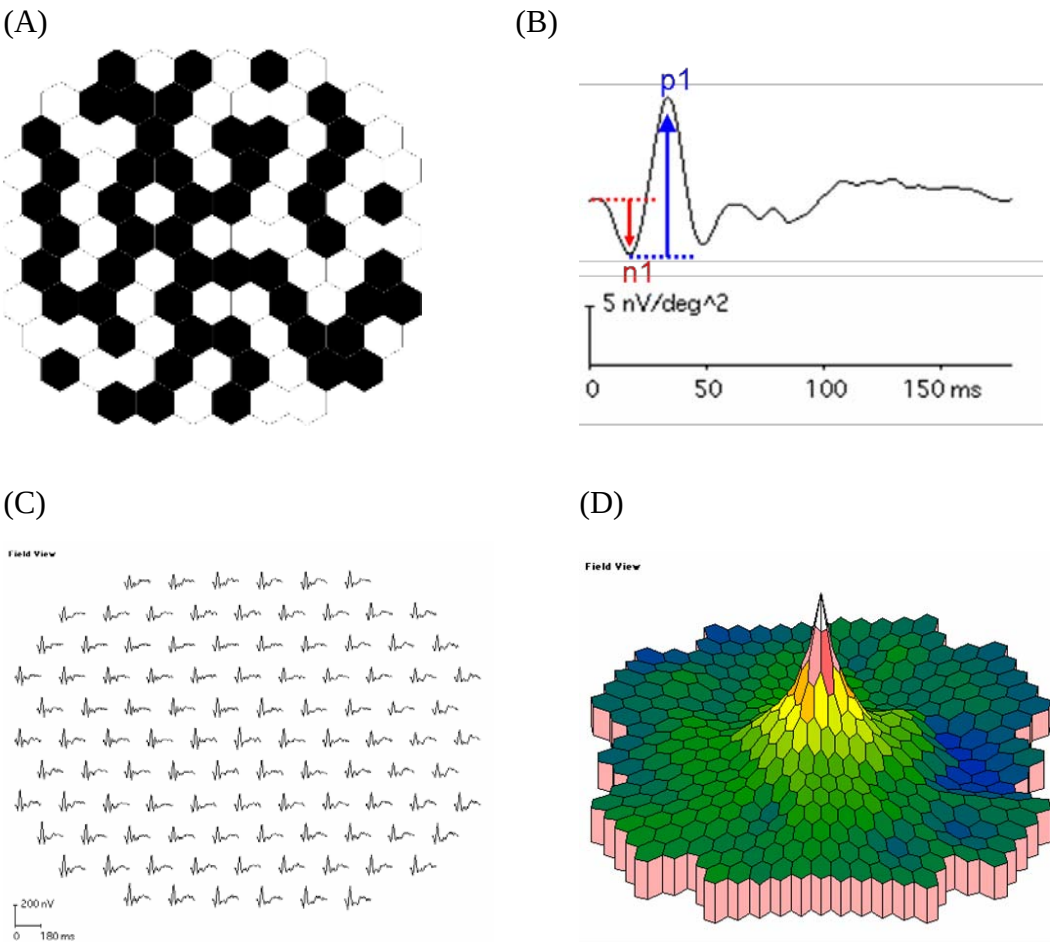

Figure 6.2. (A) 103 non-scaled hexagonal stimulation array of human mfERG. (B) Averaged first order kernel response of human mfERG. The arrows show the amplitude of n1 (red) and p1 (blue) components. (C) 103 response traces of human mfERG. (D) Three dimensional presentation of human mfERG response amplitude.

The mfERG results can be presented as an averaged response (Figure 6.2B), traces array (Figure 6.2C) over the stimulated areas and a topographical display (Figure 6.2D). The local response for each stimulus element is computed according to the m-sequence. The first order kernel response is a linear approximation of the response. It

is the averaged local response from a particular retinal area. The averaged response traces of mfERG are close to the typical full field ERG traces. Both of them contain negative and positive peaks, but their implicit times and complexities are different. It is believed to be caused by the difference in their stimulus parameters. Hood et al. (1997) inserted 7 dark frames to slow down the m-sequence to produce responses of slow flash mfERG as compared with full-field ERG response. They demonstrated the presence of oscillatory potentials in mfERG using this protocol and suggested that, under this special protocol, the negative wave of mfERG reflecting the same components as the a-wave of full field ERG, while the positive wave of mfERG and the b-wave of full-field ERG sharing similar cellular basis.

Recently, Hood et al. (2002) and Hare and Ton (2002) have used some chemicals to block and isolate various components of the monkey mfERG responses. Those chemicals included APB, PDA and TTX. The APB is a metabotropic glutamatergic receptor agonist, which selectively blocks the transmission from photoreceptors to ON-bipolar cells, the ON-responses of amacrine cells and that of ganglion cells. Thus the APB selectively blocks the ON-pathways of the outer and inner retina. The PDA, opposite to APB, is an ionotropic glutamatergic receptor antagonist. Although, it is less selective than APB, application of PDA blocks the transmission from

photoreceptors to OFF-bipolar cells and horizontal cells, but not ON-bipolar cells. The PDA also blocks the transmission from both ON- and OFF-bipolar cells to the amacrine cells and ganglion cells. The TTX is a specific blocker of the voltage gated sodium channel. The TTX sensitive sodium current has been identified in both amacrine cells and ganglion cells. Although bipolar cells usually do not fire action potentials (Lukasiewicz, 2005) and electrical signals propagate passively along their dendrites, voltage-dependent sodium current has been reported in subset of retinal bipolar cells of rat (Pan and Hu, 2000) and goldfish (Zenisek et al., 2001). TTX was reported to reduce but not remove the light response in transient ON-bipolar cell (Ichinose et al., 2005). In addition, those sustained ON-bipolar cell response and photoreceptor input were not affected by treatment of TTX (Ichinose et al., 2005) Thus, under normal conditions, amacrine cells and ganglion cells are the main retinal cell types, generating action potentials in response to light, being affected by TTX (Werblin and Dowling, 1969). In the previous studies, the application of APB caused severe attenuation of the p1 amplitude in mfERG and the n1 amplitude was mostly reduced by the PDA application. The TTX application abolished the nasal-temporal response variation and the oscillation potentials superimposed on the rear edge of the p1 component (Hare and Ton, 2002; Hood et al., 2002).

Although the waveforms of mfERG and conventional flash ERG are different in monkey, they essentially share similar cellular origins. The mfERG n1 resembles the ERG a-wave. The mfERG p1 resembles the ERG b-wave, both contributed by bipolar cells. The difference in waveforms is mainly due to the fast flickering frequency of mfERG stimuli. Thus, mfERG may provide richer temporal information about retinal adaptation.

Chapter 7 – Factors Affecting the Multifocal Electroretinogram

7. Factors affecting the retinal physiology of *in-vivo* and *in-vitro* models

The conventional flash ERG and mfERG are objective assessments of retinal physiology and they are affected by retinal conditions and retinal pathologies. The retinal pathologies which affect retinal metabolism and physiology are usually intended to be monitored and assessed. However, retinal physiology can be influenced by other factors, such as anesthesia, ocular blood flow, blood oxygenation, and core temperature of the eye. Thus, the standardization of those conditions is crucial in development of a reproducible model for study of retinal physiology.

7.1. Retinal disorders/diseases

In diseased retina, the physiology of retinal neurons and photoreceptors is usually compromised. The compromised and even impaired physiology, in some conditions, affects the retinal response to stimulation by light. As a result, retinal pathologies affecting the photoreceptors, such as retinitis pigmentosa (RP) and age related macular degeneration (ARMD), alter the retinal responses and retinal electrophysiological information obtained. However, in certain retinal diseases, there may be inconsistencies between conventional flash ERG findings and the visual disabilities of patients, because these retinal diseases may only affect a small retinal area in early stage of the condition. In such cases the conventional flash ERG may not be able to represent the visual function of patients. However, in these situations, mfERG with topographical information would be more useful in representing the functional changes localized in different retinal areas.

One of the important retinal diseases which can be assessed by ERG is retinitis pigmentosa (RP). Retinitis pigmentosa is a collection of heterogeneous, hereditary progressive retinal photoreceptor dystrophies. It affects primarily rod cells and finally cone cells. Visual field defects and night blindness are the common consequences in RP in the early stage. Eventually, loss of central vision is common in the late course

of RP. Progression of RP is different in each patient. In human patients, as there is a wide variation of visual disabilities, it is difficult to correlate mfERG changes to the progression of RP, apart from visual field constriction (Janaky et al., 2007). Thus, the understanding of physiological changes from different types of retinal cells involved in the course of RP is essential for the clinical interpretation of mfERG changes in humans.

There are different animal models for studying RP, such as retinal degeneration 10 (rd10) mice (Gargini et al., 2007), retinoblastoma gene (Lox/-) mice (Johnson et al., 2006), CNGA3(-/-) mice (Haverkamp et al., 2006), Royal College of Surgeons rat (Peng et al., 2003), Standard Wire-haired Dachshund-derived dogs (Ropstad et al., 2007) and P347L pigs (Peng et al., 2003). Although they have different genetic defects, they all show the phenotype of RP, in which they suffer primarily from rod cell death and finally from cone cell death. The development of these genetically engineered animal models provides platforms for studying the retinal functional changes following the retinal degeneration in RP. Recently, there has been evidence of neural rewiring in those genetically engineered RP models (Peng et al., 2000; Peng et al., 2003; Haverkamp et al., 2006; Johnson et al., 2006; Gargini et al., 2007; Sullivan et al., 2007). Dissection of the retinal response would help to investigate the influence

of the neural re-wiring.

7.2. Anesthesia

Anesthesia is a condition of losing feeling of pain and sensations. Anesthesia usually targets the neurons and receptors of the nervous system. This allows subjects to undergo surgically procedures, alignment and testing procedures without distress or pain. Apart from being necessary in human studies, general anesthesia is essential in nearly all *in-vivo* animal studies.

The retinal response is a summated activity of different retinal cell types, which include communication among neurons. Thus anesthesia, which desensitizes neurons, is most likely to influence ERG and mfERG results (Fortune et al., 2002; Lalonde et al., 2006). Thus, understanding the influence of different anesthetics on different retinal pathways is essential in animal studies of ERG and mfERG.

Anesthetics are classified as inhalation anesthetics and injection anesthetics. For both categories of anesthetics, the exact pharmacological mechanisms and effects of CNS are still under debate. Inhalation anesthetics are most often used to maintain general

anesthesia in surgical operations. They included a collection of volatile organic agents, such as nitrous oxide, halothane and isoflurane. In addition, there are collections of injection anesthetics such as barbiturates, benzodiazepine, propofol, etomidate and ketamine. Among them, ketamine is commonly used in animal studies, especially in electrophysiology. As in human anesthesia, propofol has recently been used to replace ketamine and isoflurane in animal studies. Thus its effects on the CNS have aroused the interest of researchers on electrophysiology (Grasshoff et al., 2005; Hans and Bonhomme, 2006; Lalonde et al., 2006). Due to ethical issues, the use of anesthesia for *in-vivo* animal studies is inevitable, however, the *in-vitro* retinal models provide us an opportunity to study electrical retinal activity with and without application of anesthetics.

7.2.1. Isoflurane

Isoflurane (2-chloro-2-(difluoromethoxy)-1,1,1-trifluoro-ethane) (Figure 7.2.1) is a common inhalation anesthetic. It is a halogen ether which replaced the flammable ethers used in the pioneer days of surgery. Although its usage in human medicine is now declining, being replaced by the intravenous anesthetic propofol, it is still

commonly used in veterinary and laboratory medicine. It is inexpensive and safe in the laboratory. Its minimum aveolar concentration (MIC) approximates 1.4 vol %, while its minimum blood concentration (MBC) approximates 0.53% (ml of ISO per ml of blood) in clinical situations (Katoh et al., 1992). Although isoflurane initiates anesthesia rapidly, its pungency irritates the respiratory system. Thus it is usually used to maintain general anesthesia that has been induced by other drugs, such as thiopentone, ketamine and propofol.

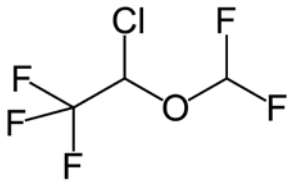

Figure 7.2.1. Isoflurane (ISO).

Similar to other classic anesthetics, the mechanism of isoflurane anesthesia is not fully understood. It reduces the sensation of pain and relaxes muscles. It causes partial suppression of action potentials and sodium channels of neurons (Duch et al., 1998). It inhibits activities of GABA receptors, glutamate receptors and glycine receptors and potassium channels (Ueno et al., 1999; Cheng and Kendig, 2003; Sonner et al., 2003). As a result, the use of isoflurane affects the response characteristics of the ERG and

the mfERG (Fortune et al., 2002; Lalonde et al., 2006).

7.2.2. Ketamine

Ketamine (Figure 7.2.2) is a fast acting anesthetic used in veterinary medicine but infrequently in human medicine, because it causes hallucinations. Its commonly used in eye research involving the ERG and the mfERG (Fortune et al., 2002; Hood et al., 2002; Lalonde et al., 2006). It can be injected intravenously or intramuscularly. Ketamine is a non-competitive NMDA antagonist and the NMDA receptor mediates analgesia (pain relief) at low doses of ketamine. It is commonly used in combination with xylazine (a sedative and muscle relaxant) to minimize the tremors caused by ketamine (Woodward et al., 2007). Although repeated re-dose of ketamine is a danger to animals, ketamine is metabolized quickly (in approximately one hour), and thus re-dose of ketamine is necessary in many animal studies. As a result, ketamine may not be a good anesthetic for long-term experiments with large animals. However, the use of ketamine has an advantage for electrophysiology monitoring in human operations because it maintains patients with good motor somatosensory evoked potential under anesthesia.

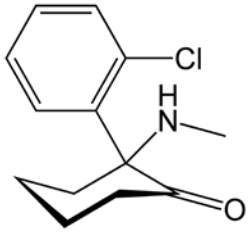

Figure 7.2.2. Ketamine.

7.2.3. Propofol

Although the mechanisms of intravenous propofol (2,6-di-isopropylphenol) (Figure 7.2.3) and inhalation ISO anesthesia are not fully understood, propofol has recently been replacing inhalation anesthesia in human medicine. It is a hypnotic agent with a fast acting time (as rapid as forty seconds after the start of intravenous perfusion). Its blood concentrations for preventing movement of 50% and 95% patients are 14.3μg/ml and 20.6μg/ml (Andrews et al., 1997). Its duration of clinical effect is short (Prassinos et al., 2005) because propofol is rapidly distributed into peripheral tissues, and its effects therefore wear off considerably within even a half hour of injection. Propofol binds to the extracellular end of the GABAa receptor, thus inducing a conformational change of the receptor (Bali and Akabas, 2004). Propofol also reduces the GABAr mediated righting reflex in rats (Sonner et al., 2003). It affects GABAa receptors in a concentration-dependent manner (Bali and Akabas, 2004). At low concentrations, it potentates sub-maximal GABA-induced currents,

while at higher concentrations, it opens the GABA-ligand channels directly in the absence of GABA. At even higher concentrations, it inhibits GABA mediated currents. In contrast to isoflurane, propofol does not suppress the sodium channels and NMDA receptors of neurons. Thus, it is suggested to cause less effects in evoked potential responses (Liu et al., 2005), such as the mfERG (Lalonde et al., 2006), than inhalation anesthetics at the same depth of anesthesia (Hans and Bonhomme, 2006).

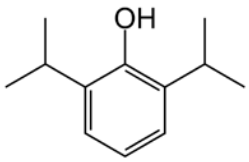

Figure 7.2.3. Propofol.

7.3. Parameters affecting retina physiology in *in-vitro* studies

In *in-vitro* studies, no matter how freshly it is isolated, the mammalian eye will suffer from a brief period of ischemia. Ischemia is a shortage of blood supply to tissue or organs, which may result in infarction of affected tissue or organs. In the present case, the reduced blood flow decreases oxygen and nutrient supply to eye. Impaired homeostasis and damage of the retina is resulted. The electrical retinal activity will be influenced according to nutrient and oxygen supply variations. In addition to the

changing supply of oxygen and nutrients to the retina, the core temperature of the eye is important. Moderate hypothermia has been reported to relieve ischemia and reperfusion injuries of the brain (Corbett and Thornhill, 2000) and retina (Wang et al., 2002). This is because hypothermia reduces oxygen demand of the tissues, the production of excitatory amino acids and reduces toxic nitric oxide synthesis (Miyazawa et al., 2003). Thus, standardization of the experimental parameters in *in-vitro* studies, such as perfusion flow rate, oxygen supply and temperature, is crucial for establishing a reproducible retinal model for physiology research.

Chapter 8 – Purpose of Investigation

The retinal electrophysiology of mammals has been studied for several decades and many *in-vivo* and *in-vitro* animal models have been proposed as alternative to human retina in physiology research. Although non-human primate is conventional accepted as the best alternative to human, ethical and legal issues prohibit to use non-human primate for physiology research in certain countries. To date, a major consensus is that porcine organs are suitable for physiology research and xenotransplantation. However, detailed evaluations that demonstrate the retinal origins of porcine mfERG and the possibilities of *in-vitro* porcine eye model are not yet available. In particular,

the alterations of mfERG induced by neural rewiring and anesthesia are not fully understood. Therefore, the aims of the present project are to:

(1) study the cellular origins of porcine mfERG *in-vivo* by use of pharmacological agents blocking specific retinal pathways.

(2) identify the alterations of porcine mfERG *in-vivo* by use of transgenic pig model with known retinal rewiring.

(3) study the cellular origins of porcine mfERG *in-vitro* by use of pharmacological agents blocking specific retinal pathways.

(4) identify the changes of porcine mfERG *in-vitro* by use of different anesthetic applications and different culture environmental parameters.

The findings from the present study could enhance our understanding of the retinal electrophysiology of the *in-vivo* porcine eye and its properties *in-vitro*.

PART II - EXPERIMENTS

Experiment I

Publication: Ng Y.F., Chan H.H.L., Chu P.H.W., Siu A.W., To C.H., Beale B.A., Gilger B.C., Wong F. (2008). Pharmacologically defined components of the normal porcine multifocal ERG. *Doc Ophthalmol 116:165-176.*

Chapter 9. Experiment I - Pharmacologically defined components of the normal porcine multifocal ERG

9.1. Abstract

Purpose:

To identify the contributions from inner retinal neurons, ON-pathway, OFF-pathway and photoreceptors to porcine mfERG.

Methods:

Multifocal electroretinograms (mfERG) from isoflurane anesthetized pigs were recorded and sequential application of TTX, NMDA, APB and PDA were used to identify contributions to the mfERG from inner retinal neurons, ON-pathway, OFF-pathway and photoreceptors.

Results:

For the first order kernel (K1) waveform, the n1 involved responses of cone photoreceptors and OFF-bipolar cells. The leading edge of p1 is dominated by ON-bipolar cell depolarization. The rear edge of p1, n2 and p2 are dominated by ON-

bipolar activities and shaped by the activities of OFF-bipolar cells and retinal cells with NMDAr and voltage gated sodium channels other than ganglion cells. The p3 is mainly inner retinal activities. For the first slice of the second order kernel (K2.1) waveform, the p1 and n1 are the summation of activities of ON-, OFF-bipolar cells and retinal cells rich in NMDAr and voltage gated sodium channels other than ganglion cells. The p2 seems to be related to the NMDA sensitive cell types other than ganglion cells.

Conclusion:

The cellular origins of the K1 and K2.1 porcine mfERG are contributed from both inner and outer retina. Better understanding of the cellular origins of the normal porcine mfERG will be useful for comparing and defining the functional changes that may occur in diseased retinas. In addition, this would help to understand the application of pig eye as a new animal model for eye research.

9.2. Introduction

In the experiment I, the pig mfERG was investigated and compared with the primate mfERG in order to understand the characteristic of pig retinal electrical response. The multifocal electroretinogram (mfERG) recordings obtained from primates before and after the injection of pharmacological agents with known effects in blocking the activities of specific neural circuits have identified and defined the contributions of specific retinal pathways in shaping the mfERG response (Hare and Ton, 2002; Hood et al., 2002). In addition, the analysis of the mfERG second-order kernels also helps to study the nonlinear characteristics of adaptation in retina (Baker and Hess, 1984; Hood, 2000). Adaptation in retina reflects underlying dynamic interactions of signaling sources, which reside in the synaptic wiring of neural circuits. Accordingly, alterations in the nonlinear characteristics of the mfERG may effectively identify changes in the retinal neural circuits of diseased eyes (Chan and Brown, 1999; Hood, 2000; Palmowski and Ruprecht, 2004; Chu et al., 2006).

The porcine eye is anatomically similar in size to the human eye (Chandler et al., 1999; Hendrickson and Hicks, 2002) and, compared to those of rodents, its retina is relatively cone photoreceptor-rich (Beauchemin, 1974; Gerke Jr et al., 1995; Chandler

et al., 1999). Its cone to rod ratio at the optic streak is very close to that of central retina in human. The color of the optic streak and fundus was orange to pale grey with pigmented epithelial cells which is very similar to human and there is no tapetum in porcine retina (Ollivier et al., 2004). Moreover, there is a porcine model of retinal degeneration in which synaptic rewiring is known to occur. Synaptic rewiring and remodeling in the retina are a reported phenomenon occurred in this animal model (Peng et al., 2000; Peng et al., 2003). Such events are expected to alter the retinal signal processing, which in turn lead to changes in visual function (Banin et al., 1999). All of these factors and circumstances make the pig an ideal large animal model for studying retinal functional changes. The experiment 1 reported herein was conducted to establish the retinal origins of the mfERG response and to investigate the nonlinear characteristics which reflect cellular interactions in the normal porcine retina.

9.3. Method

Animals:

Multifocal electroretinograms were obtained from 14 eyes of ten 6-week old Yorkshire swine. Prior to anesthesia, the animals were fasted for 12 hours. Initial anesthesia consisted of ketamine (20mg/kg IM) with xylazine (2mg/kg IV) and propofol (14-20mg/kg/hr IV). Pupils were dilated with topical tropicamide (1%), phenylephrine (10%) and anesthetized with topical proparacaine HCl (1%). After the collection of mfERG data under propofol, the anesthesia under propofol was ceased and isoflurane (ISO) (4%) in air was used to maintain anesthesia for the other parts of experiment. Artificial ventilation following orotracheal intubation was used to maintain the blood SpO_2 level at 95-100%. Throughout anesthesia, lactated Ringer's solution was administered IV and rectal temperature was maintained at 38-39°C using a circulating hot water heating pad and blanket. Heart rate and SpO_2 levels were also monitored throughout the experiment. All the experimental and animal handling procedures complied with the ARVO Statement for the Use of Animals in Ophthalmic and Vision Research and the institutional guidelines approved by North Carolina State University Institutional Animal Care and Use Committees and the Animal Ethics-subcommittee of The Hong Kong Polytechnic University.

Multifocal Electroretinography:

Grass subdermal F-E7 electrodes (Astro-med Inc; West Warwick) were placed subcutaneously at the rostrum and at the temporal canthus as ground and reference electrodes respectively. A monopolar ERG-jet contact lens electrode (Universal SA; La Chaux-de-Fons, Switzerland), as active electrode, was placed on the cornea with lubricant (Lacryvisc gel 0.3%, Alcon Cleveland, OH, USA). A stimulus pattern, consisted of 103 non-scaled white (160 cd/m^2) and black (1 cd/m^2) hexagons (Figure 9.1A) with a gray peripheral background (80 cd/m^2), for mfERG measurement was displayed on a 17" CRT monitor (s7540 CRT monitor, Hewlett-Packard; USA) with a refresh rate of 11.7 ms per frame. The mfERG stimulation was driven by VERIS (version 5.01) from EDI (Electro-Diagnostic-Imaging; San Mateo, CA, USA) according to a pseudo-random binary m-sequence of 2^{14}-1 (approximate 3.2 minutes recording). The retinal signals received were amplified (CP122 bench-top style amplifier, Grass Instruments Inc; Quincy, MA, USA) by a gain of 20,000 with a bandpass filter from 1 to 300 Hz. The signals were extracted and processed by the VERIS. Retinoscopy with the contact lens electrodes revealed +8 to +10D defocus at 20cm viewing distance and the defocus were corrected for the working distance.

To facilitate the control of ocular alignment and to prevent the drifting of ocular orientation during mfERG recording, two conjunctival sutures were placed approximately 2mm from superior and inferior limbal margins. Alignment of the eyeball to the stimulus pattern was facilitated by examination of localized traces presentation of mfERG responses from all hexagons. According to the localized traces of response, retinal features corresponding to optic nerve head and optic streak were identified as the legends for alignment (Figure 9.1B). After each intravitreal injection of drugs, the alignment of the eyeball to the stimulus pattern was verified again before mfERG measurement.

(A)

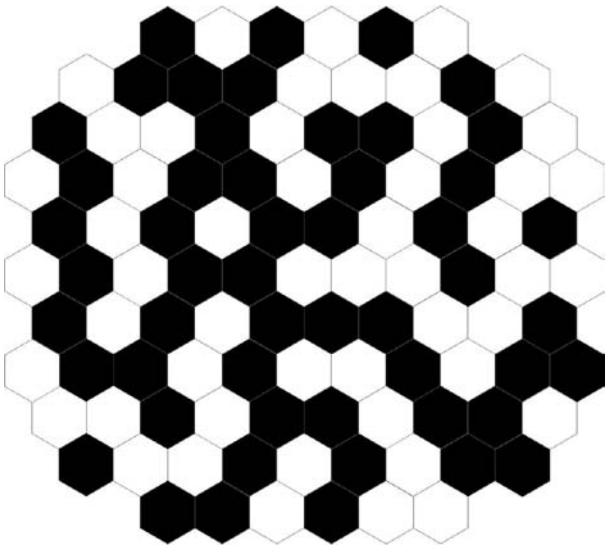

(B)

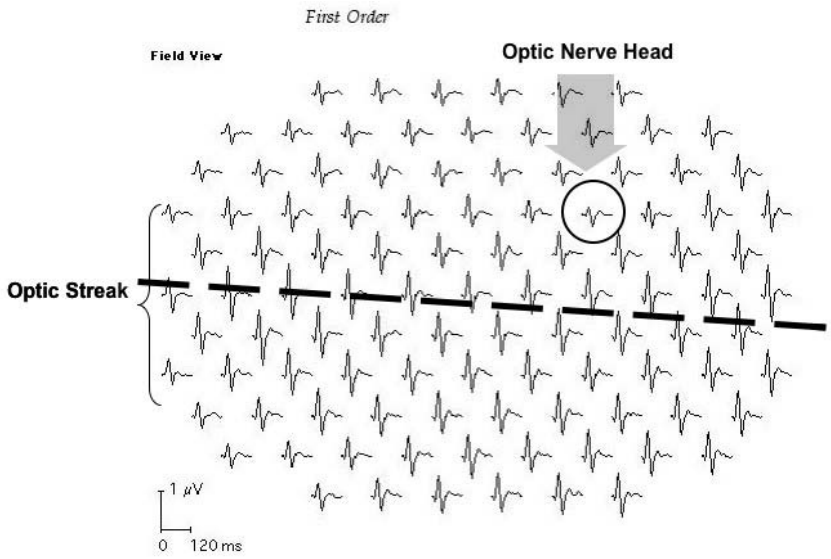

Figure 9.1. (A) 103 non-scaled hexagonal stimulus pattern of mfERG. (B) 1st order trace array of mfERG under propofol anesthesia from Pig #6. The location with the lowest response was the landmark of optic nerve head as reference point assisting alignment of stimulator.

Intravitreal Injections:

After acquisition of mfERG data in both propofol and isoflurane influenced conditions, pharmacological agents (all from Sigma-Aldrich; Missouri, USA)

including N-methyl-D-asparatic acid (NMDA), tetrodotoxin (TTX), 2-amino-4-phosphonobutyric acid (APB) and cis-2,3-piperidinedicarboylic acid (PDA) were administrated under the anesthesia of isoflurane. Using 28 gauge needles, 25ul of each medication was injected separately into vitreous, at 3mm above the superior limbus, to achieve 4mM, 5uM, 1mM and 3.5mM vitreal concentrations based on an estimated total vitreal volume of 2.0ml for each eye. The concentrations of pharmacological agents were sufficient in previous experiments in other animals (Frishman and Steinberg, 1990; Akdemir et al., 2001) and in pig (Chao et al., 1993; Lalonde et al., 2006) (Tremblay F, et al. IOVS 2005;46:ARVO E-Abstract 2247). All of these effects on the flash ERG were verified in preliminary data but not shown in this thesis. NMDA is an ionotropic glutamatergic receptor agonist that depolarizes cells with NMDA receptors (NMDAr), such as ganglion cells and amacrine cells. TTX is a voltage-gated sodium channel blocker that inhibits the voltage-gated sodium channel triggered action potential in the third order neurons, such as ganglion cells and amacrine cells. APB is a glutamate analogue that blocks signal transmission from photoreceptors to ON-bipolar cells. PDA is a glutamate analogue that blocks transmission from photoreceptors to OFF-bipolar cells and horizontal cells, and transmission from ON- and OFF-bipolar cells to ganglion cells and amacrine cells. Binocular indirect ophthalmoscopy was performed after conjunctival suturing and

each intravitreal injection to ensure the integrity of the retina. The mfERG was recorded approximately 90 minutes after administration of each drug. The NMDA and TTX were firstly injected to right and left eyes respectively for mfERG measurements and then TTX and NMDA were applied to another eye for another mfERG measurement. The sequence of injections of APB and PBA was the same. In some cases, porcine mfERG were re-recorded two days after injections of TTX and NMDA, and recovery of responses with normal mfERG waveform were noticed.

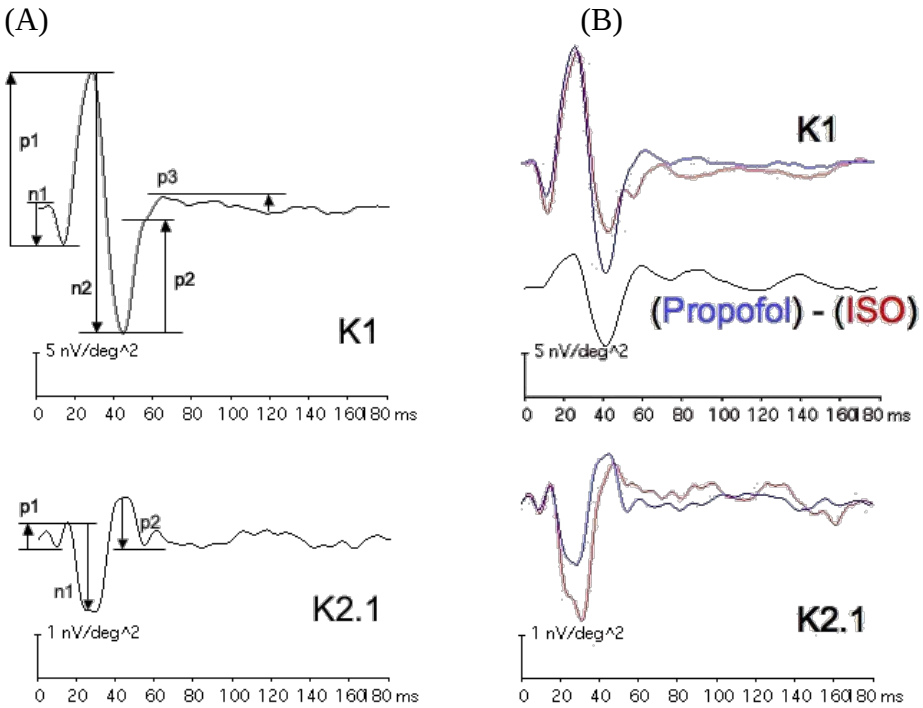

Figure 9.2. (A) First-order kernel (K1) waveform and second-order kernel first slice (K2.1) waveform of averaged mfERG from all porcine eyes under propofol anesthesia. (B) The K1 and K2.1 waveforms of averaged mfERG of both eyes from the same pig (Pig #3) under propofol (blue) and isoflurane (ISO, red) anesthesia. The dark trace is an estimate of ISO sensitive element in K1 response obtained by subtracting the red trace from the blue trace, by use of the VERIS system. It is a peak-trough-peak waveform.

Analysis:

The mfERG responses from 103 individual responses were grouped differently according to the regional response amplitude: those regions with p1 (peak-to-peak) amplitude up to the top 25 percentile were grouped as the response from optic streak, while the other regions (p1 amplitude not within the top 25 percentile) were grouped as the area outside optic streak. Amplitude and implicit time of the mfERG responses were measured. The response features are summarized in Figure 9.2A. The mfERG

data after the administration of propofol and isoflurane were compared. Then the data after the applications of NMDA, TTX and TTX+NMDA were compared with the baseline data under the anesthesia of isoflurane. Those responses under the anesthesia of isoflurane after administration of APB, PDA and APB+PDA under the effect of TTX+NMDA were compared with the data only under the TTX+NMDA. All of the comparisons were performed with repeated measures one-way ANOVA with Tukey post-hoc test.

9.4. Results

In this experiment, regions with p1 amplitude, up to the top 25 percentile, where showed the highest p1 amplitude in the topographical distribution, were grouped. The selection criterion was based on an assumption that, the p1 amplitude being proportional to the cone density of porcine retina and according to the findings reported by Gerke et al. (1995) and Chandler et al. (1999), the cone cell density of peripheral retina in porcine is less than 70% of the cone cell density of the optic streak. Except the response amplitude, the changes of mfERG waveform under effects of different pharmacological agents between the area of optic streak and the area outside optic streak were very similar, and this experiment, therefore, would focus to

report the variations of the mfERG at optic streak under different pharmacological applications.

Amplitude	n	1st order kernel (K1)					1st slice of 2nd order kernel (K2.1)		
		n1	p1	n2	p2	p3	p1	n1	p2
Propofol	14	4.89 (0.63)	22.24 (2.75)	32.92 (3.99)	16.89 (1.92)	3.78 (0.16)	0.93 (0.16)	2.93 (0.43)	2.08 (0.24)
ISO	14	6.27 (0.79)	19.30 (2.10)	21.99 (2.14)	**6.34 (0.90) *****	2.52 (0.38)	0.98 (0.22)	3.35 (0.36)	**1.03 (0.12) *****
ISO+NMDA	7	3.84 (0.82)	20.34 (4.47)	23.03 (5.67)	4.77 (1.02)	0.89 (0.23)	1.70 (0.66)	2.11 (0.66)	0.50 (0.13)
ISO+TTX	7	7.67 (1.05)	19.13 (2.82)	15.80 (2.39)	4.69 (0.94)	0.95 (0.34)	0.75 (0.22)	**1.37 (0.38) #**	1.23 (0.36)
ISO+TTX+NMDA	14	4.33 (1.24)	21.15 (3.08)	28.30 (4.37)	**12.74 (1.88) ##**	1.11 (0.25)	0.64 (0.25)	1.76 (0.52)	0.58 (0.09)
ISO+TTX+NMDA +APB	7	7.11 (0.88)	11.24 (1.26)	**6.76 (0.96) ^^**	**2.83 (0.67) ^^^**	0.43 (0.15)	0.36 (0.04)	0.94 (0.12)	0.74 (0.15)
ISO+TTX+NMDA +PDA	7	0.98 (0.30)	21.13 (3.78)	33.23 (5.67)	13.33 (1.64)	0.40 (0.08)	1.16 (0.54)	2.46 (1.05)	0.28 (0.04)
ISO+TTX+NMDA +APB+PDA	14	4.56 (0.76)	**5.81 (0.93) ^^^**	**1.82 (0.40) ^^^**	**0.89 (0.21) ^^^**	0.31 (0.06)	0.30 (0.09)	0.60 (0.06)	0.42 (0.07)

Table 9.1. Mean of amplitude (nV/degree^2) with SEM of mfERG features of 1st order kernel and 1st slice of 2nd order kernel traces at the optic streak area.

- *** ($p<0.001$) indicates significant difference from the mfERG under propofol anesthesia.
- # ($p<0.05$) and ## ($p<0.01$) indicate the level of significant difference from mfERG under isoflurane anesthesia.
- ^^ ($p<0.01$) and ^^^ ($p<0.001$) indicate levels of significant difference from the TTX+NMDA applied mfERG under isoflurane anesthesia.

Implicit time	n	1st order kernel (K1)					1st slice of 2nd order kernel (K2.1)		
		n1	p1	n2	p2	p3	p1	n1	p2
Propofol	14	12.37 (0.22)	27.07 (0.41)	43.18 (0.55)	56.98 (1.07)	69.98 (2.64)	14.32 (0.33)	25.71 (0.95)	41.57 (0.95)
ISO	14	13.01 (0.22)	28.61 (0.39)	43.84 (0.67)	**52.71 (0.39) ****	69.29 (1.52)	14.74 (0.31)	28.67 (0.99)	45.82 (1.09)
ISO+NMDA	7	13.76 (0.57)	28.56 (0.74)	44.20 (0.80)	53.87 (0.70)	77.29 (2.44)	**20.47 (1.38) ###**	**38.53 (1.54) ###**	**50.27 (1.08) ****
ISO+TTX	7	13.63 (0.40)	29.90 (0.33)	41.46 (1.12)	52.80 (0.57)	67.80 (2.50)	15.42 (0.57)	30.13 (0.64)	41.28 (2.14)
ISO+TTX+NMDA	14	12.93 (0.50)	26.76 (0.71)	43.08 (0.43)	54.98 (0.50)	74.55 (1.09)	**19.06 (0.63) ##**	30.80 (1.52)	47.07 (1.12)
ISO+TTX+NMDA +APB	7	**18.91 (0.79) ^^^**	**35.29 (0.58) ^^^**	**47.57 (0.94) ^**	**58.90 (0.98) ^**	80.33 (2.60)	**11.65 (2.19) ^^^**	**22.30 (3.53) ^**	**39.58 (2.89) ^**
ISO+TTX+NMDA +PDA	7	**8.83 (0.47) ^**	26.22 (0.87)	43.97 (0.82)	**59.28 (1.11) ^**	82.36 (3.97)	19.7 (1.28)	36.76 (1.11)	50.60 (3.10)
ISO+TTX+NMDA +APB+PDA	14	**24.68 (1.31) ^^^**	**42.80 (2.20) ^^^**	**51.74 (1.81) ^^^**	**61.67 (1.18) ^^^**	79.74 (2.42)	**11.85 (1.02) ^^^**	**22.60 (2.48) ^**	**40.50 (1.84) ^**

Table 9.2. Mean of implicit time (ms) with SEM of mfERG features from optic streak at 1st order kernel and 1st slice of 2nd order kernel traces.

- ** ($p<0.01$) indicates significant difference from the mfERG under propofol anesthesia.
- ## ($p<0.01$) and ### ($p<0.001$) indicate the level of significant difference from mfERG under isoflurane anesthesia.
- ^ ($p<0.05$), ^^ ($p<0.01$) and ^^^ ($p<0.001$) indicate levels of significant difference from the TTX+NMDA applied mfERG under isoflurane anesthesia.

The influence of ISO:

The first and second order kernel responses of mfERG at optic streak from porcine retina under two different anesthetics were shown in Figure 9.2B and the amplitudes and implicit times were listed in Table 9.1 and 9.2. There were some observable changes in the waveform of K1 and K2.1 under the influence of ISO. The n2, p2 and p3 of K1 showed different reductions of amplitude under ISO, but only p2 was statistically significantly diminished ($p<0.001$) and delayed ($p<0.01$). The n1 and p2 of K2.1 also showed different amplitude reductions but only p2 had a significant change ($p<0.001$).

(A)

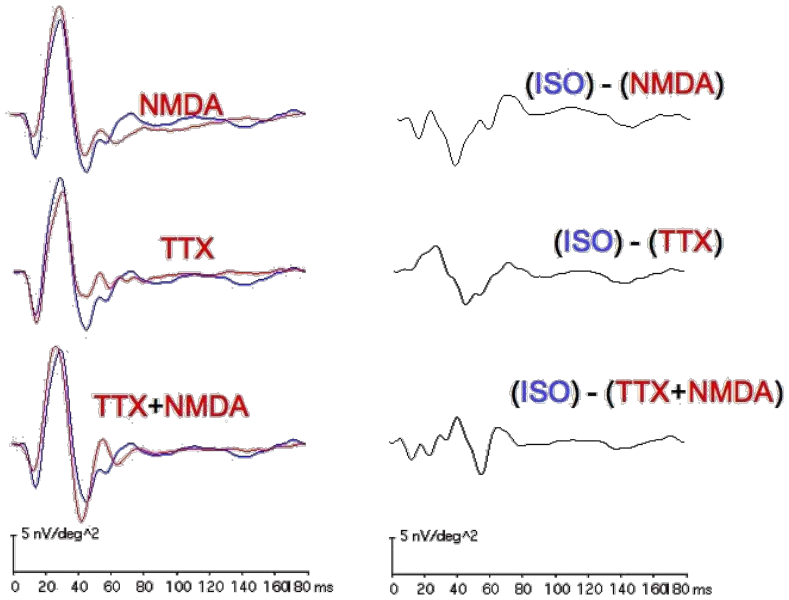

(B)

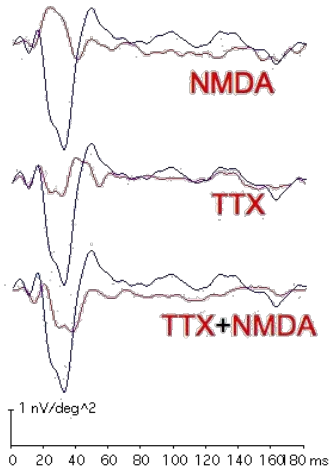

Figure 9.3. (A) The left column shows K1 waveforms of averaged mfERG under effect of NMDA, TTX and TTX+NMDA (red traces) with isoflurane anesthesia (blue trace). They are grouped responses from optic streak. The right column shows the estimates of NMDA, TTX and TTX+NMDA sensitive elements of K1 response (dark traces). The subtraction of waveform was performed by the VERIS software. They are all peak-trough-peak waveforms with similar second corneal-positive component at 60 ms. There are variations in those isolated between 20 ms to 60 ms. (B) K2.1 waveforms of averaged mfERG under effect of NMDA, TTX and TTX+NMDA (red traces) with isoflurane anesthesia (blue trace). They are grouped responses from optic streak. The traces under the effect of ISO, and TTX+NMDA were the averages of both eyes from one of the subjects (Pig #3). The traces under TTX and under NMDA

were from the right eye and the left eye of Pig #3 respectively.

The influence of TTX and NMDA:

Figure 9.3A shows the traces of the first-order kernel (K1) before and after the application of different combinations of pharmacological drugs under the anesthesia of ISO. The amplitudes and implicit times of mfERG traces are summarized in Table 9.1 and 9.2.

There were some observable changes in the waveform of K1 under the influence of TTX and NMDA, although there were no significant changes in amplitude or implicit time of n1, p1, n2, p2 and p3. The NMDA application reduced the amplitude of n1. It also reduced the amplitude and increased the implicit time of p3. The TTX application reduced the amplitude of n2 and p3. The TTX+NMDA application significantly increased the amplitude and implicit time of p2 ($p<0.01$). It also caused an observed amplitude reduction of n1, p1, p3, and an observed increase in amplitude and implicit time of n2, but none of them showed any statistical significance.

Temporal interaction of retinal responses is reflected by the first slice of the second-order kernel (K2.1) traces. Figure 9.3B shows the K2.1 waveforms before and after the application of pharmacological agents. The NMDA application caused an

observed rise of the p1 amplitude and reduction of n2 and p2 amplitude. It increased the implicit time of p1 ($p<0.001$), n2 ($p<0.001$) and p2 ($p<0.01$) significantly. The TTX application significantly decreased the amplitude of n1 ($p<0.05$) but no observed changes in the amplitude of p1 and p2. The TTX+NMDA caused a significant increase of the p1 implicit time ($p<0.01$). Although there were no significant changes of n1 and p2, an increase in n1 implicit time and reduced amplitudes of n1 and p2 were observed.

(A)

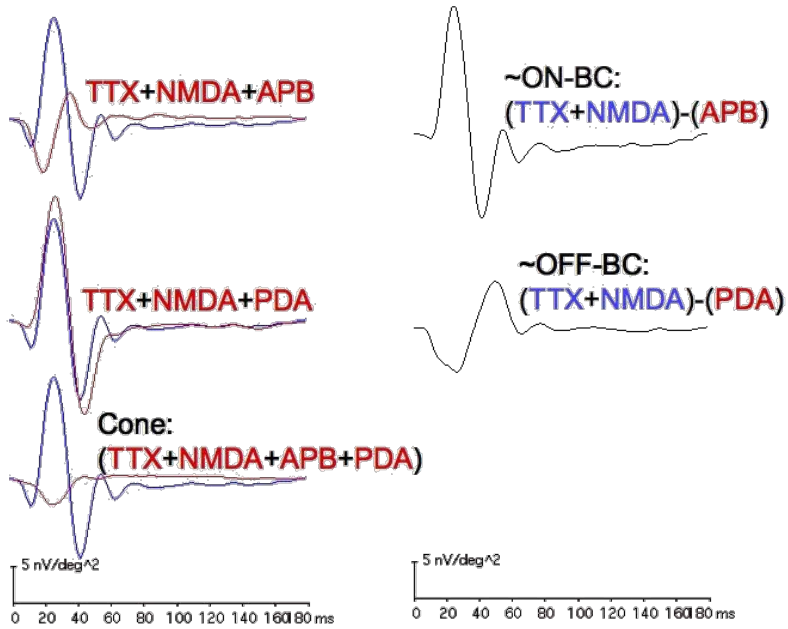

(B)

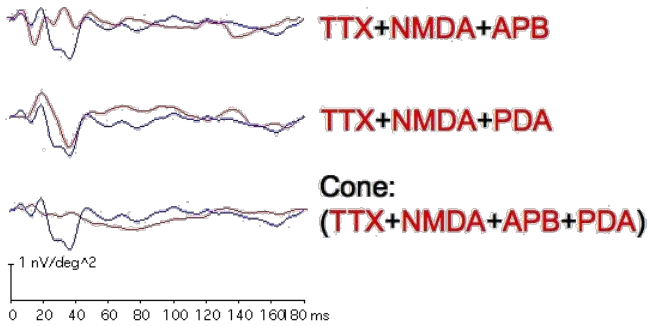

Figure 9.4. (A) The left column shows K1 waveforms of averaged mfERG under effect of APB, PDA and APB+PDA (red traces) with pre-administration of TTX+NMDA and isoflurane anesthesia (blue trace). They are grouped responses from optic streak. The bottom red trace of K1 waveform under APB+PDA is the estimate of cone photoreceptor contribution after elimination of ON- and OFF-bipolar contributions. The right column shows the estimates of ON-bipolar contributions isolated by APB (upper dark trace), and OFF-bipolar contributions isolated by PDA (lower dark trace). The subtraction of waveform was performed by the VERIS software. (B) K2.1 waveforms of averaged mfERG under effect of APB, PDA and APB+PDA (red traces) with pre-administration of TTX+NMDA and isoflurane anesthesia (blue trace). They are grouped responses from optic streak. The traces under the effect of TTX+NMDA, and APB+PDA were the averages of both eyes from

Pig #3. The traces under APB and under PDA were from the right eye and the left eye of Pig #3 respectively.

The influence of APB and PDA:

Figure 9.4A shows the K1 waveforms with TTX+NMDA under the anesthesia of ISO after the injections of APB and PDA. Amplitude and implicit time of the resultant waveforms after the application of APB and PDA are summarized in Tables 9.1 and 9.2. The APB application significantly reduced the amplitude of n2 ($p<0.01$) and p2 ($p<0.001$). It also delayed the implicit time of n1 ($p<0.001$), p1 ($p<0.001$), n2 ($p<0.05$) and p2 ($p<0.05$) significantly. The PDA significantly shortened the implicit time of n1 ($p<0.05$) and lengthened that of p2 ($p<0.05$). The application of APB+PDA reduced the amplitude of p1 ($p<0.001$), n2 ($p<0.001$) and p2 ($p<0.001$) significantly. It also significantly delayed the n1 ($p<0.001$), p1 ($p<0.001$), n2 ($p<0.001$) and p2 ($p<0.001$).

For the K2.1 traces, Figure 9.4B shows that APB and APB+PDA applications caused an observed reduction of the amplitude of p1 and n1, but the PDA application caused an observed increase of the amplitude of p1 and n1. However, all of changes were not statistically significant. Both APB and APB+PDA applications shortened the implicit time of p1 ($p<0.001$), n1 ($p<0.05$) and p2 ($p<0.05$) significantly.

9.5. Discussion

From the findings, both first order kernel (K1) and first slice of the second order kernel (K2.1) responses of the porcine mfERG contained components from both inner and outer retina.

Anesthesia:

The animals were initially anesthetized by propofol, which was suggested to have a minimal influence on evoked potentials monitoring in human surgery (Hans and Bonhomme, 2006). From the findings, the porcine mfERG under propofol anesthesia (Figure 9.2B) was similar to that under ketamine anesthesia reported from the study of Lalonde et al.(2006), but the p2 and p3 of K1 were overlapping. It may be due to the faster frame rate of stimulation used in this experiment.

In order to facilitate prolonged anesthesia, inhalation anesthesia such as isoflurane (ISO) was conventionally recommended in veterinary medicine, because of the hypotension and transient apnea experienced in long term usage of propofol. According to the study of Lalonde et al.(2006), ISO would mimic the effect of optic

nerve section in porcine mfERG with the p3 largely reduced in K1 waveform. Therefore, the ISO was also used as the agent to remove the inner retinal activity. In Figure 9.2B, the ISO reduced both p2 and p3 in K1 waveform, as well as the p2 in K2.1 waveform. However, the effect of ISO in this experiment was slightly different from the study of Lalonde et al. (2006). The difference of less reduction of p3 in this experiment might be caused by the difference in genetic background of pigs and the faster frame rate of stimulation. The dark trace in Figure 9.2B shows the ISO sensitive element in K1 obtained by subtracting the trace under ISO from that under propofol. It is a peak-trough-peak waveform with a corneal-positive component around 20 ms (approximate at p1), a corneal-negative component around 40 ms (approximate at n2) and a corneal-positive component around 60 ms (approximate at p3). Although the mechanisms of propofol and ISO anesthesia were not fully understood, propofol and ISO both reduce GABAr mediated righting reflex in rats (Sonner et al., 2003). The difference between propofol and ISO may be due to some additional properties of ISO, such as suppression of NMDAr mediated response (Ueno et al., 1999; Cheng and Kendig, 2003) and partial suppression of sodium current (Duch et al., 1998) in central nervous system. Since the ISO, in this study, could not completely remove the p3, the inner retinal activities might not be fully inhibited or removed, and hence the additional applications of TTX and NMDA were used in this experiment.

Contribution from Inner Retina:

To examine the inner retinal activities in porcine mfERG, apart from ISO, NMDA and TTX (TTX+NMDA) were injected. They are commonly used to eliminate inner retinal activities in animal studies (Bush and Sieving, 1996; Hood, 2000; Dong and Hare, 2002; Lalonde et al., 2006). Although retinal bipolar cells usually do not fire action potentials (Lukasiewicz, 2005) and propagate electrical signals passively along the dendrites, voltage-dependent sodium current has been reported in subset of retinal bipolar cells of rat (Pan and Hu, 2000) and goldfish (Zenisek et al., 2001). TTX was reported to reduce but not to totally remove the transient ON-bipolar cell light response (Ichinose et al., 2005). In contrast, the sustained ON-bipolar cell response and the photoreceptor input to bipolar cells were not affected (Ichinose et al., 2005). Thus, the TTX-sensitive component is only partially involved in the outer retinal activities, and the majority of the TTX-sensitive component is contributed in the inner retinal activities. From the findings of K1 waveform (Figure 9.3A, left / bottom), the p2 was increased and the p3 was reduced and delayed. In K2.1 waveform (Figure 9.3B), the n1 and p2 were reduced and delayed. The partially reduction of K2.1 in the porcine mfERG was consistent with the findings of Hood (2002) and Hare and Ton (2002) using TTX+NMDA in monkeys. The above findings clearly showed the K2.1

in porcine mfERG largely contributed by the inner retinal activities, but also partially contributed by the outer retina. The bottom dark trace in Figure 9.3A (right) shows the TTX+NMDA sensitive element in K1 obtained by subtracting the trace under TTX+NMDA from that under ISO. It is also a peak-trough-peak waveform with a corneal-positive component around 40 ms (approximate at n2), a corneal-negative component around 55 ms (approximate at p2) and a corneal-positive component around 65 ms (approximate at p3). These showed that the inner retinal activity is mainly contributed to the p3 of K1 and the p2 of K2.1.

Conventionally, NMDA was employed to remove the rest of inner retinal activities that cannot be inhibited by TTX (Bush and Sieving, 1996; Hood, 2000; Dong and Hare, 2002; Lalonde et al., 2006). In order to verify whether there is difference in the influence caused by NMDA and TTX in porcine mfERG, mfERGs were recorded individually under NMDA and TTX before the second injection of each others. The p3 in K1 waveform was reduced and delayed under NMDA (Figure 9.3B (left top)). For K2.1 waveform, the p1 was delayed and increased; while the n2 and p2 were both delayed and reduced. But the n2 and p3 in K1 waveform and the n1 in K2.1 waveform were reduced under TTX (Figure 9.3B (left middle)).

The NMDA and TTX shared some common influence in porcine mfERG. Figure 9.3B (right) shows both NMDA sensitive element and TTX sensitive element in K1 response with a corneal-positive component at around 65 ms (approximate at p3) which is similar to that in TTX+NMDA sensitive element. Since the loss of p3 in porcine K1 waveform was demonstrated by optic nerve section (Lalonde et al., 2006) and the loss of the second corneal-positive component in the isolated peak-trough-peak inner retinal contribution of glaucomatous monkeys (Raz et al., 2002), the second corneal-positive components in those isolated waveforms were likely to be originated by the downstream of signal propagation, such as ganglion cells.

There is difference in those NMDA, TTX and TTX+NMDA sensitive elements before 60 ms in K1 waveform. The first corneal-positive component and corneal-negative component of the NMDA sensitive element started earlier than that of TTX and TTX+NMDA sensitive elements. In between 20 ms and 60 ms, the NMDA sensitive element has a phase shift with TTX sensitive element and it is in anti-phase with the TTX+NMDA sensitive element. The target cells or target elements of NMDA and TTX are expected to be different. NMDA as glutamate receptor agonist will excite, modulate or saturate the NMDAr in post-synaptic membrane. Thus, the physiological NMDAr dependent electrical activities would be masked. The excitabilities of those

neurons processing NMDAr would be provoked. In turn, the firing of action potential will be enhanced. Although there is no proof of the speculation, in K2.1 waveforms (Figure 9.3B (top)), the administration of NMDA caused an enhanced p1, which was blocked by co-administration of TTX. Thus the corneal-negative component of NMDA sensitive element in K1 between 20 ms and 60 ms would be originated from retinal elements rich with NMDAr and voltage gated sodium channels other than ganglion cells.

Contribution from Outer Retina:

The porcine mfERG response has dominated ON-pathway and OFF-pathway components with a smaller contribution from the photoreceptors. After the pharmacological removal of most inner retinal activities, the contributions from major cell types, such as ON- and OFF- bipolar cells and cone cells, can be observed more easily.

The K1 waveform of TTX+NMDA is mainly a summated contribution from ON- and OFF-bipolar cell pathways. APB application caused a delay in the K1 waveform with an enhancement on the n1 component and suppression on the p1 and n2 components.

(Figure 9.4A (left top)) PDA application, also demonstrated a fast-depolarized p1 component with a large hyperpolarized n2 component. (Figure 9.4A (left middle)) By using the method of subtraction, the contributions of ON- and OFF-pathways in porcine mfERG response can be estimated. The resultant APB-sensitive waveform shown in Figure 9.4A (right top) is an estimated contribution of ON-bipolar cell pathway to the K1 response. There is a large depolarization at 20 ms followed by a corneal-negative component at 40 ms and a small corneal-positive component at 55-60 ms. All of these components approximately occurred at the time course of p1, n2 and p2 of the control K1 waveform. The resultant PDA-sensitive waveform shown in Figure 9.4A (right bottom) is an estimated contribution of OFF-bipolar cell pathway to the K1 response and it is an exaggerated corneal-negative component followed by a corneal-positive component at about 55 ms which is at the time course of p2. The estimated contributions from the ON- and OFF-pathway activities in K1 waveform are in opposite natures. This demonstrates the antagonistic nature between ON- and OFF-pathways. After the combined application of APB+PDA, there was only a small corneal-negative component at about 25 ms and it is similar to the findings of other studies using primates (Hare and Ton, 2002; Hood et al., 2002). This small corneal-negative component is most likely from the cone photoreceptors.

The K2.1 waveform after the TTX+NMDA application involved contribution from the ON- and OFF-bipolar cell pathways and/or the residual inner retinal activities which is not blocked by the effect of ISO and TTX+NMDA (Hood et al., 2002). Under the effect of APB, there was no conspicuous K2.1 feature resembling the features of control K2.1 waveform and those with TTX+NMDA application. This is consistent with the assumption of K2.1 receiving its main contribution from the inner retinal activities. Interestingly, the applications of PDA caused a positive feature of K2.1 at 20 ms and a negative tough at about 40 ms in the optic streak region but this was not so obvious in the outside-streak region. It is similar to the mfERG waveform of monkeys after PDA application (Hare and Ton, 2002). It seems that blocking OFF-pathway activity may unveil a contribution of ON-pathway activity likely masked by the OFF-pathway in K2.1. This also shows that both ON- and OFF-pathways contribute to K2.1 in different ways. It is further complicated if the combination of ISO+TTX+NMDA cannot totally block all the inner retinal activities because PDA also blocks some synaptic transmissions from bipolar cells to ganglion cells and amacrine cells. There may involve some residual PDA-sensitive inner retinal activity that is not eliminated by ISO+TTX+NMDA and this residual activity influenced the contribution of ON-pathway activity to the K2.1 response.

The outer retinal contribution is mainly a summated result from both ON- and OFF-bipolar cell pathway activities. For the K1 waveform, the n1 is dominated by OFF-bipolar cells activities and partially contributed by the corneal-negative component of cone cells. The p1 and n2 are dominated by the ON-bipolar cell pathway activities and the p2 is a combined effect of the ON- and OFF-bipolar cell pathway activities. For the K2.1 response, it seems to have some contributions from both ON- and OFF-bipolar cell pathway activities.

The possible cellular origins of the K1 and K2.1 porcine mfERG are contributed from both inner and outer retina. For the K1 waveform, the n1 involved responses of cone photoreceptors and OFF-bipolar cells. The leading edge of p1 is dominated by ON-bipolar cell corneal-positive component. The rear edge of p1, n2 and p2 are dominated by ON-bipolar activities and shaped by the activities of OFF-bipolar cells and those retinal cells rich in NMDAr and voltage gated sodium channels other than the ganglion cells. The p3 is mainly ganglion cell activities. For the K2.1 waveform, the p1 and n1 are the summation of activities of ON-, OFF-bipolar cells and those retinal cells rich in NMDAr and voltage gated sodium channels other than the ganglion cells. The p2 is the NMDAr activities.

There are similarities and differences among porcine and monkey mfERGs. In their mfERGs, the K1 waveforms were similar in general. However, the double-peak feature of monkey mfERG (Hood et al., 2002) was not observed in porcine mfERG. Although both showed n2 and p2 following the p1 (Hare and Ton, 2002), the p2 implicit time of monkey mfERG was shorter than that of porcine mfERG. The TTX, PDA and APB sensitive elements in K1 were similar in waveforms in both porcine and monkey mfERGs (Hare and Ton, 2002; Hood et al., 2002), although the oscillations of the TTX-sensitive element from monkey were not observed in porcine mfERG. But this kind of oscillations was also not observed in human mfERG. Thus the porcine mfERG may be another viable alternative for retinal physiological studies.

Finally, care should be taken when comparing porcine and primate mfERGs, because of the structural differences in retina, such as the photoreceptors and ganglion cells distribution. On the other hand, by the understanding of the waveform properties of porcine mfERG under various pharmacological agents, the changes of retinal signal processing in porcine disease eye model with synaptic re-wiring, can be investigated to study whether the pig eye is a good alternative for retinal physiological studies.

Experiment II

Ng Y.F., Chan H.H.L., Chu P.H.W., To C.H., Beale B.A., Gilger B.C., Petters R.M., Wong F. (2008). Multifocal Electroretinogram in Rhodopsin P347L Transgenic Pigs.

Invest Ophthalmol Vis Sci 49:2208-2215.

Chapter 10. Experiment II - Multifocal Electroretinogram in Rhodopsin P347L Transgenic Pigs

10.1. Abstract

Purpose:

Neural ectopic re-wiring in retinal degeneration such as retinitis pigmentosa (RP) may form functional synapses between cones and rod bipolar cells which cause atypical signal processing. In this experiment, the multifocal electroretinograms (mfERG) of a large animal model of RP, the rhodopsin P347L transgenic pig (Tg), were measured to examine the sources and nature of altered signal processing.

Methods:

MfERG responses from 6-week old Tg were recorded before and after sequential application of TTX, NMDA, APB and PDA to identify contributions to the retinal signal from inner retinal neurons, the ON-pathway, the OFF-pathway and photoreceptors. The mfERG response contributions from different retinal components of Tg were estimated and compared with control data from age-matched wild-type

(WT) pigs.

Results:

There was a prominent difference in the estimates of inner retinal response and ON-bipolar cell pathway contribution between the Tg and WT mfERG responses. In particular, the early components of the inner retinal contribution were obviously altered in Tg mfERG; the inner retinal components at about 24 and 40ms appeared to be inverted. Differences in the estimates of OFF-bipolar cell pathway contributions were minimal. There was no change of cone cell responses in Tg mfERG.

Conclusion:

In Tg pigs, ectopic synapses formed between cones and rod bipolar cells probably altered signal processing of the ON-bipolar cell pathway. In response to the altered visual signal input from outer retina, signal processing in inner retinal neurons was also modified.

10.2. Introduction

In the previous experiment, the characteristics and origins of mfERG in normal pig eye were investigated and had better understanding. In the experiment II, a pig model with retinal disease was selected to investigate whether the pig eye is a good alternative for retinal physiological studies. Photoreceptor cell death is common in many retinal diseases, such as age-related macular degeneration (ARMD), Stargardt's disease, Leber's congenital amaurosis and retinitis pigmentosa (RP). Different animal models have been developed to study these retinal diseases (Petters et al., 1997; Narfstrom et al., 2001; Chader, 2002; Koenekoop, 2004), and histological evidence of neural rewiring and ectopic synaptogenesis (involving surviving photoreceptors and bipolar cells) concomitant with, or following, photoreceptor cell death has been reported. Ectopic synaptogenesis occurs in the degeneration of rods (Peng et al., 2000; Peng et al., 2003; Johnson et al., 2006; Gargini et al., 2007) and cones (Haverkamp et al., 2006; Sullivan et al., 2007), and in the absence of rods during development (Strettoi et al., 2004; Johnson et al., 2006). In the current experiment, the retinal response alterations in a model known to have ectopic synapses between surviving cones and rod bipolar cells was investigated.

When the visual signal is transmitted from the outer plexiform layer to the inner retina via ectopic synapses, a different inner retinal response due to the altered visual input might occur. Thus an electrophysiological method can be applied to examine changes in response of photoreceptors, bipolar cell pathways and inner retinal neurons.

The multifocal electroretinogram (mfERG) can measure responses from multiple retinal regions (Sutter and Tran, 1992). Multifocal ERG recordings have been used to identify the contributions of different retinal pathways to the response in primates (Hare and Ton, 2002; Hood et al., 2002). This strategy has been adopted to define the retinal signal contributions of different retinal pathways of wild type pigs in experiment 1 (Ng et al., 2008b).

In this experiment, the mfERG changes were measured in the P347L transgenic pig (Tg), which is a large animal model known to have ectopic synaptogenesis between cones and rod bipolar cells (Peng et al., 2000) and altered retinal electrical response (Banin et al., 1999). The ectopic synaptic connection between rod-bipolar cells and cone pedicles is expected to alter the physiology of the outer retina and to affect signal processing in the inner retina. Although the mfERG theoretically provides information only on cone pathways, it is believed that the signal processing in the

cone pathway will be altered because of ectopic synaptogenesis involving both rod and cone pathways (Peng et al., 2000; Peng et al., 2003).

10.3. Method

The mfERG of the transgenic pig (Tg) and wild type pig (WT) were compared. The retinal cellular contribution of the wild type porcine mfERG has been published and shown in experiment 1 (Ng et al., 2008b) and the data of the WT mfERG has been used in this experiment to compare with the findings of Tg mfERG. The applications of pharmacological agents known to block activities of specific neural circuits have identified and defined the contributions of specific retinal pathways in shaping the mfERG response (Hare and Ton, 2002; Hood et al., 2002; Ng et al., 2008b). The pharmacological agents used include: isoflurane (ISO), N-methyl-D-asparatic acid (NMDA), tetrodotoxin (TTX), 2-amino-4-phosphonobutyric acid (APB) and cis-2,3-piperidinedicarboylic acid (PDA). The activities of different retinal cell types of WT was presented in experiment 1 (Ng et al., 2008b) by application of different combinations of those pharmacological agents. The combined application of ISO+TTX+NMDA essentially eliminates the activities of inner retinal neurons. Application of APB after ISO+TTX+NMDA also inhibits ON-bipolar pathway

activity and the application of PDA after ISO+TTX+NMDA inhibits OFF-bipolar pathway activity in the retina. The application of ISO+TTX+NMDA+APB+PDA inhibits most of the activity of retinal cell types except the photoreceptor response to light stimulation. By subtraction of responses measured under these various conditions, the responses of photoreceptors, outer retina, inner retina and ON- and OFF-bipolar pathways can be estimated. The differences of retinal activities of Tg and WT were investigated in this experiment.

Animals:

Multifocal electroretinograms were obtained from 16 eyes of eight 6-week old transgenic (Tg) Yorkshire pigs. The normal pig data used for comparison were obtained from 14 eyes of ten 6-week old wild-type Yorkshire pigs. Prior to anesthesia, the animals were fasted for 12 hours and initial anesthesia consisted of ketamine (20mg/kg IM) with xylazine (2mg/kg IV) and propofol (14-20mg/kg/hr IV). Pupils were dilated with topical tropicamide (1%) and phenylephrine (10%); the cornea was anesthetized with topical proparacaine HCl (1%). After the collection of mfERG control data, propofol anesthesia was replaced by isoflurane (ISO) (4%) in air for the other parts of the experiment. The use of ISO anesthetic is the standard method used in the veterinary surgical procedures and ISO is suitable for prolonged anesthetic in

large animals. Artificial ventilation following orotracheal intubation was used to maintain the blood SpO_2 level at 95-100%; heart rate was monitored throughout the experiment. Throughout anesthesia, lactated Ringer's solution was administered IV and rectal temperature was maintained at 38-39°C using a circulating hot water heating pad and blanket. All experimental and animal handling procedures complied with the ARVO Statement for the Use of Animals in Ophthalmic and Vision Research, as well as the institutional guidelines approved by North Carolina State University Institutional Animal Care and Use Committees, and the Animal Ethics-subcommittee of The Hong Kong Polytechnic University.

Multifocal Electroretinogram:

Two Grass subdermal F-E7 electrodes (Astro-med Inc; West Warwick, RI) were placed subcutaneously at the temporal canthus and at the rostrum as reference and ground electrodes respectively. An ERG-jet contact lens monopolar electrode (Universal SA; La Chaux-de-Fons, Switzerland) was placed on the cornea with Lacryvisc lubricant gel (0.3%, Alcon; Cleveland, OH) as active electrode. A stimulus pattern, with 103 non-scaled white (160 cd/m^2) and black (1 cd/m^2) hexagons (Figure 10.1B) and a grey peripheral background (80 cd/m^2), was displayed on a 17" CRT monitor (Model s7540, Hewlett-Packard; Palo Alto, CA) with a refresh rate of 85 Hz

(11.7 ms per frame) for mfERG measurement. The mfERG stimulation was driven by VERIS 5.01 software (Electro-Diagnostic-Imaging; San Mateo, CA) according to a pseudo-random binary m-sequence of 2^{14}-1, providing 3.2 minutes of recording, which is sufficient to minimize random noise (Sutter and Tran, 1992). The signals generated were amplified (Grass Model CP122, Astro-med Inc; West Warwick, RI) with a gain of 20,000 and bandpass from 1 to 300 Hz before processing by the VERIS system. This experiment would focus on the first order kernel responses, not the second order kernel responses, because the K1 results have been reported to include both inner and outer retinal activity (Hare and Ton, 2002; Hood et al., 2002) and this would be sufficient to investigate the alteration of retinal signals in the Tg pigs.

(A)

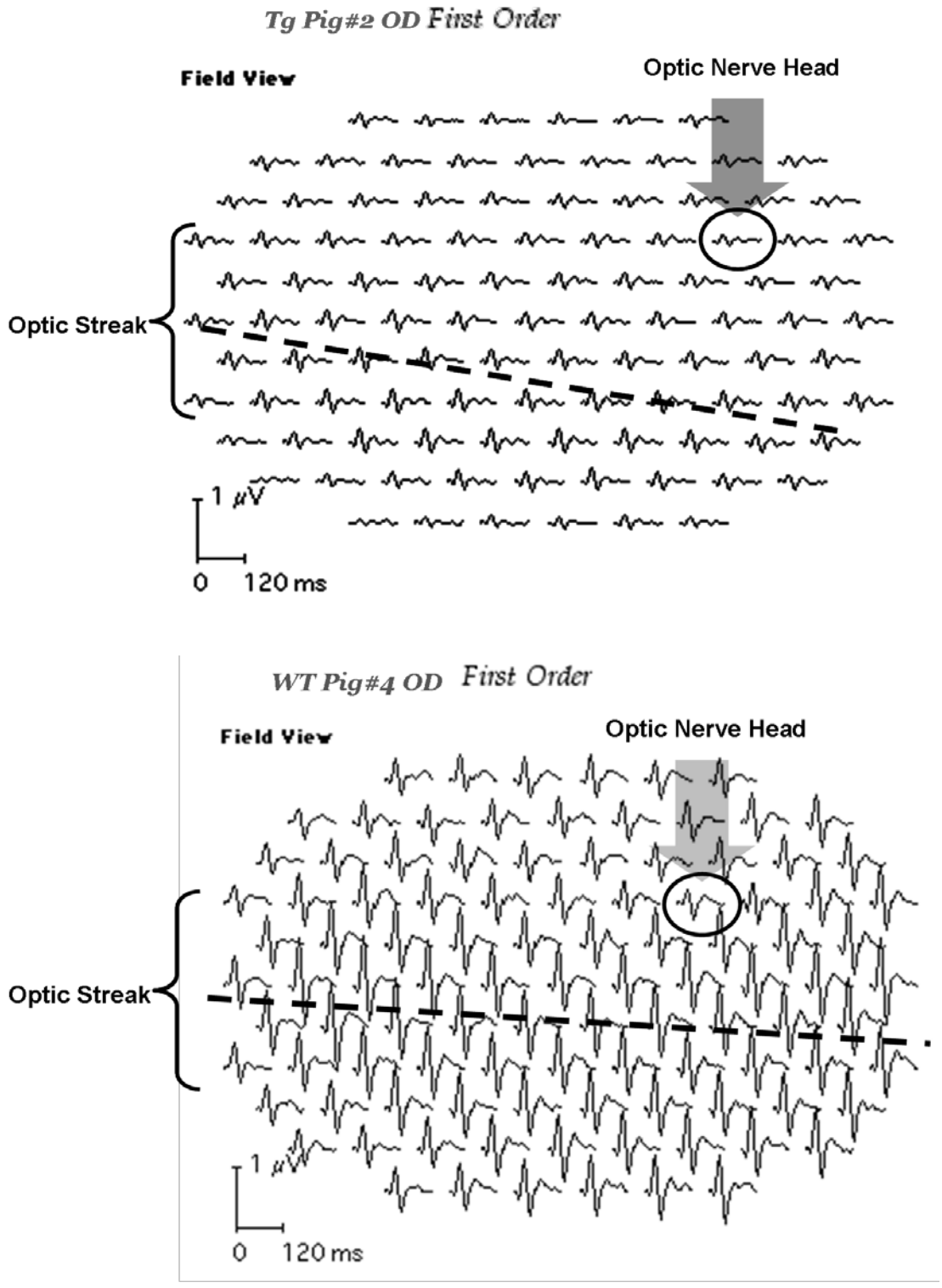
Tg Pig#2 OD First Order
Field View
Optic Nerve Head
Optic Streak
1 μV
0
120 ms
WT Pig#4 OD First Order
Field View
Optic Nerve Head
Optic Streak
1 μV
0
120 ms

(B)

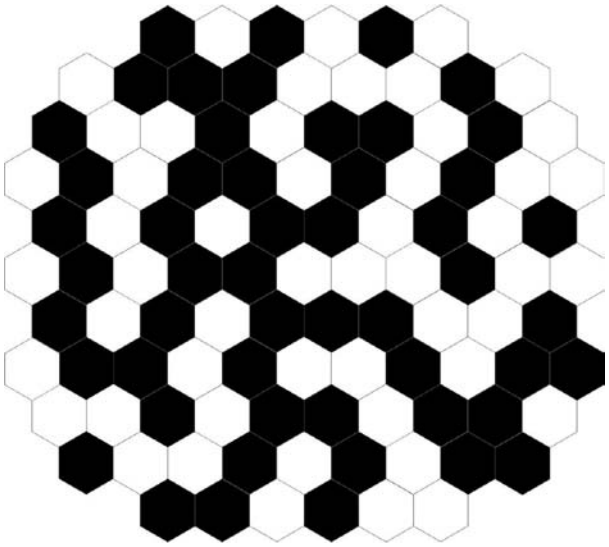

(C)

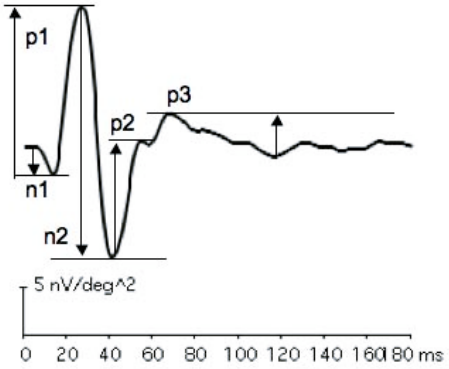

Figure 10.1. (A) 1st order trace array of mfERG under propofol anesthesia from Tg Pig#2 right eye and WT Pig #4 right eye. The location with the lowest response was the landmark of optic nerve head as the reference point assisting alignment of stimulator. (B) 103 non-scaled hexagonal stimulus pattern of mfERG. (C) First-order kernel (K1) waveform of averaged mfERG from right eye of WT Pig#4 under propofol anesthesia.

To control ocular alignment and prevent drift of ocular orientation during mfERG recording, two conjunctival sutures were placed approximately 2 mm from superior and inferior limbal margins. Alignment of the eyeball to the stimulus pattern was facilitated by using the trace arrays of localized mfERG responses; retinal features, such as optic nerve head and optic streak, were identified as the basis for alignment (Figure 10.1A). The alignment of the eyeball to the stimulus pattern was checked after each intravitreal drug injection. Refractive error was corrected using ophthalmic lenses placed in front of the eye under test after retinoscopy had been performed with the contact lens electrode in place.

Intravitreal Injections:

After acquisition of mfERG data under propofol and isoflurane, pharmacological agents (all from Sigma-Aldrich; Missouri, USA) including N-methyl-D-asparatic acid (NMDA), tetrodotoxin (TTX), 2-amino-4-phosphonobutyric acid (APB) and cis-2,3-piperidinedicarboylic acid (PDA) were administrated under isoflurane anesthesia; 25ul of each agent was injected (using 28-gauge needles) separately into the vitreous, 3mm above the superior limbus, to achieve 4 mM, 5 uM, 1 mM and 3.5 mM vitreal concentrations respectively based on an estimated vitreal volume of 2.0 ml for each

eye. The concentrations of pharmacological agents were sufficient to achieve the required effects in other animals (Frishman and Steinberg, 1990; Hare and Ton, 2002) and in porcine mfERG (Chao et al., 1993; Lalonde et al., 2006; Ng et al., 2008b) (Tremblay F, et al. IOVS 2005;46:ARVO E-Abstract 2247). Sixteen eyes of eight Tg pigs were used. TTX+NMDA were injected for all eyes after mfERG under ISO were recorded. APB and PDA were then injected to right and left eyes respectively before mfERG measurements; PDA and APB were applied again to the opposite eyes (so that ultimately each eye had both APB and PDA applied) prior to additional mfERG measurements. In the control group, 14 eyes of ten WT pigs were used. Both eyes of four WT pigs received the same procedures as the Tg pigs. In the other six WT pigs, only one eye was used (3 right eyes for APB and 3 left eyes for PDA before APB+PDA applications).

After conjunctival suturing and each intravitreal injection, binocular indirect ophthalmoscopy was performed to ensure retinal integrity. The mfERG was recorded approximately 90 minutes after administration of each drug.

Analysis:

The mfERG responses from 103 individual responses were grouped by region: hexagons with p1 (peak-to-peak) amplitude in the top 25th percentile were grouped as the response from the optic streak, while the other hexagons (p1 amplitude not within the top 25th percentile) were grouped as the area outside the optic streak. The waveform features (Figure 10.1C) were defined conventionally according to Lalonde and co-workers (2006); details are given by Lalonde et al. (2006) and experiment 1 (Ng et al., 2008b). Amplitude and implicit time of the mfERG responses of Tg pigs before and after applications of ISO, TTX, NMDA, APB and PDA were measured and compared with the control data of WT pigs in experiment 1(Ng et al., 2008b). In addition, the inner retinal mfERG responses of WT and Tg pigs were also compared. Repeated measures one-way ANOVA with the Tukey *post-hoc* test was used for statistical analysis.

(A) (B)

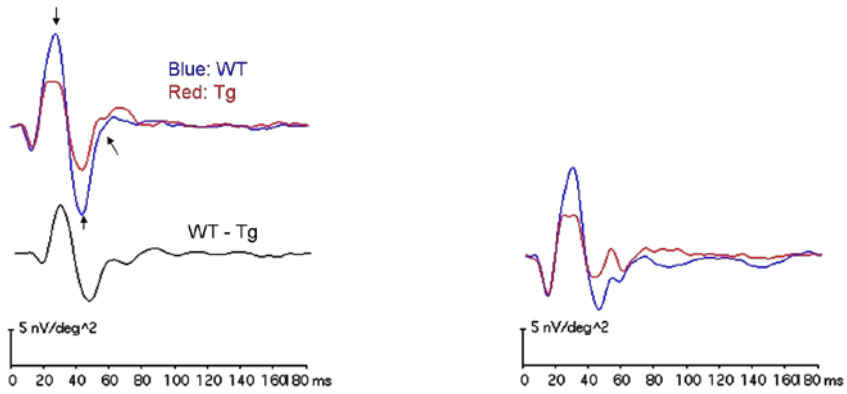

Figure 10.2. First-order kernel (K1) waveform of averaged mfERG from both eyes of WT Pig#4 (blue traces) and Tg Pig#2 (red traces) under propofol (A) and isoflurane (B) anesthesia. The p1, n2 and p2 of Tg K1 waveform were smaller than that of wild type. The black trace in (A) is the difference between averaged mfERG of all WT and Tg porcine eyes.

10.4. Results

The first-order kernel mfERG waveforms at the optic streak from Tg and WT retina under propofol and isoflurane (ISO) anesthesia are shown in Figure 10.2 and the amplitudes and implicit times are listed in Tables 10.1 and 10.2. The mfERG amplitude of the Tg was generally smaller than that of the WT. In the baseline data (under propofol anesthesia), the amplitude of the Tg mfERG were significantly smaller than the WT mfERG for the p1 ($p<0.01$), n2 ($p<0.001$) and p2 ($p<0.001$) components. The implicit time of p2 was also significantly shorter ($p<0.05$) in the Tg

pig. Under ISO anesthesia, although there were no significant differences in amplitude or implicit time between the Tg and WT mfERG, the p1 and n2 amplitude were somewhat smaller in the Tg mfERG.

Amplitude		n	1st order kernel (K1)				
			n1	p1	n2	p2	p3
Propofol	WT	14	4.89 (0.63)	22.24 (2.75)	32.92 (3.99)	16.89 (1.92)	3.78 (0.16)
	Tg	16	3.71 (0.38)	**11.21 (1.15) ****	**14.66 (1.60) *****	**8.06 (1.06) *****	3.21 (0.39)
ISO	WT	14	6.27 (0.79)	19.30 (2.10)	21.99 (2.14)	6.34 (0.90)	2.52 (0.38)
	Tg	16	5.80 (0.55)	13.53 (1.28)	12.17 (1.34)	5.51 (0.64)	2.43 (0.36)
ISO+TTX +NMDA	WT	14	4.33 (1.24)	21.15 (3.08)	28.30 (4.37)	12.74 (1.88)	1.11 (0.25)
	Tg	16	3.17 (0.82)	19.56 (2.62)	28.85 (3.49)	**16.51 (2.33) ***	1.73 (0.22)
ISO+TTX +NMDA +APB	WT	7	7.11 (0.88)	11.24 (1.26)	6.76 (0.96)	2.83 (0.67)	0.43 (0.15)
	Tg	8	7.45 (1.23)	11.82 (1.80)	6.82 (1.10)	1.93 (0.42)	0.48 (0.14)
ISO+TTX +NMDA +PDA	WT	7	0.98 (0.30)	21.13 (3.78)	33.23 (5.67)	13.33 (1.64)	0.40 (0.08)
	Tg	8	0.66 (0.26)	18.90 (5.11)	32.77 (9.22)	19.10 (5.89)	1.55 (0.92)
ISO+TTX +NMDA +APB+PDA	WT	14	4.56 (0.76)	5.81 (0.93)	1.82 (0.40)		
	Tg	16	5.07 (0.97)	7.00 (1.37)	2.89 (0.62)		

Table 10.1. Mean of amplitude (nV/degree^2) of 1st order kernel traces with SEM of mfERG at optic streak. * ($p<0.05$), ** ($p<0.01$) and *** ($p<0.001$) indicate significant difference from the wild type mfERG.

Implicit time		n	1st order kernel (K1)				
			n1	p1	n2	p2	p3
Propofol	WT	14	12.37 (0.22)	27.07 (0.41)	43.18 (0.55)	56.98 (1.07)	69.98 (2.64)
	Tg	16	12.11 (0.24)	23.56 (0.89)	41.40 (0.48)	**53.13 (0.79) ***	65.14 (1.04)
ISO	WT	14	13.01 (0.22)	28.61 (0.39)	43.84 (0.67)	52.71 (0.39)	69.29 (1.52)
	Tg	16	13.06 (0.35)	26.19 (0.96)	42.53 (1.29)	53.12 (1.43)	72.66 (2.74)
ISO+TTX +NMDA	WT	14	12.93 (0.50)	26.76 (0.71)	43.08 (0.43)	54.98 (0.50)	74.55 (1.09)
	Tg	16	11.81 (0.36)	25.22 (0.61)	41.85 (0.33)	55.79 (0.61)	77.60 (1.39)
ISO+TTX +NMDA +APB	WT	7	18.91 (0.79)	35.29 (0.58)	47.57 (0.94)	58.90 (0.98)	80.33 (2.60)
	Tg	8	**16.90 (0.96) ***	33.68 (1.75)	46.53 (2.03)	55.97 (1.79)	71.15 (1.82)
ISO+TTX +NMDA +PDA	WT	7	8.83 (0.47)	26.22 (0.87)	43.97 (0.82)	59.28 (1.11)	82.36 (3.97)
	Tg	8	8.83 (0.79)	25.09 (0.57)	42.30 (0.35)	56.59 (0.82)	77.02 (2.19)
ISO+TTX +NMDA +APB+PDA	WT	14	24.68 (1.31)	42.80 (2.20)	51.74 (1.81)		
	Tg	16	26.33 (1.16)	45.36 (1.36)	**65.28 (2.76) *****		

Table 10.2. Mean of implicit time (ms) of 1st order kernel traces with SEM of mfERG at optic streak. * ($p<0.05$) and *** ($p<0.001$) indicate significant difference from the wild type mfERG.

Figure 10.3A shows the waveforms of the first-order kernel after the application of different combinations of TTX, NMDA, PDA and APB under ISO anesthesia. The amplitudes and implicit times are listed in Tables 10.1 and 10.2. After TTX+NMDA application, the difference between the Tg and WT mfERG waveforms was reduced. For the Tg mfERG, n1 and p1 amplitudes showed small reductions under TTX+NMDA, and p2 was significantly increased ($p<0.05$) compared to the WT mfERG. After PDA injection, there were no significant changes in amplitude or implicit time of Tg and WT mfERG, but the n1 and p1 amplitude were relatively smaller in the Tg mfERG, and the p2 amplitude was relatively larger in the Tg mfERG. After APB injection, there were no significant amplitude changes in the Tg mfERG, but the implicit time of n1 was shortened significantly ($p<0.05$). After APB+PDA had been injected together, apart from a significant delay of the n2 implicit time ($p<0.001$) in the Tg mfERG, there were no significant differences in amplitudes or implicit times between the two groups.

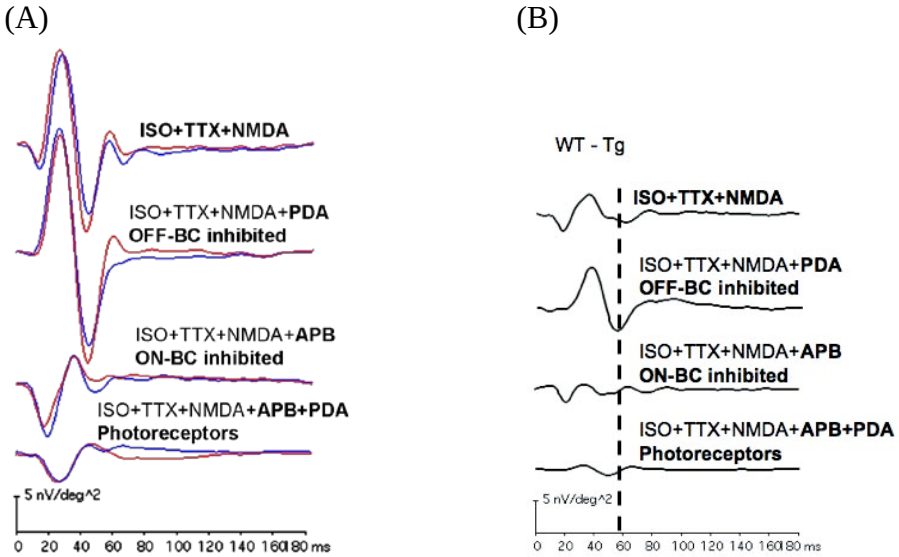

Figure 10.3. (A) First-order kernel (K1) waveform of mfERG from WT Pig#4 (blue traces) and Tg Pig#2 (red traces) after TTX, NMDA, PDA and APB administration under isoflurane anesthesia. The traces under the effect of ISO+TTX+NMDA, and APB+PDA were the averages of both eyes from WT Pig#4 and Tg Pig#2. The traces under APB and under PDA were from the right eye and the left eye of WT Pig#4 and Tg Pig #2 respectively. There was a positive peak at 57ms in K1 waveform of Tg mfERG but not in wild type mfERG after PDA administration. (B) The estimates of difference between the K1 waveforms of averaged mfERG of all Tg and WT porcine eyes.

Figure 10.3B shows the estimates of difference among the waveforms between the Tg and WT mfERG. The estimated waveforms were obtained by subtracting the waveform before drug application from that after drug application. The subtraction of waveforms was performed using VERIS, a method which has also been used in

previous studies (Hood et al., 1999; Hare and Ton, 2002; Hood et al., 2002). These waveforms show components of the mfERG which are altered in the Tg. There was a loss of a corneal negative-positive-negative component after TTX+NMDA and a positive-negative component after PDA application. However, there was only a loss of small oscillations after APB application and there was almost no difference between the two types of mfERG after all drugs had been injected.

The estimates of response of the inner retinal elements in the Tg and WT mfERG shown in Figure 10.4 were markedly different. The estimates were produced by subtraction of the waveforms under ISO anesthesia after TTX+NMDA application from those under propofol anesthesia. The major features of the response are oscillatory wavelets arbitrarily named OW1, OW2 and OW3. OW1 and OW2 in Tg showed opposite characteristics compared to those in WT. The amplitudes and implicit times are summarized in Table 10.3 and 10.4. There were significant differences of amplitudes of OW1 ($p<0.001$) and OW2 ($p<0.001$) between Tg and WT mfERG, but no difference in OW3.

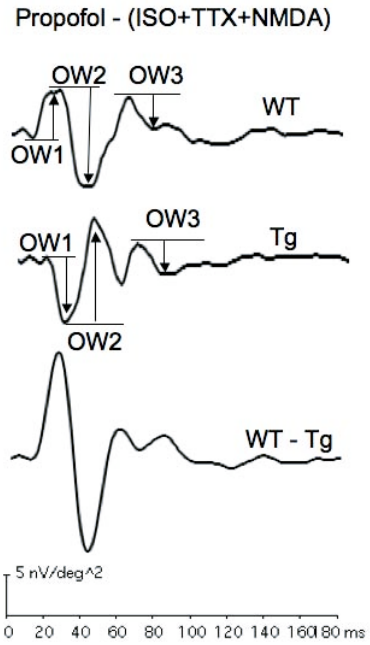

Figure 10.4. The averaged estimates of inner retinal response from both eyes of WT Pig#4 and Tg Pig#2. There were three features arbitrarily named OW1, OW2 and OW3. The OW1 and OW2 were altered in Tg mfERG. The bottom trace is the difference between the estimates of inner retinal element of all WT and Tg porcine eyes.

Amplitude		Inner retinal elements		
		OW1	OW2	OW3
Propofol – (ISO+TTX+NMDA)	WT	8.19 (4.48)	14.39 (6.71)	6.28 (1.06)
	Tg	**-7.71 (2.60) *****	**-10.31 (3.27) *****	4.19 (0.38)

Table 10.3. Mean of amplitude (nV/degree^2) of 1st order kernel traces with SEM of inner retinal elements at optic streak. *** ($p<0.001$) indicates significant difference from the wild type mfERG.

Implicit time		Inner retinal elements		
		OW1	OW2	OW3
Propofol – (ISO+TTX+NMDA)	WT	23.89 (1.27)	40.25 (1.05)	63.85 (1.15)
	Tg	24.72 (1.12)	41.30 (1.19)	64.65 (0.79)

Table 10.4. Mean of implicit time (ms) of 1st order kernel traces with SEM of inner retinal elements at optic streak.

10.5. Discussion

Recently, there has been increasing histological evidence of neural rewiring, such as ectopic synaptogenesis, following photoreceptor cell death (Peng et al., 2000; Peng et al., 2003; Haverkamp et al., 2006; Johnson et al., 2006; Gargini et al., 2007; Sullivan et al., 2007). The P347L transgenic pig (Tg) is an important large animal model shown to have ectopic synaptogenesis between cones and rod bipolar cells (Peng et al., 2000) and altered retinal electrophysiological response (Banin et al., 1999). Six-week old P347L transgenic pigs were chosen for this experiment because of their relatively spared cone physiology with extensive loss of rods (Petters et al., 1997). A previous study using flash ERG found that the cone response amplitudes were the same in Tg and WT, while there was no detectable rod mediated b-wave in 4-week old Tg animals (Banin et al., 1999). This experiment further demonstrated signal alterations in the Tg pigs in both outer and inner retinal responses, most likely as a consequence of retinal neural re-wiring.

Although there has been no direct evidence of different glutamate receptor types in porcine retina, Peng and co-workers (2000) reported the presence of GoG protein, which is related to mammalian metabotropic glutamate receptor 6 in Tg rod-bipolar cells after ectopic synaptogenesis. Furthermore, the effects of PDA and APB on WT

porcine mfERG in experiment 1 (Ng et al., 2008b) suggested the presence of corresponding receptors in porcine retina. In addition, the PDA and APB sensitive waveforms or components in porcine mfERG in experiment 1 (Ng et al., 2008b) resemble those of primates (Hare and Ton, 2002; Hood et al., 2002). All of these findings suggest that the porcine retina is a viable alternative to primate retina for dissecting the cellular contributions to the retinal signal using mfERG.

It is unlikely that the observed mfERG alterations are caused by transient increase of intraocular pressure or mechanical effects of injection because the injection volume of pharmacological solution in normal saline form was referenced to that of injection in monkey (Hare and Ton, 2002; Hood et al., 2002) and porcine eye (Lalonde et al., 2006). Furthermore, the effect of normal saline injection on perfused isolated porcine eye have been tested in the pilot investigation of the experiment III and found no alteration of mfERG with the same volume of normal saline injection.

Outer retinal signal alteration in Tg mfERG:

Under propofol anesthesia, the mfERG of Tg was smaller than that of WT (Figure 10.2A). This agrees with most of the studies on human RP subjects (Chan and Brown, 1998; Hood et al., 1998; Greenstein et al., 2004; Gerth et al., 2007; Janaky et al.,

2007). The mfERG contributed by the outer retina can be estimated after the removal of inner retinal activity by administration of ISO+TTX+NMDA (Figure 10.3A, top trace). The ISO was shown to remove only part of the inner retinal contribution in porcine mfERG (Lalonde et al., 2006; Ng et al., 2008b) and the PDA and APB sensitive elements under ISO were well preserved in experiment 1 (Ng et al., 2008b). Accordingly, signals originating from cells affected by photoreceptor degeneration and synaptic rearrangement, such as surviving cone photoreceptors in contact with rod bipolar cells, should be detected. The estimate of outer retinal mfERG response is mainly a summated contribution from ON- and OFF- bipolar cell pathways.

The changes in the outer retinal response as a consequence of rod photoreceptor cell death between the Tg and WT porcine mfERG are illustrated by subtracting the outer retinal elements of Tg mfERG from WT mfERG (Figure 10.3B). Although the outer retinal mfERG of Tg approximates that of WT (Figure 10.3A, top trace), a corneal negative-positive-negative component appears to be lost in Tg (Figure 10.3B, top trace), demonstrating that outer retinal activity in Tg is not identical to that of WT. It may be caused by the difference in implicit time between the outer retinal responses of Tg and WT. When OFF-bipolar cells are blocked, the Tg seems to have a loss of a corneal positive component followed by a corneal negative wavelet (2^{nd} trace in

Figure 10.3B). When ON-bipolar cells are blocked, a series of small oscillating wavelets following a corneal negative component are likely to be diminished in Tg (3rd trace in Figure 10.3B).

In Tg, a substantial number of cones remains (Banin et al., 1999) and there is no significant loss of rod bipolar cells after extensive rod degeneration (Peng et al., 2000). Consistent with these morphological data, mfERG findings showed no conspicuous waveform change in the cone response of Tg (4th trace in Figure 10.3B). The mfERG findings are also consistent with the absence of significant difference in the isolated cone response, between Tg and WT as reported by Banin and co-workers (1999). Therefore, the source of waveform difference between Tg and WT mfERG at the level of the outer retina seemed to arise mainly from the ON-bipolar cell pathway (2nd trace in Figure 10.3B), with a small contribution from the OFF-bipolar cell pathway (3rd trace in Figure 10.3B).

Neural re-wiring and ectopic synaptogenesis are important features in the degenerating retina and the synaptogenesis starts early in the neural development of retina (Strettoi et al., 2004; Johnson et al., 2006; Gargini et al., 2007) or after the onset of rod cell degeneration (Peng et al., 2000; Peng et al., 2003; Haverkamp et al., 2006).

After forming the ectopic contacts with cone photoreceptors, the rod bipolar cells retain the characteristics of ON-bipolar cells (Yang, 2004) and thus likely continue to utilize the mGluR6 mediated signaling pathway. This might explain why the waveform difference between Tg and WT mfERG at the level of the outer retina occurs mainly in the ON pathway.

Marc and co-workers (2007) recently reported increased ionotropic glutamate receptor response (OFF-response) and loss of rod bipolar cell signatures in a human RP retina. However, the Tg shows an alteration largely in the ON-bipolar cell pathway response, with minimal alteration in OFF-bipolar cell pathway response. The difference between the current findings and those of Marc et al. (2007) may be due to differences in the stages of retinal degeneration studied.

Inner retinal signal alteration in Tg mfERG:

In rod ablated retina, cellular components of the rod-specific signal pathway downstream from rods may persist long after rod degeneration. The altered signaling in the ON pathway as observed at the level of the outer retina could in turn cause alterations in the inner retina.

In this experiment, ISO would partially affect the inner retinal activity and the further application of TTX+NMDA would suppress nearly all inner retinal activity (Robson and Frishman, 1995; Hood et al., 2002). However, some types of inner retinal neurons that do not process NMDA receptors (Lukasiewicz, 2005) rather involve GABA receptors. GABA was not used for the suppression of inner retinal activity in this study because the use of GABA could affect the outer retina (Lukasiewicz, 2005). According to the findings from Hood and co-workers (2002), despite the difference in action of NMDA and GABA, the effects of TTX+NMDA are sufficient to suppress nearly most of inner retinal activity.

The estimates of inner retinal elements of Tg and WT were obtained by subtracting their mfERG responses after administration of ISO+TTX+NMDA from those before administration of ISO+TTX+NMDA (Figure 10.4). Both Tg and WT showed waveforms with oscillatory wavelets, OW1, OW2 and OW3, at approximately 24, 40 and 64 ms. No signal filtering was used to extract the OWs from the mfERG. Thus, they may not be the same as the oscillatory potentials of the full field ERG (Wachtmeister, 1998). These oscillatory wavelets or components are attributed to inner retinal cells because they were removed by ISO+TTX+NMDA, which presumably inhibited or removed most of the inner retinal contribution. Interestingly,

the inner retinal response was a corneal positive-negative-positive component (top trace in Figure 10.4) in the WT but was a corneal negative-positive-positive component (middle trace in Figure 10.4) in the Tg animal. But OW3 is very similar in both Tg and WT; its implicit time matches that of p3 from the normal porcine mfERG, which is reported to be eliminated by optic nerve section (Lalonde et al., 2006). As the Tg shows altered OW1 and OW2, but no change in OW3, the involvement of optic nerve due to retinal dystrophy in Tg is suspected to be minimal. This agrees with the reported preservation of retinal ganglion cells in young RP patients (Flannery et al., 1989). It may be that insufficient time has elapsed after the death of the photoreceptors for marked transneuronal degeneration to occur at the inner retinal level in this animal model (Milam et al., 1998).

Therefore, at the level of the inner retina, the difference between the estimates of response of WT and Tg retinas are reflected in the changes in OW1 and OW2 (Figure 10.4). Although the cellular origins of these wavelets are not known, these changes in the inner retina are likely due to alterations in synaptic circuitry induced by altered activity from the outer retina.

Although there was small number of significant differences between Tg and WT

porcine mfERG in this experiment, the results pointed to specific retinal pathways and regions that were altered in Tg. These results were made possibly by combining the mfERG technique with sequential application of pharmacological agents with known effects on the retina. The difference in the ON pathway of Tg compared to WT is likely to arise because of ectopic synaptogenesis involving cone photoreceptors and rod bipolar cells and the differences in OW1 and OW2 are likely the result of adaptive responses from the inner retinal neurons due to altered input from the outer retina. The neural re-wiring in degenerating retina is an example of neural plasticity which provides dynamic and adaptive changes to maintain the integrity of the retina despite profound loss of photoreceptors. In addition, the inner retinal neurons and their connections may be modified by the light stimulated signal from the outer retina to make the remaining neural circuits more suitable for the cone mediated pathways. This experiment showed that the pig eye model with retinal disease is useful to study the retinal pathophysiological changes. In addition, it further demonstrates that the porcine eye is a good alternative animal model for retinal research.

Experiment III

Ng Y.F., Chan H.H.L., To C.H., Yap, M. (2008). The characteristics of multifocal electroretinogram in isolated perfused porcine eye. *Doc Ophthalmol, 117:205-14.*

Chapter 11. Experiment III - The characteristics of multifocal electroretinogram in isolated perfused porcine eye

11.1. Abstract

Purpose:

To investigate the characteristics of multifocal electroretinograms (mfERG) from *in-vitro* perfused porcine eyes and the effect of commonly used anesthesia.

Methods:

TTX, NMDA, APB and PDA were used to identify contributions to the mfERG from inner retinal neurons, ON-pathway, OFF-pathway and photoreceptors. In addition, applications of isoflurane and propofol caused interference with the mfERG response was monitored.

Results:

The cellular contributions of the first-order kernel (K1) in an isolated perfused porcine mfERG came from both inner and outer retina, and were similar to those of *in-vivo* porcine mfERG. Isoflurane and propofol caused influence on mfERG resembled inner

retinal activities sensitive to TTX+NMDA application. The isoflurane sensitive element was a peak-trough-peak waveform, while the propofol sensitive element was a trough-peak-trough waveform.

Conclusion:

Improved understanding of the cellular origins of the isolated perfused porcine mfERG, in the absence of anesthetic agents, is useful for identifying changes shown in the waveform under anesthesia. The isolated perfused pig eye model is a good *in-vitro* model for retinal research.

11.2. Introduction

Multifocal electroretinogram (mfERG) recordings obtained from anesthetized primates (Hare and Ton, 2002; Hood et al., 2002) and pig (Lalonde et al., 2006; Ng et al., 2008b) have been measured before and after the injection of pharmacological agents with known effects in blocking the activities of specific neural circuits. These findings have been used to define the contributions of specific *in-vivo* retinal pathways to the mfERG response. However, general anesthesia is inevitable in such animal studies, and the anesthetics commonly used in human and veterinary medicine

are notorious for their effects on electrophysiological assessment (Fortune et al., 2002; Hans and Bonhomme, 2006; Lalonde et al., 2006). The *in-vitro* perfused eye model provides the integrity of the whole eyeball and the ability to apply anesthetic and other agents for retinal research.

The whole-eye perfusion method preserves the optical property of eyeball and the architecture of retina. Niemeyer and co-workers (2001) have extensively studied a perfused feline eye model. Recently, an isolated perfused bovine eye was showed to give stable and reproducible mfERG responses (Shahidullah et al., 2005b). The bovine eye, however, is very different from the human eye in globe size and types of cone photoreceptors. From the findings of the experiment 1 (Ng et al., 2008b) and 2 (Ng et al., 2008a), the porcine eye is relatively more close to the primate eye, even the human eye. This makes the perfused porcine eye can be developed as an alternative *in-vitro* model for eye research and the influence of various anesthetic and other agents can be studied by using this model. The present experiment was conducted to establish the characteristics of mfERG response in the isolated perfused porcine eye using pharmacological dissection techniques using TTX, NMDA, APB and PDA, and to investigate the effect of anesthetic agents, isoflurane (ISO) and propofol.

11.3. Method

Isolated eye preparation:

Fresh porcine eyes were collected from a local abattoir immediately after death of the animal. The ophthalmic artery was isolated, cannulated and perfused with oxygenated Krebs' solution at 30.5ºC; perfusion was started within 20 minutes of death of the animal. The cannulation and perfusion were carried out as previously described. Briefly, the ophthalmic artery was identified, incised and cannulated proximal to its bifurcation to form the two long posterior ciliary arteries (Shahidullah et al., 2003).

The Krebs' solution comprised of the following (mM): NaCl, (118); KCl, (4.7); $MgSO_4$, (1.2); $CaCl_2$, (2.5); $NaHCO_3$, (25); KH_2PO_4, (1.2); glucose, (11.5); ascorbate, (0.05); glutathione (1.0) and allopurinol (1.8)**.** It was bubbled with 95% oxygen and 5% carbon dioxide for 30 minutes and continued throughout the experiments. The dissolved oxygen in Krebs' solution exceeded 20mg/L (pO_2 > 365mmHg) and was monitored by a dissolved oxygen meter (Cole-Parmer, YSI Model 52 Field DO/BOD Meter). The pH of the Krebs' solution was maintained at 7.4 throughout the experiment. Eyes were oriented so that the multifocal ERG stimulus pattern from a computer monitor could be directed through the pupil (see below). Perfusion through

the ophthalmic artery ensured the supply of the Krebs' solution to retina as well as other parts of the eyeball including ciliary body and iris (Prince et al., 1960). Perfusion was driven by a digital peristaltic pump (Watson-Marlow, 505S) at 2.0ml per minute (Niemeyer, 1981). Successful perfusion was signaled by the appearance of blood and Krebs' solution outflow from vortex veins. Recording of the mfERG was commenced after the intra-ocular pressure (IOP), which was monitored by the use of tonometer (Tono-Pen XL, Reichert; Depew, NY, USA), had reached a steady state in 15–20 minutes. The arterial perfusion pressure was continuously monitored using a digital pressure transducer (Harvard Apparatus, 60-3003) and a dual-channel chart recorder (Kipp and Zonen, BD 112). Vascular perfusion pressure was typically stabilized between 20 and 60 mmHg. Eyes showing vascular perfusion pressure above 60 mmHg and/or IOP above 20 mmHg were excluded from the experiment.

Multifocal electroretinography:

Grass subdermal F-E7 electrodes (Astro-med Inc; West Warwick) were placed at the extraocular muscle and the cut end of optic nerve approximately 2.5 cm from the globe as ground and reference electrodes respectively (Figure 11.1A). Placing the reference electrode at the optic nerve minimizes the response amplitude variation caused by limbal-reference distance variation (Cringle et al., 1986), and improves the

signal to noise ratio when compared to placing it at the extra-ocular muscles. A monopolar ERG-jet contact lens electrode (Universal SA; La Chaux-de-Fons, Switzerland), as active electrode, was placed on the cornea using a lubricant (Lacryvisc gel 0.3%, Alcon Cleveland, OH, USA). With the contact lens electrode in place, retinoscopy showed +4 to -2D defocus at the 40cm working distance; this was corrected before mfERG recording.

(A)

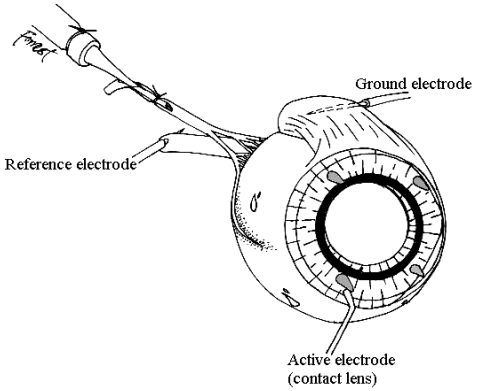

(B)

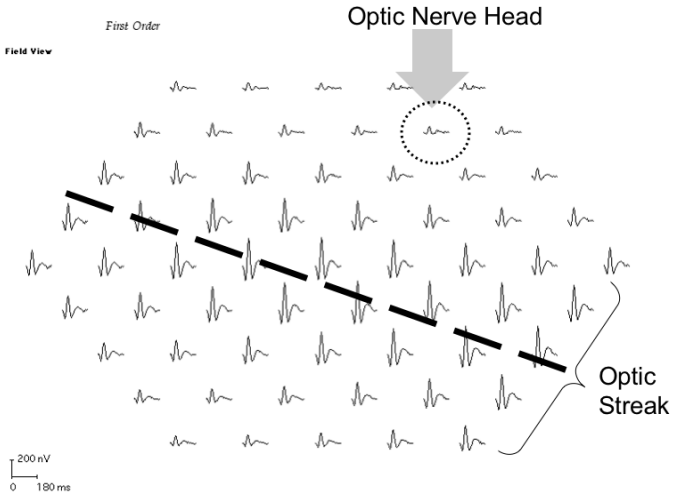

(C)

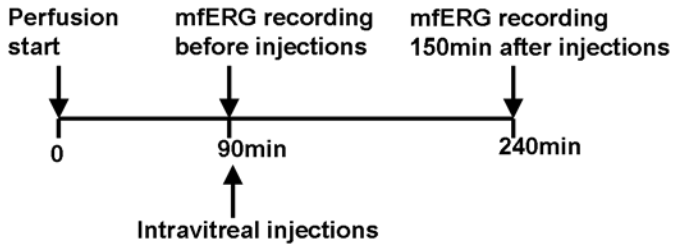

Figure 11.1 (A) Electrodes configuration of the perfused eye. **(B)** The K1 mfERG trace array after 90 minutes perfusion from eye (#2007-06-08e1). The location with the weakest response was the landmark of optic nerve head as reference point to assist the alignment of stimulator. **(C)** Time line depicturing the time of mfERG recording and intravitreal injections.

The mfERG stimulus pattern, consisting of 61 non-scaled white (160 cd/m^2) and black (1 cd/m^2) hexagons with a gray background (80 cd/m^2), was displayed on a 15" CRT monitor (591S CRT monitor, Samsung; USA) with a refresh rate of 75 Hz (13.3ms per frame). The mfERG stimulation was driven by VERIS software (version 5.01) (Electro-Diagnostic-Imaging; San Mateo, CA, USA) according to a pseudo-random binary m-sequence of 2^{15}-1 (approximate 7 minutes recording); mfERG responses were re-measured every 30 minutes. Retinal signals were amplified x20,000 (P511K amplifier, Grass Instruments Inc; Quincy, MA, USA) and filtered (bandpass: 1 to 300Hz). Local responses were extracted and processed by VERIS software.

Alignment of the eyeball to the stimulus pattern was facilitated by using the mfERG trace array; retinal features corresponding to the optic nerve head and optic streak were identified as reference points for the alignment (Figure 11.1B). After each intravitreal injection, the alignment of the eyeball to the stimulus pattern was verified again.

Drug administration:

Baseline mfERG data were obtained after 90 minutes (stabilization period) of perfusion (Figure 11.1C); pharmacological agents (all from Sigma-Aldrich; MO, USA) including N-methyl-D-asparatic acid (NMDA), tetrodotoxin (TTX), 2-amino-4-phosphonobutyric acid (APB) and cis-2,3-piperidinedicarboylic acid (PDA), isoflurane (ISO) and propofol were administered. Using 28 gauge needles, 25ul of NMDA, TTX, APB, PDA and ISO were injected separately into vitreous, 3mm above the superior limbus, to achieve 4mM, 5uM, 1mM, 3.5mM and 0.2mM vitreal concentrations respectively based on an estimated total vitreal volume of 2.0ml for each eye. Propofol (0.1mM) was transported into the eyes in the Krebs' solution perfusate. Clinically, the arterial concentration of propofol for preventing movement in 95% of patients is approximately 20.6ug/ml (0.115mM) (Andrews et al., 1997). For ISO, the minimum alveolar concentration (MIC) is approximately 1.4 vol %, while its minimum blood concentration (MBC) is approximately 0.53% in clinical situations (Katoh et al., 1992). Assuming that the minimum vitreous concentration of ISO approximates its clinical MBC, 25ul ISO in intra-vitreal injection would be double the minimum amount of ISO required. The concentrations of pharmacological agents, besides ISO and propofol, were evidently sufficient in previous experiments in other animals (Frishman and Steinberg, 1990; Akdemir et al., 2001) and in pig (Chao et al.,

1993; Lalonde et al., 2006; Ng et al., 2008b) (Tremblay et al. IOVS 2005;46:ARVO E-Abstract 2247). All of these effects on the flash ERG were verified.

Binocular indirect ophthalmoscopy was performed after each intravitreal injection to examine the retina and ensure its integrity. The mfERG was measured every 30 minutes for 180 minutes after the administrations of pharmacological agents (Figure 11.1C). For eyes injected with more than one pharmacological agent, such as TTX+NMDA, TTX+NMDA+APB, TTX+NMDA+PDA and TTX+NMDA+APB+PDA, those pharmacological agents were injected separately after the stabilization of perfusion pressure.

Analysis:

The 61 individual mfERG traces were grouped according to the regional response amplitude: those traces with p1 (peak-to-peak) amplitude up to the top 25 percentile were grouped as the response 'from optic streak', while the other traces (p1 amplitude not within the top 25 percentile) were grouped as 'outside optic streak'. The selection criterion was based on the assumption that the p1 amplitude (Figure 11.2) was proportional to the cone density. According to data of Gerke et al. (Gerke Jr et al., 1995) and Chandler et al. (Chandler et al., 1999), the cone cell density of peripheral

porcine retina is less than about 70% of the cone cell density of the optic streak. Amplitude and implicit time of the mfERG responses were measured.

Implicit time and the percentage amplitude change were used for statistical analysis and all comparisons were performed with repeated measures one-way ANOVA with Tukey *post-hoc* tests. In order to minimize the effect of baseline response variations among eyes before drug application, amplitudes after drug application were compared to the amplitude before administration (Equation 11.1 and Table 11.2). Responses after administration of APB, PDA and APB+PDA under the effect of TTX+NMDA were compared to the TTX+NMDA baselines. The data of percentage change at 150 minutes after the applications of TTX, NMDA, TTX+NMDA, ISO and propofol were compared with the averaged results of the control group after 240 minutes (90 minutes of stabilization period + 150 minutes) of perfusion.

$$\text{Amplitude \%} = A_{90min} / A_{240min}$$

Equation 11.1. Percentage amplitude calculation. A_{90min} and A_{240min} are the amplitude of mfERG waveform features at 90 minutes and 240 minutes perfusion respectively.

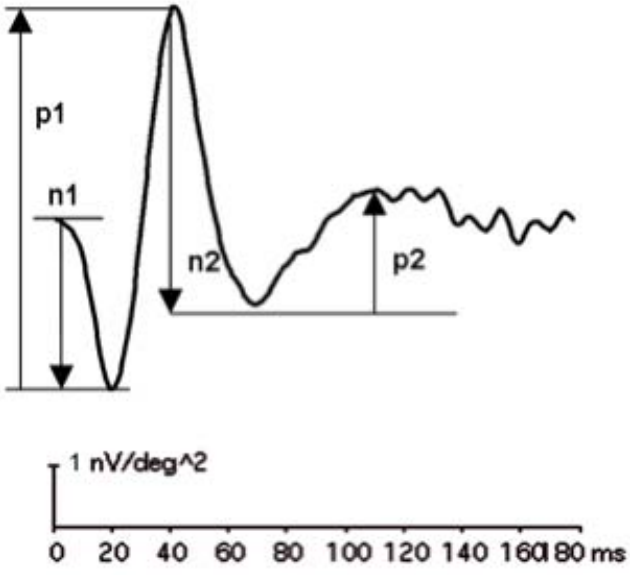

Figure 11.2. K1 waveform of averaged mfERG from all perfused porcine eyes after 90 minutes of perfusion without pharmacological agent administrations.

Implicit time (ms)	n	Before drug application								150 min after drug application							
		n1		p1		n2		p2		n1		p1		n2		p2	
Control	13	21.02	(1.01)	44.09	(0.99)	70.90	(1.94)	120.40	(3.38)	23.41	(1.13)	46.43	(1.73)	77.86	(3.30)	116.20	(2.56)
TTX	5	19.56	(1.20)	42.84	(0.72)	70.94	(1.55)	112.40	(3.69)	22.24	(2.04)	46.96	(2.33)	78.40	(3.50)	119.70	(4.08)
NMDA	5	20.10	(1.67)	40.98	(1.09)	70.60	(4.53)	116.00	(6.90)	20.54	(2.72)	42.78	(2.34)	73.86	(5.50)	103.60	(10.18)
TTX+NMDA	5	17.72	(0.32)	40.62	(1.65)	62.84	(4.25)	105.60	(7.39)	20.88	(1.41)	46.26	(1.30)	74.70	(2.92)	119.00	(5.62)
TTX+NMDA+PDA	6	21.47	(1.83)	42.12	(2.76)	67.07	(4.91)	104.90	(4.03)	21.47	(1.46)	42.22	(2.32)	68.97	(4.71)	108.00	(5.97)
TTX+NMDA+APB	4	21.78	(1.96)	42.20	(2.08)	66.25	(5.47)	117.70	(8.27)	26.98	(2.15)	50.58	(5.47)	73.78	(8.20)	108.70	(15.18)
TTX+NMDA+APB+PDA	5	15.45	(4.19)	43.68	(2.07)	71.43	(0.98)	104.20	(4.57)	24.45	(5.15)	42.23	(1.29)	65.00	(2.37)	113.50	(8.06)
Propofol	5	24.10	(1.25)	52.54	(3.76)	86.16	(7.18)	137.00	(11.70)	36.64 ***	(2.30)	64.56 ***	(4.08)	109.90 ***	(1.79)	151.20 ***	(7.79)
ISO	7	22.70	(1.38)	48.37	(3.34)	76.11	(2.74)	126.00	(5.06)	21.03	(0.94)	44.90	(1.64)	74.14	(2.48)	119.50	(6.19)

Table 11.1. Mean of implicit time with SEM of first-order kernel mfERG features at optic streak.

*** ($p<0.001$) indicates significant difference from the control mfERG

Amplitude %	n=	n1		p1		n2		p2	
Control	13	74.89	(9.88)	55.78	(5.75)	49.64	(5.92)	63.63	(7.45)
TTX	5	92.35	(15.77)	77.40	(6.57)	80.83	(5.63)	89.41	(15.78)
NMDA	5	98.96	(25.30)	78.85	(11.15)	75.65	(11.78)	94.03	(16.72)
TTX+NMDA	5	82.69	(15.12)	82.02	(6.23)	91.61	(14.85)*	113.40	(26.38)
TTX+NMDA+PDA	6	88.14	(10.24)	107.10	(17.40)	109.50	(18.35)	115.90	(15.23)
TTX+NMDA+APB	4	87.58	(19.89)	43.29	(7.80)	36.93	(7.19)#	55.81	(15.92)
TTX+NMDA+APB+PDA	5	75.95	(11.67)	42.33	(10.22)	34.84	(8.15)#	116.70	(35.82)
Propofol	5	82.92	(18.25)	48.28	(10.80)	38.75	(11.11)	47.85	(15.22)
ISO	7	82.68	(8.53)	86.57	(10.04)*	112.40	(10.55)**	103.50	(7.86)*

Table 11.2. Mean of percentage amplitude with SEM of mfERG first-order kernel traces at optic streak. The percentage amplitude of different response features was obtained by dividing the amplitude 150 min after drug applications by the corresponding response amplitude before drug applications.

* ($p<0.05$) indicates significant difference from the control mfERG

** ($p<0.001$) indicates significant difference from the control mfERG

($p<0.05$) indicates significant difference from the mfERG under TTX+NMDA

11.4. Results

Figure 11.2 shows a typical mfERG waveform obtained from the perfused pig eye; typically responses from optic streak and the area outside optic streak were very similar even across the various drug treatment used (Figure 11.1B). This experiment will focus on the changes of the mfERG in the optic streak under different pharmacological conditions. The response implicit times of first-order kernel (K1) mfERG at optic streak from perfused porcine retina before and 150 minutes after administration of pharmacological agents are listed in Table 11.1. The percentage amplitude changes are listed in Table 11.2.

The influence of TTX and NMDA:

Figure 11.3A shows the averaged trace of the K1 mfERG without pharmacological agents and the averaged traces of the K1 mfERG under effects of TTX, NMDA and TTX+NDMA. Implicit times and percentage amplitude of the K1 responses with and without application of TTX and NMDA are summarized in Tables 11.1 and 11.2. Although there were no significant changes of the mfERG response in terms of amplitude or implicit time under the influence of TTX and NMDA, some changes in the K1 waveforms were noticed. After the application of TTX, the oscillatory

wavelets in the K1 response became more obvious. The TTX+NMDA application significantly increased the percentage amplitude of n2 ($p<0.01$); application of NMDA diminished the oscillatory wavelets in K1 caused by TTX.

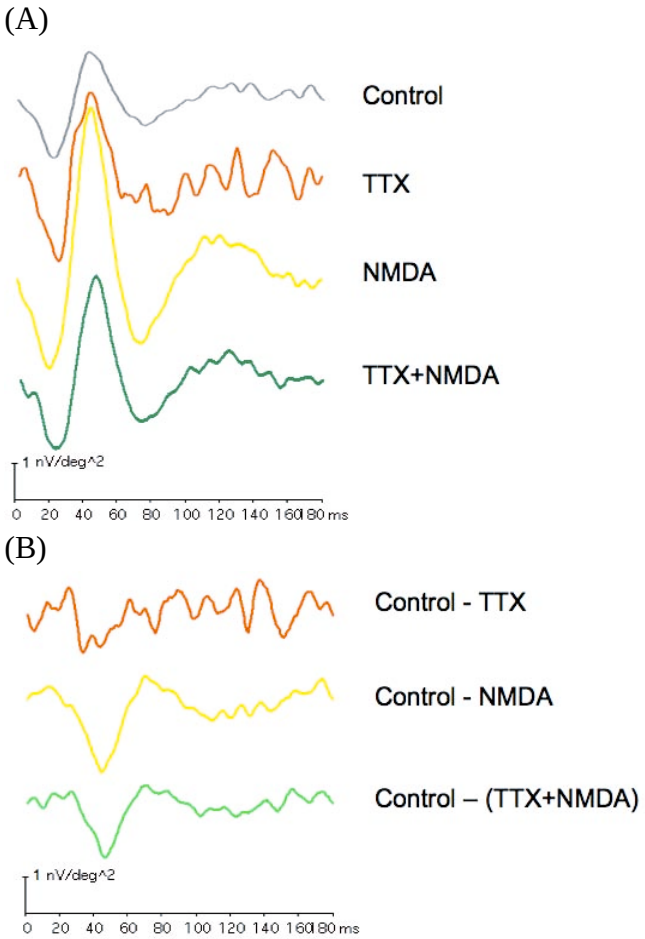

Figure 11.3. (A) Averaged K1 waveforms of mfERG responses at 150 minutes after pharmacological administration (ie. 240 minutes after perfusion). The top trace (black) is waveform of averaged mfERG without pharmacological agents, while the rest of traces are waveforms of averaged mfERG under effects of TTX (orange trace), NMDA (yellow trace), and TTX+NMDA (green trace). They are grouped responses at optic streak. (B) Estimates of TTX (orange trace), NMDA (yellow trace), TTX+NMDA (green trace) sensitive elements of the K1 mfERG responses. The subtraction of waveform was performed by the VERIS software. The TTX-sensitive element is mainly a corneal-positive component at 25 ms. The NMDA- and TTX+NMDA-sensitive elements are peak-trough-peak waveforms with similar corneal-positive, -negative and -positive component at 15-25, 45 and 70 ms.

(A)

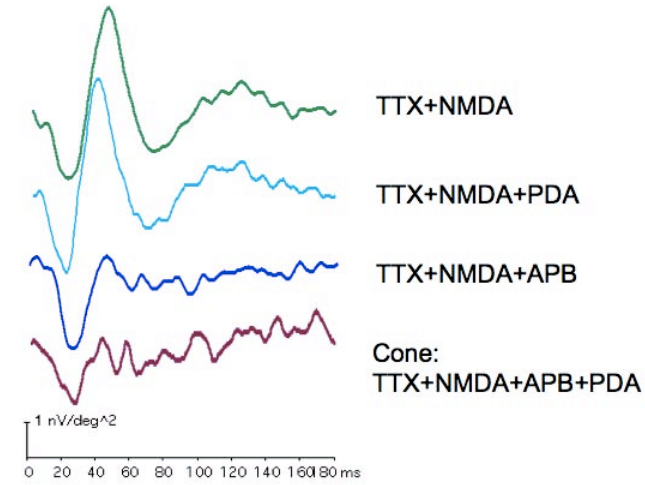

(B)

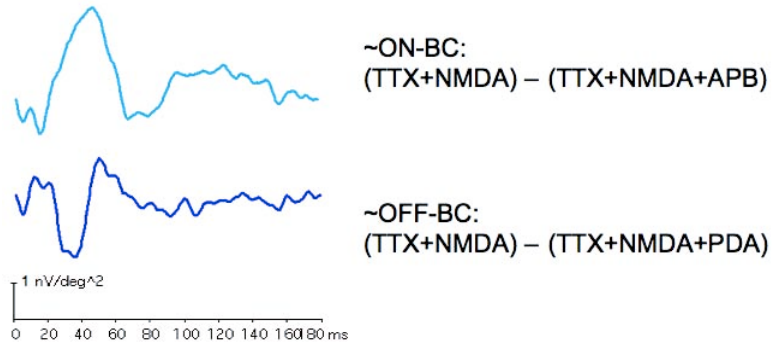

Figure 11.4. (A) Averaged K1 waveforms of mfERG responses at 150 minutes after application of TTX+NMDA (green trace) with co-administration of PDA (turquoise trace), APB (blue) and APB+PDA (purple trace) (ie. 240 minutes after perfusion). They are grouped responses at optic streak. The bottom purple trace under APB+PDA is the estimate of cone photoreceptor contribution after elimination of ON- and OFF-bipolar contributions. (B) Estimates of APB (turquoise trace) and PDA (blue trace) sensitive elements of the K1 mfERG responses at 150 minutes after pharmacological administrations (ie. 240 minutes after perfusion). The subtraction of waveform was performed by the VERIS software.

The influence of APB and PDA:

Figure 11.4A shows the averaged traces of the K1 mfERG under the effect of APB, PDA and APB+PDA with co-administration of TTX+NDMA. Implicit times and percentage amplitude of the K1 responses after the application of APB and PDA are summarized in Tables 11.1 and 11.2. The APB application significantly reduced the amplitude of n2 ($p<0.05$). The application of APB+PDA reduced the amplitude of n2 significantly ($p<0.05$).

(A)

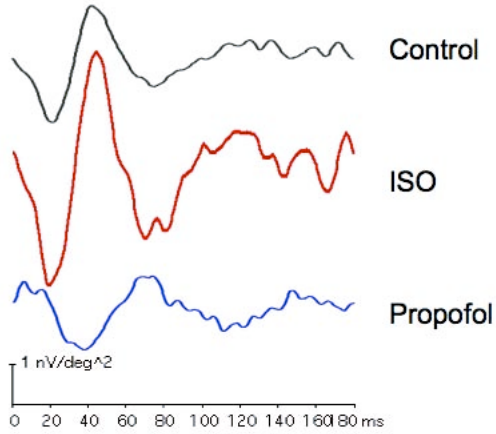

(B)

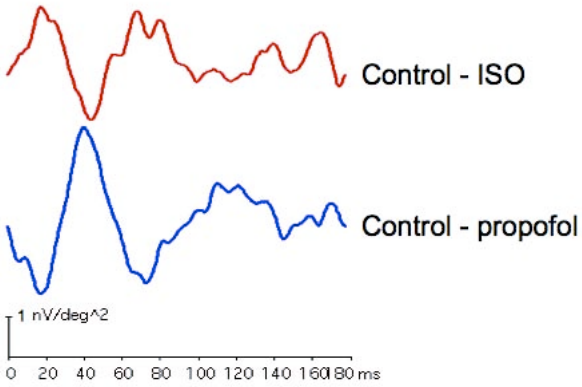

Figure 11.5. (A) Averaged K1 waveforms of mfERG responses at 150 minutes after ISO and propofol administration (ie. 240 minutes after perfusion). The black trace is the averaged K1 waveform of control group. They are grouped responses at optic streak. (B) Estimates of ISO (red trace) and propofol (blue trace) sensitive elements of the K1 mfERG responses at 150 minutes after pharmacological administrations (ie. 240 minutes after perfusion). The subtraction of waveform was performed by the VERIS software. The ISO- and propofol-sensitive elements show opposite in nature.

The influence of propofol and ISO:

Figure 11.5A shows the averaged traces of the K1 mfERG after ISO and propofol administration. Implicit time and percentage amplitude of the K1 responses are summarized in Tables 11.1 and 11.2. The ISO application caused significant amplitude increase of p1 ($p<0.01$), n2 ($p<0.01$) and p2 ($p<0.01$). The propofol application caused significant increase of n1 ($p<0.001$), p1 ($p<0.001$), n2 ($p<0.001$) and p2 ($p<0.001$) implicit times. Figure 11.5B shows the ISO- and propofol-sensitive components from the mfERG measurement. The appearance of these two components was different and had opposite in nature.

11.5. Discussion

While the K1 responses of perfused porcine mfERG differ from *in-vivo* porcine mfERG in experiment 1 (Ng et al., 2008b), variation in factors such as time after enucleation, ambient temperature after enucleation, imperfect perfusion, and extraocular vascular leakage of perfusion medium (Niemeyer, 2001) would contribute to these differences. The baseline mfERG of perfused eyes were generally delayed and reduced when compared to *in-vivo* porcine mfERG in experiment 1 (Ng et al., 2008b). There is only very weak p3 (which was obvious from *in-vivo* mfERG) found

for *in-vitro* mfERG. The discrepancy between *in-vivo* and *in-vitro* mfERG possibly relates to the different oxygen carrying capacity of Krebs' solution as compared to blood and hypothermia of *in-vitro* system. Nevertheless, the *in-vitro* mfERG still contained components from both inner and outer retina. The general anesthetics commonly used in animal studies *in-vivo* affect the K1 responses.

Contribution from inner retina:

The amplitude of p1, n2 and p2 were increased after removal of inner retinal contribution (Figure 11.3A, lower green trace). The increase of p2 amplitude is consistent with the findings of *in-vivo* porcine mfERG (Ng et al., 2008b). Figure 11.3B (lower green trace) shows the TTX+NMDA-sensitive element obtained by subtracting the trace under TTX+NMDA (Figure 11.3A, lower green trace) from that without pharmacological effect (Figure 11.3A, top black trace). It is a peak-trough-peak waveform with a corneal-positive component around 25 ms (approximate at n1), a corneal-negative component around 45 ms (approximate at p1) and a corneal-positive component around 70 ms (approximate at n2). These showed that there is certain inner retinal activity in K1 porcine mfERG of the isolated perfused eyes. In contrast to *in-vivo* porcine mfERG, a corneal positive component following the p2 (the p3 of *in-vivo* porcine mfERG in experiment 1 (Ng et al., 2008b)) was not

obvious, which being susceptible to the cut of optic nerve (Lalonde et al., 2006). Although there were differences in implicit times, the waveform of inner retinal activity of perfused porcine mfERG was close to that of *in-vivo* porcine mfERG (Lalonde et al., 2006; Ng et al., 2008b) and monkey (Raz et al., 2002).

Comparing the results under TTX or NMDA application, both K1 waveforms under TTX or NMDA showed increased amplitude of n1, p1 and p2. However, their sensitive elements were different. Conventionally, NMDA was employed to remove the rest of inner retinal activities that cannot be inhibited by TTX (Bush and Sieving, 1996; Hood, 2000; Dong and Hare, 2002; Lalonde et al., 2006). In experiment 1 (Ng et al., 2008b), TTX- and NMDA-sensitive elements were not exactly the same in the K1 response. Figure 11.3B shows a small peak-trough waveform of the TTX-sensitive element (orange trace), while the NMDA-sensitive element (yellow trace) is a peak-trough-peak waveform. This indicates that the retinal cells being sensitive to either TTX or NMDA were still function in the isolated perfused porcine eye and the effects of TTX and NMDA on removal of inner retinal activity are different. In addition, the waveform of TTX+NMDA-sensitive element is similar to that of NMDA sensitive element, but different from that of TTX-sensitive element (Figure 11.3B). This confirms that the retinal components influenced by NMDA are located prior to the

components inhibited by TTX in the retinal hierarchy.

Contribution from outer retina:

The K1 mfERG response of perfused porcine eyes involved dominated ON-pathway and OFF-pathway components with a small contribution from the photoreceptors. After the pharmacological removal of most inner retinal activities, the contributions from major cell types, such as ON-, OFF-bipolar cells and cone cells, can be observed.

The application of PDA caused the implicit time decrease and amplitude increase of p1 and n2. The application of APB caused the decrease in amplitude of p1 and n2. By using the method of subtraction, the contributions of ON- and OFF-pathways in perfused porcine mfERG K1 response can be estimated. The APB-sensitive element (Figure 11.4B, turquoise trace) is an estimated contribution of ON-bipolar cell pathway to the K1 response. There is a large corneal-positive component around 45 ms (approximate at p1 of control waveform) following by a corneal-negative component around 65-80 ms and a corneal-positive component around 100-120 ms (approximate at p2 of control waveform). The PDA-sensitive element (Figure 11.4B, blue trace) is an estimated contribution of OFF-bipolar cell pathway to the K1

response. It comprised of a corneal-negative component around 35 ms followed by a corneal positive component around 50 ms. The estimated contributions from the ON- and OFF-pathway activities in the K1 response are in opposite or antagonistic natures. Under APB+PDA (Figure 11.4A, purple trace), there was only a small corneal-negative component at about 25 ms, similar to that of *in-vivo* porcine mfERG (Ng et al., 2008b) and other studies using primates (Hare and Ton, 2002; Hood et al., 2002). This small component is most likely from the cone photoreceptors. Because the implicit times of the estimated cone photoreceptors and OFF-bipolar cell contributions in perfused porcine mfERG are similar to those of *in-vivo* porcine mfERG, the delayed ON-bipolar cell contribution in perfused porcine mfERG may be the cause of delayed K1 response. The applause explanations are the lower physiological temperature of perfused porcine eye, the higher oxygen partial pressure of Krebs' solution and the damage of retinal neurons during transient ischemia before perfusion. The ON-bipolar cells are likely to be more sensitive to the above changes.

Effect of anesthetics on mfERG:

Most of the anesthetics commonly used in human and veterinary medicine interfere with evoked potentials measured in electrophysiology assessment (Fortune et al., 2002; Hans and Bonhomme, 2006; Lalonde et al., 2006). An *in-vitro* perfused eye

model is a good platform for investigating effects of anesthetic agents on neural tissue.

Isoflurane (ISO) is an anesthetic agent conventionally used in veterinary medicine. The mechanism of ISO anesthesia is not fully understood. It causes partial suppression of action potential and sodium channels (Duch et al., 1998), and inhibits activities of GABA receptors, glutamate receptors, glycine receptors and potassium channels (Ueno et al., 1999; Cheng and Kendig, 2003; Sonner et al., 2003). Isoflurane has been reported to reduce mfERG response amplitudes (Fortune et al., 2002; Lalonde et al., 2006; Ng et al., 2008b). However, in this experiment, the application of ISO caused increased amplitude of n1, p1, n2 and p2 (Figure 11.5A) in K1 mfERG. Figure 11.5B (red trace) shows the ISO-sensitive element obtained by subtracting the trace under ISO at 150 minutes from the control. It is a peak-trough-peak waveform with two corneal-positive components around 20 ms and 70 ms, and a corneal-negative component around 40 ms. The ISO-sensitive element is very similar to the inner retinal activity isolated by TTX+NMDA application and the ISO sensitive element from *in-vivo* porcine mfERG in experiment 1 (Ng et al., 2008b). The discrepancy between ISO effect on K1 mfERG response *in-vivo* and *in-vitro* may be due to the delayed K1 response *in-vitro*.

Propofol has recently been replacing ISO in anesthesia for human surgery. The mechanism of propofol anesthesia is also not fully understood. Propofol appears to induce conformational change in GABAa receptors (Bali and Akabas, 2004) and has been reported to reduce GABAr mediated righting reflex in rats (Sonner et al., 2003). In contrast to isoflurane, propofol does not suppress the sodium channels and NMDA receptors of neurons. Propofol produces less alteration in evoked potential responses, such as mfERG (Lalonde et al., 2006) and somato-sensatory evoked potentials (Liu et al., 2005), than inhalation anesthetics at the same depth of anesthesia (Hans and Bonhomme, 2006). However, propofol was showed to cause reduction and delay of p1 in the perfused porcine eye (Figure 11.5A, blue trace). Figure 11.5B (blue trace) shows that the propofol-sensitive component is a trough-peak-trough waveform with corneal-negative components around 20 ms and 70 ms, and a corneal-positive component around 40ms. The propofol-sensitive element is very different from the ISO-sensitive element (Figure 11.4B). The difference may be due to the antagonistic effects of ISO and propofol on evoked potentials. A possible explanation is that propofol affects GABAa receptors in a concentration-dependent manner (Bali and Akabas, 2004). At low concentrations, it potentiates sub-maximal GABA-induced currents, which, in turn, enhances certain GABA-mediated inner retinal pathway. In contrast, the ISO suppresses activities of GABA receptors (Ueno et al., 1999; Cheng

and Kendig, 2003; Sonner et al., 2003), which may inhibit certain GABA-mediated inner retinal pathway. As GABAa receptors mediate inhibitory neurotransmission (Lukasiewicz, 2005), propofol, which enhances GABAa receptor activities, would reinforce the inhibition activity. However, ISO, which suppresses GABAr activities, would suppress the inhibition responses.

The K1 porcine mfERG arises from both inner and outer retina, as does the *in-vivo* porcine mfERG. The n1 of K1 mfERG involved responses of cone photoreceptors and OFF-bipolar cells. The leading edge of p1 is dominated by ON-bipolar cell corneal-positive component. The trailing edge of p1 and n2 are dominated by reduction of ON-bipolar activities and shaped by the activities of OFF-bipolar cells and those retinal cells express NMDAr, because of the small TTX-sensitive component comparing to the NMDA-sensitive component. The p2 reflects mainly ON-bipolar cell activity.

There are differences between *in-vivo* and perfused porcine mfERGs, despite their similarities; the p3 of *in-vivo* porcine mfERG was very weak in perfused porcine mfERG. This may be related to the optic nerve section because of the enucleation process. The delayed and reduced K1 response in perfused porcine mfERG is likely

caused by the impaired ON-bipolar cell response affected by the experimental conditions.

The perfused porcine eye model allows a platform free of anesthetic agents. Both ISO and propofol altered inner retinal activity, albeit in different ways. Care should be taken in comparing retinal electrical activities under ISO and propofol anesthesia, because of the alteration in the baseline.

Chapter 12. Discussion and Conclusions

Discussion

In addition to the close relationship of physiology and anatomy between human eye and pig eye, there are advantages in choosing the porcine eye for research. First of all, pig eye models are readily available. For example, the retinitis pigmentosa (RP) transgenic pig (Peng et al., 2000) which is a genetically engineered pig model, is more readily prepared than a corresponding primate model. Pig models of retinal detachment (Kyhn et al., 2008) and diabetes mellitus (Hara et al., 2008) are also available. Secondly, breeding of pigs is easier than breeding of primates and the rate of reproduction is also quite high. In addition, for *in-vitro* experiments, there is

abundant supply of fresh porcine eyes from slaughterhouses. Thus, the usage of porcine eye *in-vivo* and *in-vitro* in retinal research can overcome a number of obstacles in human and primate experiments, such as the availability of normal and diseased animals and current stringent ethical constraints.

As a good alternative to primate retina in mfERG studies, we need a model with cellular origins of the mfERG comparable to that of the primate mfERG. In experiment 1, the cellular origins of porcine mfERG *in-vivo* were found to be generally similar to those of monkey mfERG (Hare and Ton, 2002; Hood et al., 2002), although lacking the double-peak feature observed in monkey mfERG (Hood et al., 2002). Both K1 and K2.1 of the porcine mfERG contained components from both inner and outer retina. For the K1 waveform, the n1 involved responses of cone photoreceptors and OFF-bipolar cells. The leading edge of p1 is dominated by an ON-bipolar cell corneal-positive component. The rear edge of p1, n2 and p2 are dominated by ON-bipolar activities and shaped by the activities of OFF-bipolar cells and retinal cells rich in NMDAr and voltage gated sodium channels, other than the ganglion cells. The p3 component is driven mainly by ganglion cell activity (Lalonde et al., 2006). For the K2.1 waveform, the p1 and n1 are the summation of activities of ON-, OFF-bipolar cells and retinal cells rich in NMDAr and voltage gated sodium channels

other than the ganglion cells. The p2 component reflects mainly NMDAr activities and is insensitive to TTX. The detailed dissection of the mfERG waveforms in the pig eye helps us to further understand the cellular origins of mfERG in humans. Since both K1 and K2.1 waveforms were investigated in this study, this would help to explain the changes of mfERG in cases of different retinal diseases. For example, the loss of p2 and p3, which approximates the p60 component in the human mfERG, could suggest altered inner retinal physiology. In addition, the superimposition of activities from inner and outer retina arouses the concern of response component examination in future because the altered components, such as p1, may involve physiology changes of more than a single retinal cell type. Although there are some differences between human eye and pig eye, the findings in this study give us a framework for the interpretation of mfERG results in some retinal diseases which are not easily simulated in monkey models, such as some genetic disorders.

The TTX, PDA and APB sensitive elements in K1 were similar in waveforms in both porcine and monkey mfERGs (Hare and Ton, 2002; Hood et al., 2002), although the oscillations of the TTX-sensitive element from monkey were not observed in the porcine mfERG. Oscillations in the mfERG waveform of this kind are not observed in human mfERG, and thus the porcine mfERG may be a better alternative for studies of

retinal physiology.

There are some alternations in retinal circuitry or neural re-wiring reported for animal models associated with photoreceptor degenerations (Peng et al., 2000; Peng et al., 2003; Strettoi et al., 2004; Haverkamp et al., 2006; Johnson et al., 2006; Gargini et al., 2007). However, these models are usually genetically engineered and are not usually available in primates. In experiment 2, the alteration in porcine mfERG associated with neural re-wiring in the degenerating porcine RP model (six-week P347L transgenic pig) was demonstrated. The signal alterations in the Tg pigs involved both outer and inner retinal responses. Although the lack of solid information on the cellular origin of the inner retinal activities related to OW1, OW2 and OW3, the close relationship of the OW3 and p3 in timing suggested lack of involvement of optic nerve in the alteration of inner retinal activities associated with neural re-wiring. This is an example of neural plasticity, which is believed to make certain dynamic and adaptive changes to maintain integrity of retinal function despite profound loss of photoreceptors. In addition, the inner retinal neurons and their connections, from the experiment 2, are likely to be modified in response to the light stimulated signal from the outer retina in order to make the remaining neural circuits better accommodated to the cone mediated pathways. In this study, the mfERG changes in the diseased pig eye

were demonstrated and this further supports the notion that the diseased pig eye can be a good alternative model for study of pathological changes in the human eye. The findings from the porcine RP model in this study showed a modified or adjusted inner retinal response which is likely to be caused by abnormal neural rewiring. This important new finding supports the issue of neural plasticity and helps us to understand the mechanism of neural adaptation under pathological changes. The modified response caused by abnormal rewiring may influence or overload other pathways in the diseased retina (eg the cone pathway), which finally induces pathological or degenerative changes. In order to explore the consequence of neural rewiring, longitudinal study of the mfERG alteration of degenerating porcine retina is recommended. This is a new concept in neural plasticity of the diseased eye and may be a new area in developing new treatment for different retinal diseases.

Apart from the diseased porcine retinal model, the enucleated porcine eye as a by-product from slaughter houses provides a large supply of material for *in-vitro* study. Although the experiments of retina *in-vivo* (experiments 1 and 2) provide an intact retinal network and physiology, there are still some practical disadvantages. General anesthetics are essentials in animal experiments *in-vivo*. The ISO anesthesia affects the retinal physiology and signal transmission (Fortune et al., 2002; Lalonde et al.,

2006; Ng et al., 2008b) as shown in experiment 1. The metabolism of animals also affects drug delivery to the retina. Sometimes, animal models *in-vivo* limit the dosage and type of drugs used due to toxicity issues. Studies of retina *in-vitro* can overcome these limitations although the retinal physiology and structures are not totally the same as those of the retina *in-vivo*.

A sound retinal model *in-vitro* has to show comparable electrophysiological cellular components to those of *in-vivo* retinal electrophysiology. In addition, a good *in-vitro* model requires well preserved optical and retinal architecture to simulate the *in-vivo* environment. In experiment 3, the whole eye perfusion method reported by Niemeyer (2001) was simplified by using an enucleated porcine eye from a local slaughterhouse. The functional cellular components of porcine mfERG *in-vitro* were demonstrated by use of pharmacological agents as in experiment 1 and other experiments using primates (Hare and Ton, 2002; Hood et al., 2002). The K1 mfERG *in-vitro* was generally diminished and delayed when comparable to that of K1 mfERG *in-vivo*. Although there were differences between K1 mfERG *in-vitro* and *in-vivo*, the cellular origins of the K1 porcine mfERG *in-vitro* are also contributed from both inner and outer retina in a manner similar to the *in-vivo* porcine mfERG. The n1 of K1 mfERG involved responses of cone photoreceptors and OFF-bipolar cells. The

leading edge of p1 is dominated by the ON-bipolar cell corneal-positive component. The rear edge of p1 and n2 are dominated by ON-bipolar cell activities and shaped by the activities of OFF-bipolar cells and those retinal cells express NMDAr, because of the small TTX-sensitive component comparing to the NMDA-sensitive component of *in-vitro* porcine mfERG. The p2 reflects mainly ON-bipolar cell activity. However, the p3 of the *in-vivo* porcine mfERG was very weak in the perfused porcine mfERG. This may be related to the optic nerve section after the enucleation process. The delayed and reduced K1 response in the perfused porcine mfERG may be caused by the impaired ON-bipolar cell response produced by the experimental conditions. Apart from the minor disadvantages, the *in-vitro* pig eye model is quite similar and comparable to the *in-vivo* pig eye model and this suggests that both models are valuable for retinal research.

The *in-vitro* perfused porcine eye can act as a platform free of anesthetic agents and the alteration of K1 mfERG associated with the application of two commonly used anesthetics, including ISO and propofol, (experiment 3) was tested. Both agents altered inner retinal activity, but in different ways. The ISO sensitive element with waveform approximates that of TTX+NMDA sensitive element *in-vitro* and *in-vivo* (experiment 1), while the propofol sensitive element with waveform in reversed

polarity to TTX+NMDA and ISO sensitive elements. A plausible explanation for this difference may lie in their different mechanisms of producing anesthesia. ISO suppresses GABA receptor activities (Ueno et al., 1999; Cheng and Kendig, 2003; Sonner et al., 2003) while propofol enhances GABA receptor activities (Bali and Akabas, 2004). This indicates that different kinds of anesthetics, such as ISO or propofol, would have predictable influences on retinal activities *in-vivo*. Thus, care should be taken in using anesthesia for all kind of *in-vivo* experiment, because of the alteration in the baseline of retinal activity. The isolated whole eye perfusion *in-vitro* model provides a good alternative when such issues are of primary importance.

Conclusions

The porcine eye provides a good alternative to the primate eye for retinal physiology studies. Experiment 1 and 3 showed the possibilities of assessing usable mfERG information and the close similarity of cellular origins of the mfERG between pig and primate. They help to consolidate the foundation of interpretation of porcine mfERG. Experiment 2 and 3 showed an example of using the porcine mfERG *in-vivo* and *in-vitro* for experiments that may not be easily performed in the monkey. Experiment 2 provided new understanding and interpretation of neural plasticity using mfERG from a diseased eye. Experiment 3 demonstrated the possibility of using an *in-vitro* porcine

model and the effect of common anesthetics. This experiment arouses the re-consideration of what are the best anesthetics for use in retinal electrophysiology.

APPENDICES

Appendix A - Multifocal electroretinogram (mfERG) in isolated porcine eye: the effects of temperature

A.1. Introduction

Multifocal electroretinography (mfERG) is a procedure for recording the local electrical responses from different retinal regions over a short period of time using multi-input stimulation (Sutter and Tran, 1992; Marmor et al., 2003). It gives a spatial functional map of the retina (Hood, 2000) which is useful for detecting the abnormalities in retinal function as in the case of retinal diseases (Hood, 2000), including glaucoma (Chan and Brown, 1999), diabetic retinopathy (Onozu and Yamamoto, 2003), and macular degeneration (Jurklies et al., 2002).

In experiment 1, the mfERG from isoflurane anesthetized *in-vivo* pigs (Ng et al., 2008b) was reported with sequential application of TTX, NMDA, APB and PDA to identify contributions to the mfERG from inner retinal neurons, ON-pathway, OFF-pathway and photoreceptors. However, general anesthesia is usually inevitable in *in-vivo* animal studies and the anesthetics commonly used in human and veterinary medicine are known to interfere evoked potentials in electrophysiological assessment

(Fortune et al., 2002; Hans and Bonhomme, 2006; Lalonde et al., 2006). *In-vitro* perfused whole eye model is the only platform that provides the integrity of retinal architecture and optical system, and the absence of application of anesthetic agents for retinal research.

It was reported previously that conventional flash ERG (Imaizumi et al., 1972) could be obtained in arterially perfused eyes. Attention has been drawn to the potential use of isolated mammalian eye in studying retinal electrophysiology (Niemeyer, 2001). Recently, *in-vitro* perfused bovine eye model was reported to give stable and reproducible mfERG recordings (Shahidullah et al., 2005b). However, the retinal structure and the photoreceptor profile in the bovine eye are very different from humans (Hebel, 1976), and therefore bovine eye may not be a good model. Pig and human eyes share many similarities in terms of their sizes, anatomy and histology (Beauchemin and Babel, 1973). In particular, the pig retina has a high cone density of both S and M cone types (Beauchemin, 1974; Braekevelt, 1983) which resembles the human eye very well (Hendrickson and Hicks, 2002). Therefore, pig has been proposed as a good alternative non-primate model for retinal research (Chandler et al., 1999; Hendrickson and Hicks, 2002).

As common to most *in-vitro* studies, no matter how freshly it is isolated, mammalian organs suffer from brief period of ischemia. Moderate hypothermia has been reported to relieve ischemia and reperfusion injury of the brain (Corbett and Thornhill, 2000) and retina (Wang et al., 2002). It is because hypothermia reduces oxygen demand of the tissues, the production of excitatory amino acids and the toxic nitric oxide synthesis (Miyazawa et al., 2003). In addition, the oxygen carrying capacity of perfusion medium is increased as the temperature decreases and thus, under hypothermia, this also benefits the physiological functioning of the *in-vitro* tissues. This experiment attempted to investigate the effects of temperature on mfERG recordings in order to optimize the condition for future use of the isolated porcine eye model. The mfERG, rather than flash ERG, was used to assess the retinal function in this experiment because it can provide higher spatial resolution, rather than summed overall response, from retina and the future use of mfERG is believed to become more important.

A.2. Method

Isolated eye preparation:

Fresh porcine eyes were collected from a local abattoir immediately after killing of pigs. The eyes were transported to laboratory by iced Krebs' solution bath. The ophthalmic artery was isolated, cannulated and perfused with oxygenated Krebs' solution. The solution was perfused via a warming water jacket so that the corresponding intravitreal temperatures were adjusted to 32.5, 30.5 or 28.5 ºC. The perfusion was started within 20 minutes post mortem time. The connection and perfusion were carried out according to the method described in the experiment 3 which is the same as the previous study (Shahidullah et al., 2003). Briefly, the ophthalmic artery was identified and cannulated proximal to its bifurcation to form the two long posterior ciliary arteries. Eyes were perfused with oxygenated modified Krebs' solution (pH 7.4) comprising (mM): NaCl, (118); KCl, (4.7); $MgSO_4$, (1.2); $CaCl_2$, (2.5); $NaHCO_3$, (25); KH_2PO_4, (1.2); glucose, (11.5); ascorbate, (0.05); glutathione (1.0) and allopurinol (1.8mM). The Krebs' solution was bubbled with 95% oxygen and 5% carbon dioxide for 30 minutes and continued throughout the experiments. The pH of perfusate was monitored and maintained at pH 7.4 throughout the experiment for different temperatures. The eyes were oriented in such a way that

the multifocal ERG stimulus pattern from a computer monitor could be directed into the retina through the pupil. Perfusion through the ophthalmic artery ensured supply of the Krebs' solution to retina as well as other parts of the eye including ciliary body and iris (Prince et al., 1960). Perfusion was driven by a digital peristaltic pump (Watson-Marlow, 505S) at flow rate of 2.0ml per minute (Niemeyer, 1981) at the pre-set temperature described above. The recording of mfERG was commenced after the arterial perfusion pressure and intra-ocular pressure (IOP) had reached a steady state in 15–20 minutes monitored by use of digital pressure transducer (Harvard Apparatus, 60-3003) and applanated tonometer (Tono-Pen XL, Reichert; Depew, NY, USA). The arterial perfusion pressure was typically stabilized between 20 and 60 mmHg. Eyes showing arterial perfusion pressure above 60 mmHg or IOP above 20 mmHg were excluded from the experiment, because of suspicion of blockage and rupture of the vascular meshwork.

Multifocal electroretinography:

Grass subdermal F-E7 electrodes (Astro-med Inc; West Warwick) was placed at the extraocular muscle and the cut end of optic nerve approximate one inch from the globe as ground and reference electrodes respectively (Figure 11.1A). A monopolar ERG-jet contact lens electrode (Universal SA; La Chaux-de-Fons, Switzerland), as

active electrode, was placed on the cornea with lubricant (Lacryvisc gel 0.3%, Alcon Cleveland, OH, USA). A stimulus pattern, consisted of 61 non-scaled white (160 cd/m^2) and black (1 cd/m^2) hexagons with a gray peripheral background (80 cd/m^2), for mfERG measurement was displayed on a 15" CRT monitor (591S CRT monitor, Samsung; USA) with a refresh rate of 75 Hz (13.3ms per frame). The mfERG stimulation was driven by VERIS (version 5.01, from Electro-Diagnostic-Imaging; San Mateo, CA, USA) according to a pseudo-random binary m-sequence of 2^{15}-1 (approximate 7 minutes recording). Recording of mfERG response was done at 90 min and 240 min after the commence of perfusion (Figure A1)**.** The retinal signals received were amplified (P511K amplifier, Grass Instruments Inc; Quincy, MA, USA) by a gain of 20,000 with a bandpass filter from 1 to 300Hz. The signals were extracted and processed by the VERIS. With the contact lens electrodes, the optical defocus at 40cm working distance was revealed by retinoscopy and the defocus at this working distance was corrected for mfERG recording.

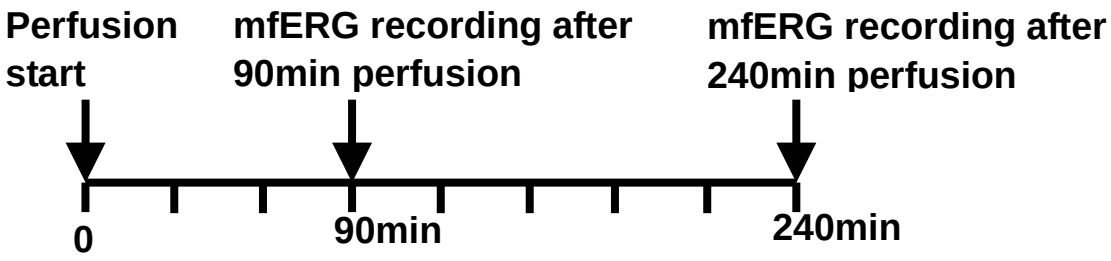

Figure A1. Time line depicturing the time of mfERG recording.

Alignment of the eyeball to the stimulus pattern was facilitated by examination of localized trace array of mfERG from all hexagons. According to the localized traces, retinal features corresponding to optic nerve head and optic streak were identified as the legends for alignment (Figure 11.1B).

Collection, Presentation and Statistical Analysis of Data:

The mfERG recording was started after obtaining target perfusion flow rate and stabilization of IOP, which usually took 30 minutes. Recording was repeated every 30 minutes. The 61 mfERG traces were grouped differently according to the regional response amplitude: those traces with p1 (peak-to-peak) amplitude up to the top 25 percentile were grouped as the response from optic streak, while the other traces (p1 amplitude not within the top 25 percentile) were grouped as the area outside optic streak. Amplitude and implicit time of the mfERG responses were measured. The response features are summarized in Figure 11.2. To reflect the initial stabilization period in the presentation of data, the time for the first measurement was designated

as 30 minutes. Results were expressed as the mean (± SEM) of separate experiments. Statistical analysis of mfERG findings were performed with repeated measures one-way ANOVA with Tukey post-hoc test.

A.3. Results

The mfERG waveforms showed typical troughs (n1 and n2) and peak (p1) as of *in-vivo* porcine mfERG at 61 different retinal locations (Figure 11.1B). In this experiment, regions with p1 amplitude, up to the top 25 percentile, where showed the highest p1 amplitude in the topographical distribution, were grouped as in experiment 1 (Ng et al., 2008b). Except the response amplitude, the mfERG waveform between the area of optic streak and the area outside optic streak were very similar, and this experiment, therefore, would focus to report the changes of the mfERG at optic streak at different temperatures, and the data outside optic streak would not be shown. The response amplitude and implicit time of first-order kernel (K1) mfERG at optic streak from perfused porcine retina after 45 minutes and 240 minutes perfusion were listed in Tables A1A to D and 2A to D. The initial and final IOP were 14.5 ± 3.5mmHg and 13.0 ± 4.7mmHg (n=24). The initial and final refractive errors were -0.34 ± 1.33DS and -0.54 ± 1.23DS (n=20). There were no significant differences among the initial

and final IOP (p=0.11) and refractive errors (p=0.12) of the eyes.

Implicit time at 90 minutes	32.5°C	30.5°C	28.5°C
Number of eyes	13	15	10
n1	20.15 (0.95)	20.96 (0.94)	**24.70* (1.62)**
p1	42.60 (1.14)	44.09 (0.99)	**52.95***### (1.22)**

Table A1A. Mean of implicit time (ms) with SEM of first-order kernel mfERG features at optic streak after 90 minutes of perfusion with different temperatures.
* ($p<0.05$) indicates significant difference from the mfERG recorded at 32.5°C
*** ($p<0.001$) indicates significant difference from the mfERG recorded at 32.5°C
($p<0.001$) indicates significant difference from the mfERG recorded at 30.5°C

Amplitude at 90 minutes	32.5°C	30.5°C	28.5°C
Number of eyes	13	15	10
n1	1.34 (0.11)	**3.21*** (0.28)**	**1.05### (0.11)**
p1	3.00 (0.45)	**6.69*** (0.68)**	**6.06** (0.53)**

Table A1B. Mean of amplitude (nV/degree^2)with SEM of first-order kernel mfERG features at optic streak after 90 minutes of perfusion with different temperatures.
** ($p<0.01$) indicates significant difference from the mfERG recorded at 32.5°C
*** ($p<0.001$) indicates significant difference from the mfERG recorded at 32.5°C
($p<0.001$) indicates significant difference from the mfERG recorded at 30.5°C

Implicit time at 240 minutes	32.5°C	30.5°C	28.5°C
Number of eyes	13	15	10
n1	21.63 (1.68)	23.41 (1.13)	27.13 (1.66)
p1	44.04 (1.99)	46.43 (1.73)	**53.89**,# (1.55)**

Table A1C. Mean of implicit time (ms) with SEM of first-order kernel mfERG features at optic streak after 240 minutes of perfusion different temperatures.
** ($p<0.01$) indicates significant difference from the mfERG recorded at 32.5°C

($p<0.05$) indicates significant difference from the mfERG recorded at 30.5°C

Amplitude at 240 minutes	32.5°C	30.5°C	28.5°C
Number of eyes	13	15	10
n1	0.98 (0.08)	**2.21*** (0.23)**	**0.89### (0.17)**
p1	1.37 (0.18)	**3.47*** (0.33)**	**3.45*** (0.29)**

Table A1D. Mean of amplitude (nV/degree^2) with SEM of first-order kernel mfERG features at optic streak after 240 minutes of perfusion with different temperatures.
*** ($p<0.001$) indicates significant difference from the mfERG recorded at 32.5°C
($p<0.001$) indicates significant difference from the mfERG recorded at 30.5°C

The mfERG at 28.5ºC and 30.5ºC revealed higher response amplitude than that obtained at 32.5ºC but the mfERG at 28.5ºC was generally delayed. (Tables A1A—D) The p1 implicit time was delayed significantly at 28.5ºC compared to those obtained at 30.5ºC and 32.5ºC. The n1 implicit time at 90 minutes was significantly delayed at 28.5ºC compared to that obtained at 32.5ºC. The p1 amplitudes were significantly increased at 30.5 and 28.5ºC. The n1 amplitude at 30.5ºC was significantly increased compared to those obtained at 28.5ºC and 32.5ºC.

A.4. Discussion

This experiment attempted to optimize the temperature for *in-vitro* arterially perfused porcine eye model as an experimental platform for mfERG measurement. Different

temperature conditions showed obvious influences on the retinal physiology in terms of mfERG result. Moderate hypothermia has been reported to relieve ischemia and reperfusion injury of the brain (Corbett and Thornhill, 2000; Miyazawa et al., 2003) and retina (Wang et al., 2002). Table A1B and A1D show that moderate hypothermia (30.5ºC and 28.5ºC) improved the p1 amplitude of mfERG. Because the perfusion medium at 30.5ºC and 28.5ºC may carry higher oxygen content than 32.5ºC. These results agree with previous histological findings on the neural protective effect of hypothermia on retinal ischemia in rat (Wang et al., 2002) and chick (Zeevalk and Nicklas, 1996). However, 28.5ºC caused significant increase of implicit time, which may be due to the slowed metabolic activities under hypothermia, even though the plausible increase of oxygen content in perfusate. Thus, to obtain the reproducible mfERG in isolated perfused porcine eyes, 30.5ºC is more suitable than 28.5ºC for *in-vitro* porcine mfERG recordings.

Appendix B - Morphological investigation of isolated, perfused porcine eyes.

B.1. Introduction

In the experiments of using isolated perfused eye, fresh porcine eyes were collected from a local abattoir immediately after killing of pigs. The perfusion usually started at around 20 minutes after enucleation and the histological changes in retina is unknown. Hence, in this appendix, the retina of *in-vitro* isolated perfused porcine eyes was studied after standardized perfusion and multifocal electroretinograph (mfERG) testing. Thin sections of retina were stained and studied microscopically to evaluate the architecture of retina after perfusion process.

B.2. Method

The preparation and perfusion of *in-vitro* isolated porcine eyes were described by previous chapters. Porcine eyes were grouped as “control”, “perfused” and “non-perfused” according to the conditions right before preparation for histology assessment. The control group (n=31) was dissected immediately after transportation of porcine eyes to the laboratory. For the perfused group (n=15) and non-perfused

group (n=9), the eyes were dissected after five hours at 30.5°C with and without perfusion with Krebs' solution. The preparation of retina for histology assessment was briefly described as below:

1. The eyeballs were transected parallel to the equator of globe.
2. The core mass of vitreous body was excised before preserving the eye cups in 10% neutral buffered formalin for 24 hours.
3. Formalin preserved eye cups were sectioned (Figure B1) prior to processing to paraffin block. Five-micrometer sections were prepared, stained with haematoxylin and eosin (H&E) and examined by bright field microscopy (Figure B2).

The slides of H&E stained retina were captured digitally. The thickness of retinal layers was measured and summarized in Figure B3. The thickness of retinal layers among the three groups was compared. All of the comparisons were performed with repeated measures one-way ANOVA with Tukey post-hoc test.

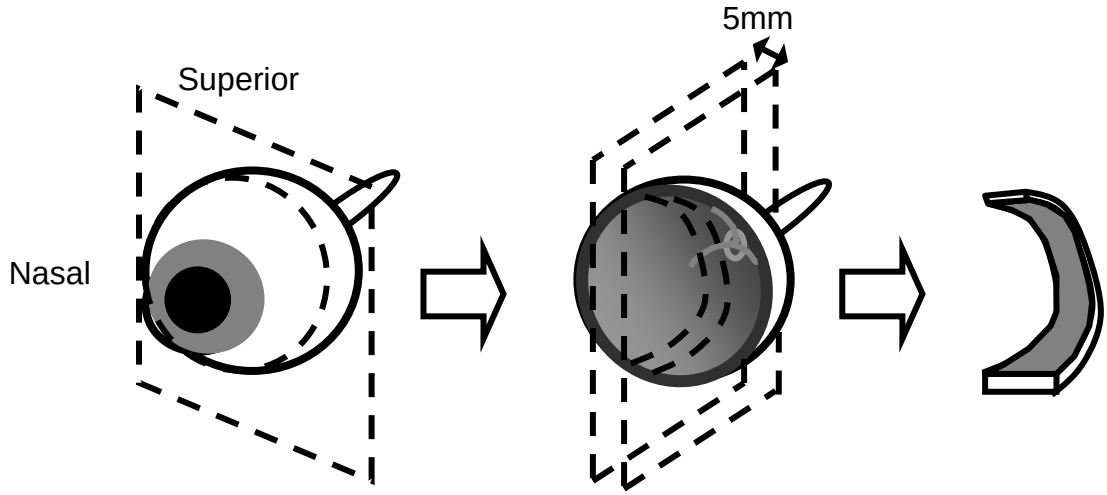

Figure B1. Porcine retinal paraffin blocks preparation. Porcine eyeball was transected parallel to the equator. After removal of vitreous body, the eye cup was transected perpendicular to equator to facilitate the paraffin block preparation.

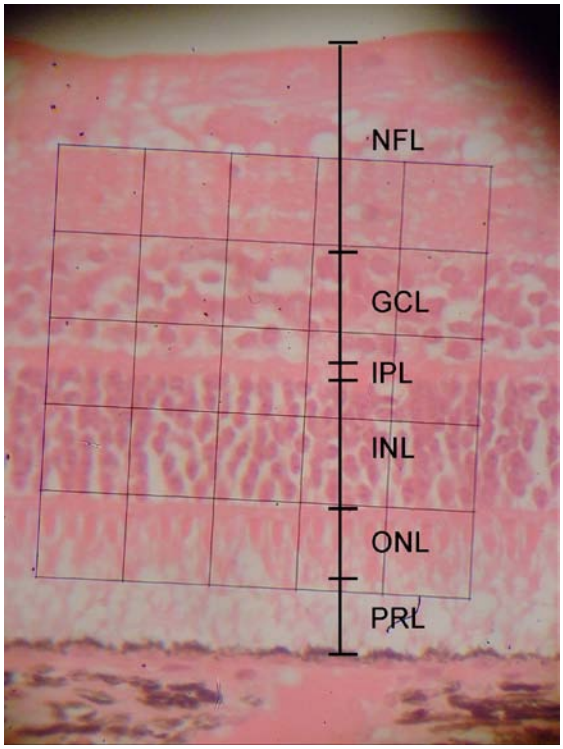

Figure B2. Porcine retinal section prepared after five hours of perfusion. The thickness of different retinal layers was measured. The mire grid was 125x125um^2.

B.3. Results

The retinal layers were generally reduced in thickness after five hours of perfusion (Figure B3). The thickness of photoreceptor layer was reduced significantly for the perfused group. The thickness of outer nuclear layer was reduced significantly for the perfused group and increased significantly for the non-perfused group. There was no obvious change of thickness of the inner nuclear layer and inner plexiform layer for all groups. Although there was no significant change of thickness, there were observed reductions of thickness of ganglion cell layer and nerve fiber layer from the perfused group. The total retinal thickness was reduced for the perfused group and increased for the non-perfused group, although there was no statistical significance.

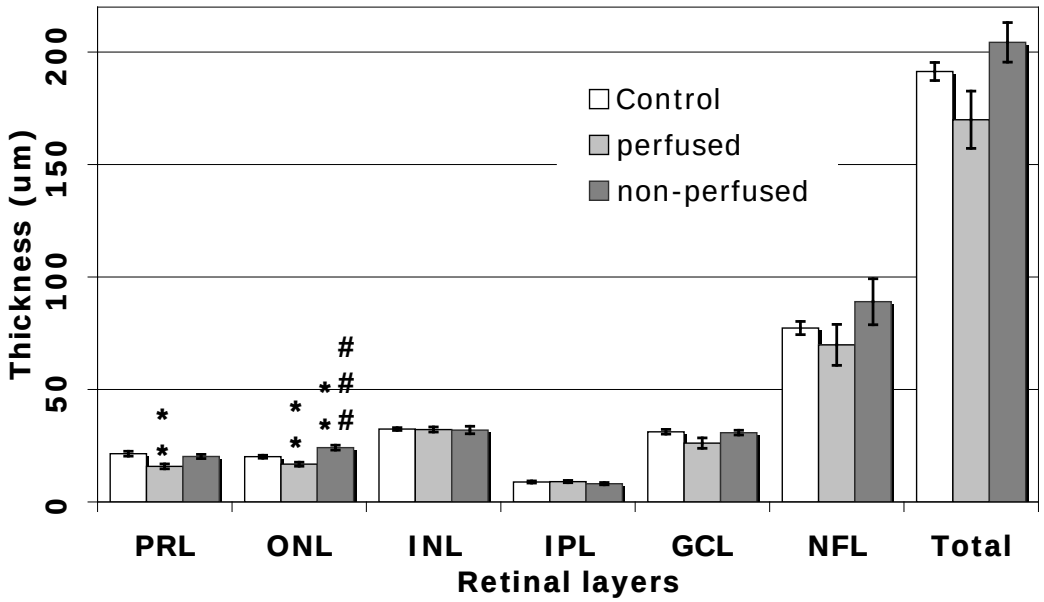

Figure B3. Mean thickness (um) with SEM of retina layers after enucleation (control), after five hours with perfusion (perfused) and without perfusion (non-perfused).
** ($p<0.01$) indicates significant difference from the control group.
($p<0.001$) indicates significant difference from the group perfused for five hours.

B.4. Discussion

The retinal layer thickness was generally reduced after five hours of perfusion with oxygenated Krebs' solution, but the histopathological examination cannot show deterioration of retinal layers after five hours of perfusion and all retinal layers remained well defined. However, there were mild to moderate deterioration of inner retinal layers after five hours of storage without perfusion. The reduction of total retinal thickness after perfusion compared to control group may be caused by the possible relief of short term retinal ischemia due to around 20 minutes of transportation from slaughter house to the laboratory. Thus *in-vitro* arterial perfusion may rescue the porcine retina from acute ischemia. The retinal edema caused by ischemia was relieved by *in-vitro* arterial perfusion. Thus, the histological alteration in the perfused retina under *in-vitro* arterial perfusion should be less than that in the non-perfused retina for five hours.

REFERENCES

Akdemir H, Asik Z, Pasaoglu H, Karakucuk I, Oktem IS, Koc RK (2001) The effect of allopurinol on focal cerebral ischaemia: an experimental study in rabbits. *Neurosurg Rev 24:131-135.*

Amano S, Shimomura N, Kaji Y, Ishii K, Yamagami S, Araie M (2003) Antigenicity of porcine cornea as xenograft. *Curr Eye Res 26:313-318.*

Ames A, 3rd, Nesbett FB (1981) In vitro retina as an experimental model of the central nervous system. *J Neurochem 37:867-877.*

Andrews DT, Leslie K, Sessler DI, Bjorksten AR (1997) The arterial blood propofol concentration preventing movement in 50% of healthy women after skin incision. *Anesth Analg 85:414-419.*

Baker CL, Jr., Hess RF (1984) Linear and nonlinear components of human electroretinogram. *J Neurophysiol 51:952-967.*

Bali M, Akabas MH (2004) Defining the propofol binding site location on the GABAA receptor. *Mol Pharmacol 65:68-76.*

Ball SL, Petry HM (2000) Noninvasive assessment of retinal function in rats using multifocal electroretinography. *Invest Ophthalmol Vis Sci 41:610-617.*

Banin E, Cideciyan AV, Aleman TS, Petters RM, Wong F, Milam AH, Jacobson SG (1999) Retinal rod photoreceptor-specific gene mutation perturbs cone pathway development. *Neuron 23:549-557.*

Beauchemin ML (1974) The fine structure of the pig's retina. *Albrecht Von Graefes Arch Klin Exp Ophthalmol 190:27-45.*

Beauchemin ML, Babel J (1973) Proceedings: A preliminary study on the ultrastructure of the pig retina. *Exp Eye Res 17:400.*

Birch DG (2001) The focal and multifocal electroretinogram. *In: Electrophysiologic testing in disorders of the retina, optic nerve, and visual pathway, 2 Edition (Fishman GA, ed), pp 177-195. Singapore: Foundation of the American Academy of Ophthalmology.*

Block F, Schwarz M (1998) The b-wave of the electroretinogram as an index of retinal ischemia. *Gen Pharmacol 30:281-287.*

Bohnke M, Eggli P, Engelmann K (1999) Transplantation of cultured adult human or porcine corneal endothelial cells onto human recipients in vitro. Part II: Evaluation in the scanning electron microscope. *Cornea 18:207-213.*

Boycott BB, Wassle H (1991) Morphological Classification of Bipolar Cells of the Primate Retina. *Eur J Neurosci 3:1069-1088.*

Braekevelt CR (1983) Fine structure of the retinal rods and cones in the domestic pig. *Graefes Arch Clin Exp Ophthalmol 220:273-278.*

Bush RA, Sieving PA (1996) Inner retinal contributions to the primate photopic fast flicker electroretinogram. *J Opt Soc Am A 13:557-565.*

Chader GJ (2002) Animal models in research on retinal degenerations: past progress and future hope. *Vision Res 42:393-399.*

Chan HL, Brown B (1998) Investigation of retinitis pigmentosa using the multifocal electroretinogram. *Ophthalmic Physiol Opt 18:335-350.*

Chan HL, Brown B (1999) Multifocal ERG changes in glaucoma. *Ophthalmic Physiol Opt 19:306-316.*

Chandler MJ, Smith PJ, Samuelson DA, MacKay EO (1999) Photoreceptor density of the domestic pig retina. *Vet Ophthalmol 2:179-184.*

Chao TI, Pannicke T, Reichelt W, Reichenbach A (1993) Na+ channels are expressed by mammalian retinal glial (Muller) cells. *Neuroreport 4:575-578.*

Cheng G, Kendig JJ (2003) Enflurane decreases glutamate neurotransmission to spinal cord motor neurons by both pre- and postsynaptic actions. *Anesth Analg 96:1354-1359.*

Choy EP, Cho P, Benzie IF, Choy CK (2006) Investigation of corneal effect of different types of artificial tears in a simulated dry eye condition using a novel porcine dry eye model (pDEM). *Cornea 25:1200-1204.*

Chu PH, Chan HH, Brown B (2006) Glaucoma detection is facilitated by luminance modulation of the global flash multifocal electroretinogram. *Invest Ophthalmol Vis Sci 47:929-937.*

Cohen ED, Miller RF (1994) The role of NMDA and non-NMDA excitatory amino acid receptors in the functional organization of primate retinal ganglion cells. *Vis Neurosci 11:317-332.*

Cohen ED, Zhou ZJ, Fain GL (1994) Ligand-gated currents of alpha and beta ganglion cells in the cat retinal slice. *J Neurophysiol 72:1260-1269.*

Cooper DK (1992) Is xenotransplantation a realistic clinical option? *Transplant Proc 24:2393-2396.*

Corbett D, Thornhill J (2000) Temperature modulation (hypothermic and hyperthermic conditions) and its influence on histological and behavioral outcomes following cerebral ischemia. *Brain Pathol 10:145-152.*

Cringle SJ, Alder VA, Brown MJ, Yu DY (1986) Effect of scleral recording location on ERG amplitude. *Curr Eye Res 5:959-965.*

Curcio CA, Sloan KR, Kalina RE, Hendrickson AE (1990) Human photoreceptor topography. *J Comp Neurol 292:497-523.*

De Schaepdrijver L, Simoens P, Pollet L, Lauwers H, De Laey JJ (1992) Morphologic and clinical study of the retinal circulation in the miniature pig. B: Fluorescein angiography of the retina. *Exp Eye Res 54:975-985.*

DeVries SH (2000) Bipolar cells use kainate and AMPA receptors to filter visual information into separate channels. *Neuron 28:847-856.*

Dhingra A, Lyubarsky A, Jiang M, Pugh EN, Jr., Birnbaumer L, Sterling P, Vardi N (2000) The light response of ON bipolar neurons requires G[alpha]o. *J Neurosci 20:9053-9058.*

Dhingra NK, Reddy R, Govindaiah, Hemavathy U, Raju TR, Ramamohan Y (2001) Synaptic development in semi-dissociated cultures of rat retina. *Int J Dev Neurosci 19:533-540.*

Dong CJ, Hare WA (2002) GABAc feedback pathway modulates the amplitude and kinetics of ERG b-wave in a mammalian retina in vivo. *Vision Res 42:1081-1087.*

Duch DS, Rehberg B, Vysotskaya TN (1998) Volatile anesthetics significantly suppress central and peripheral mammalian sodium channels. *Toxicol Lett 100-101:255-263.*

Dvorak D (1984) Off-pathway synaptic transmission in the outer retina of the axolotl is mediated by a kainic acid-preferring receptor. *Neurosci Lett 50:7-11.*

Engelsberg K, Ghosh F (2007) Transplantation of cultured adult porcine full-thickness retina. *Cell Transplant 16:31-39.*

Fishman GA (2001) Components and origins of the ERG. *In: Electrophysiologic testing in disorders of the retina, optic nerve, and visual pathway, 2 Edition (Fishman GA, ed), pp 2-10. Singapore: Foundation of the American Academy of Ophthalmology.*

Flannery JG, Farber DB, Bird AC, Bok D (1989) Degenerative changes in a retina affected with autosomal dominant retinitis pigmentosa. *Invest Ophthalmol Vis Sci 30:191-211.*

Fletcher EL, Hack I, Brandstatter JH, Wassle H (2000) Synaptic localization of NMDA receptor subunits in the rat retina. *J Comp Neurol 420:98-112.*

Fortune B, Cull G, Wang L, Van Buskirk EM, Cioffi GA (2002) Factors affecting the use of multifocal electroretinography to monitor function in a primate model of glaucoma. *Doc Ophthalmol 105:151-178.*

Frishman LJ, Steinberg RH (1990) Origin of negative potentials in the light-adapted ERG of cat retina. *J Neurophysiol 63:1333-1346.*

Gargini C, Terzibasi E, Mazzoni F, Strettoi E (2007) Retinal organization in the retinal degeneration 10 (rd10) mutant mouse: a morphological and ERG study. *J Comp Neurol 500:222-238.*

Gerke Jr CG, Hao Y, Wong F (1995) Topography of rods and cones in the retina of the domestic pig. *Hong Kong Med J 1:302-303.*

Gerth C, Wright T, Heon E, Westall CA (2007) Assessment of central retinal function

in patients with advanced retinitis pigmentosa. *Invest Ophthalmol Vis Sci 48:1312-1318.*

Gouras P, Hoff M (1970) Retinal function in an isolated, perfused mammalian eye. *Invest Ophthalmol 9:388-399.*

Grasshoff C, Rudolph U, Antkowiak B (2005) Molecular and systemic mechanisms of general anaesthesia: the 'multi-site and multiple mechanisms' concept. *Curr Opin Anaesthesiol 18:386-391.*

Greenstein VC, Holopigian K, Seiple W, Carr RE, Hood DC (2004) Atypical multifocal ERG responses in patients with diseases affecting the photoreceptors. *Vision Res 44:2867-2874.*

Hamasaki DI, Machemer R, Norton EW (1969) Experimental retinal detachment in the owl monkey. VI. The ERG of the detached and reattached retina. *Albrecht Von Graefes Arch Klin Exp Ophthalmol 177:212-221.*

Hanitzsch R, Lichtenberger T, Mattig WU (1996) The influence of MgCl2 and APB on the light-induced potassium changes and the ERG b-wave of the isolated superfused rat retina. *Vision Res 36:499-507.*

Hanna N, Lachapelle P, Roy MS, Orquin J, Varma DR, Chemtob S (1995) Alterations in the electroretinogram of newborn piglets by propionic acid-derivative nonsteroidal antiinflammatory drugs but not by indomethacin and diclofenac. *Pediatr Res 37:81-85.*

Hans P, Bonhomme V (2006) Why we still use intravenous drugs as the basic regimen for neurosurgical anaesthesia. *Curr Opin Anaesthesiol 19:498-503.*

Hara H, Lin YJ, Zhu X, Tai HC, Ezzelarab M, Balamarugan AN, Bottino R, Houser SL, Cooper DK (2008) Safe induction of diabetes by high-dose streptozotocin in pigs. *Pancreas 36:31-38.*

Hare WA, Ton H (2002) Effects of APB, PDA, and TTX on ERG responses recorded using both multifocal and conventional methods in monkey. Effects of APB, PDA, and TTX on monkey ERG responses. *Doc Ophthalmol 105:189-222.*

Haverkamp S, Michalakis S, Claes E, Seeliger MW, Humphries P, Biel M, Feigenspan A (2006) Synaptic plasticity in CNGA3(-/-) mice: cone bipolar cells react on the missing cone input and form ectopic synapses with rods. *J Neurosci 26:5248-5255.*

Hebel R (1976) Distribution of retinal ganglion cells in five mammalian species (pig, sheep, ox, horse, dog). *Anat Embryol (Berl) 150:45-51.*

Hendrickson A, Hicks D (2002) Distribution and density of medium- and short-wavelength selective cones in the domestic pig retina. *Exp Eye Res 74:435-444.*

Hoff M, Gouras P (1973) Tolerance of mammalian retina to circulatory arrest. *Doc*

Ophthalmol Proc Ser 2:57-63.

Hood DC (2000) Assessing retinal function with the multifocal technique. *Prog Retin Eye Res 19:607-646.*

Hood DC, Seiple W, Holopigian K, Greenstein V (1997) A comparison of the components of the multifocal and full-field ERGs. *Vis Neurosci 14:533-544.*

Hood DC, Frishman LJ, Saszik S, Viswanathan S (2002) Retinal origins of the primate multifocal ERG: implications for the human response. *Invest Ophthalmol Vis Sci 43:1673-1685.*

Hood DC, Frishman LJ, Viswanathan S, Robson JG, Ahmed J (1999) Evidence for a ganglion cell contribution to the primate electroretinogram (ERG): effects of TTX on the multifocal ERG in macaque. *Vis Neurosci 16:411-416.*

Hood DC, Holopigian K, Greenstein V, Seiple W, Li J, Sutter EE, Carr RE (1998) Assessment of local retinal function in patients with retinitis pigmentosa using the multi-focal ERG technique. *Vision Res 38:163-179.*

Huettner JE (2003) Kainate receptors and synaptic transmission. *Prog Neurobiol 70:387-407.*

Ichinose T, Shields CR, Lukasiewicz PD (2005) Sodium channels in transient retinal bipolar cells enhance visual responses in ganglion cells. *J Neurosci 25:1856-1865.*

Imaizumi H (1974) [Influence of sodium ion concentration on electroretinogram of the living extracorporeal bovine eye (author's transl)]. *Nippon Ganka Gakkai Zasshi 78:831-843.*

Imaizumi K, Tazawa Y, Ogawa K, Mera H, Otsuka T (1972) Electrophysiological application of the living extracorporeal bovine eye. *Adv Exp Med Biol 24:119-123.*

Jacoby RA, Wu SM (2001) AMPA-preferring receptors mediate excitatory non-NMDA responses of primate retinal ganglion cells. *Vis Neurosci 18:703-710.*

Janaky M, Palffy A, Deak A, Szilagyi M, Benedek G (2007) Multifocal ERG reveals several patterns of cone degeneration in retinitis pigmentosa with concentric narrowing of the visual field. Invest Ophthalmol *Vis Sci 48:383-389.*

Johnson DA, Donovan SL, Dyer MA (2006) Mosaic deletion of Rb arrests rod differentiation and stimulates ectopic synaptogenesis in the mouse retina. *J Comp Neurol 498:112-128.*

Johnson MA, Lutty GA, McLeod DS, Otsuji T, Flower RW, Sandagar G, Alexander T, Steidl SM, Hansen BC (2005) Ocular structure and function in an aged monkey with spontaneous diabetes mellitus. *Exp Eye Res 80:37-42.*

Jurklies B, Weismann M, Husing J, Sutter EE, Bornfeld N (2002) Monitoring retinal function in neovascular maculopathy using multifocal electroretinography -

early and long-term correlation with clinical findings. *Graefes Arch Clin Exp Ophthalmol 240:244-264.*

Katoh T, Suguro Y, Nakajima R, Kazama T, Ikeda K (1992) Blood concentrations of sevoflurane and isoflurane on recovery from anaesthesia. *Br J Anaesth 69:259-262.*

Kishida K, Kodama T, O'Meara PD, Shichi H (1985) Glutathione depletion and oxidative stress: study with perfused bovine eye. *J Ocul Pharmacol 1:85-99.*

Koenekoop RK (2004) An overview of Leber congenital amaurosis: a model to understand human retinal development. *Surv Ophthalmol 49:379-398.*

Kolb H, Nelson R, Mariani A (1981) Amacrine cells, bipolar cells and ganglion cells of the cat retina: a Golgi study. *Vision Res 21:1081-1114.*

Kong CW, Li KK, To CH (2006) Chloride secretion by porcine ciliary epithelium: New insight into species similarities and differences in aqueous humor formation. *Invest Ophthalmol Vis Sci 47:5428-5436.*

Kyhn MV, Kiilgaard JF, Lopez AG, Scherfig E, Prause JU, la Cour M (2008) Functional implications of short-term retinal detachment in porcine eyes: study by multifocal electroretinography. *Acta Ophthalmol (Oxf) 86:18-25.*

Lalonde MR, Chauhan BC, Tremblay F (2006) Retinal ganglion cell activity from the multifocal electroretinogram in pig: optic nerve section, anaesthesia and intravitreal tetrodotoxin. *J Physiol 570:325-338.*

Li ZY, Wong F, Chang JH, Possin DE, Hao Y, Petters RM, Milam AH (1998) Rhodopsin transgenic pigs as a model for human retinitis pigmentosa. *Invest Ophthalmol Vis Sci 39:808-819.*

Liu EH, Wong HK, Chia CP, Lim HJ, Chen ZY, Lee TL (2005) Effects of isoflurane and propofol on cortical somatosensory evoked potentials during comparable depth of anaesthesia as guided by bispectral index. *Br J Anaesth 94:193-197.*

Lukasiewicz PD (2005) Synaptic mechanisms that shape visual signaling at the inner retina. *Prog Brain Res 147:205-218.*

Lutjen-Drecoll E, Kaufman PL, Barany EH (1977) Light and electron microscopy of the anterior chamber angle structures following surgical disinsertion of the ciliary muscle in the cynomolgus monkey. *Invest Ophthalmol Vis Sci 16:218-225.*

Marc RE, Jones BW, Anderson JR, Kinard K, Marshak DW, Wilson JH, Wensel T, Lucas RJ (2007) Neural reprogramming in retinal degeneration. *Invest Ophthalmol Vis Sci 48:3364-3371.*

Marmor MF, Hood DC, Keating D, Kondo M, Seeliger MW, Miyake Y; International Society for Clinical Electrophysiology of Vision (2003) Guidelines for basic multifocal electroretinography (mfERG). *Doc Ophthalmol 106:105-115.*

Milam AH, Li ZY, Fariss RN (1998) Histopathology of the human retina in retinitis pigmentosa. *Prog Retin Eye Res 17:175-205.*

Millar JC, Shahidullah M, Wilson WS (1997) Atriopeptin lowers aqueous humor formation and intraocular pressure and elevates ciliary cyclic GMP but lacks uveal vascular effects in the bovine perfused eye. *J Ocul Pharmacol Ther 13:1-11.*

Miyazawa T, Tamura A, Fukui S, Hossmann KA (2003) Effect of mild hypothermia on focal cerebral ischemia. Review of experimental studies. *Neurol Res 25:457-464.*

Narfstrom K, Ehinger B, Bruun A (2001) Immunohistochemical studies of cone photoreceptors and cells of the inner retina in feline rod-cone degeneration. *Vet Ophthalmol 4:141-145.*

Nawy S, Jahr CE (1990) Suppression by glutamate of cGMP-activated conductance in retinal bipolar cells. *Nature 346:269-271.*

Neitz J, Jacobs GH (1989) Spectral sensitivity of cones in an ungulate. *Vis Neurosci 2:97-100.*

Nelson R, Kolb H (1983) Synaptic patterns and response properties of bipolar and ganglion cells in the cat retina. *Vision Res 23:1183-1195.*

Ng YF, Chan HH, Chu PH, To CH, Gilger BC, Petters RM, Wong F (2008a) Multifocal Electroretinogram in Rhodopsin P347L Transgenic Pigs. *Invest Ophthalmol Vis Sci 49:2208-2215.*

Ng YF, Chan HH, Chu PH, Siu AW, To CH, Beale BA, Gilger BC, Wong F (2008b) Pharmacologically defined components of the normal porcine multifocal ERG. *Doc Ophthalmol 116:165-176.*

Nicholls D, Attwell D (1990) The release and uptake of excitatory amino acids. *Trends Pharmacol Sci 11:462-468.*

Niekrasz M, Ye Y, Rolf LL, Zuhdi N, Cooper DK (1992) The pig as organ donor for man. *Transplant Proc 24:625-626.*

Niemeyer G (1973a) ERG dependence on flow rate in the isolated and perfused mammalian eye. *Brain Res 57:203-207.*

Niemeyer G (1973b) Intracellular recording from the isolated perfused mammalian eye. *Vision Res 13:1613-1618.*

Niemeyer G (1975) The function of the retina in the perfused eye. *Doc Ophthalmol 39:53-116.*

Niemeyer G (1981) Neurobiology of perfused mammalian eyes. *J Neurosci Methods 3:317-337.*

Niemeyer G (2001) Retinal research using the perfused mammalian eye. *Prog Retin Eye Res 20:289-318.*

Nixon PJ, Bui BV, Armitage JA, Vingrys AJ (2001) The contribution of cone responses to rat electroretinograms. *Clin Experiment Ophthalmol 29:193-196.*

Ollivier FJ, Samuelson DA, Brooks DE, Lewis PA, Kallberg ME, Komaromy AM (2004) Comparative morphology of the tapetum lucidum (among selected species). *Vet Ophthalmol 7:11-22.*

Olsen TW, Sanderson S, Feng X, Hubbard WC (2002) Porcine sclera: thickness and surface area. *Invest Ophthalmol Vis Sci 43:2529-2532.*

Onozu H, Yamamoto S (2003) Oscillatory potentials of multifocal electroretinogram retinopathy. *Doc Ophthalmol 106:327-332.*

Palmowski AM, Ruprecht KW (2004) Follow up in open angle glaucoma. A comparison of static perimetry and the fast stimulation mfERG. Multifocal ERG follow up in open angle glaucoma. *Doc Ophthalmol 108:55-60.*

Pan ZH, Hu HJ (2000) Voltage-dependent Na(+) currents in mammalian retinal cone bipolar cells. *J Neurophysiol 84:2564-2571.*

Peachey NS, Green DJ, Ripps H (1993) Ocular ischemia and the effects of allopurinol on functional recovery in the retina of the arterially perfused cat eye. *Invest Ophthalmol Vis Sci 34:58-65.*

Peng YW, Hao Y, Petters RM, Wong F (2000) Ectopic synaptogenesis in the mammalian retina caused by rod photoreceptor-specific mutations. *Nat Neurosci 3:1121-1127.*

Peng YW, Senda T, Hao Y, Matsuno K, Wong F (2003) Ectopic synaptogenesis during retinal degeneration in the royal college of surgeons rat. *Neuroscience 119:813-820.*

Petters RM (1994) Transgenic livestock as genetic models of human disease. *Reprod Fertil Dev 6:643-645.*

Petters RM, Alexander CA, Wells KD, Collins EB, Sommer JR, Blanton MR, Rojas G, Hao Y, Flowers WL, Banin E, Cideciyan AV, Jacobson SG, Wong F (1997) Genetically engineered large animal model for studying cone photoreceptor survival and degeneration in retinitis pigmentosa. *Nat Biotechnol 15:965-970.*

Pourcho RG, Qin P, Goebel DJ (2001) Cellular and subcellular distribution of NMDA receptor subunit NR2B in the retina. *J Comp Neurol 433:75-85.*

Prassinos NN, Galatos AD, Raptopoulos D (2005) A comparison of propofol, thiopental or ketamine as induction agents in goats. *Vet Anaesth Analg 32:289-296.*

Prince JH, Diesem CD, Eglitis I, Ruskell GL (1960) Anatomy and Hiostology of the Eye and Orbit in Domestic Animals. *Illianois: Thomas Springfield.*

Quinones-Hinojosa A, Ames A, 3rd, Malek JY, Maynard KI (1999) An in vitro rabbit retina model to study electrophysiologic and metabolic function during and

following ischemia. *J Neurosci Methods 90:107-115.*

Raz D, Seeliger MW, Geva AB, Percicot CL, Lambrou GN, Ofri R (2002) The effect of contrast and luminance on mfERG responses in a monkey model of glaucoma. *Invest Ophthalmol Vis Sci 43:2027-2035.*

Robson JG, Frishman LJ (1995) Response linearity and kinetics of the cat retina: the bipolar cell component of the dark-adapted electroretinogram. *Vis Neurosci 12:837-850.*

Ropstad EO, Bjerkas E, Narfstrom K (2007) Clinical findings in early onset cone-rod dystrophy in the Standard Wire-haired Dachshund. *Vet Ophthalmol 10:69-75.*

Rosolen SG, Rigaudiere F, Le Gargasson JF (2003) [A new model of induced ocular hyperpressure using the minipig]. *J Fr Ophtalmol 26:259-267.*

Rosolen SG, Rigaudiere F, LeGargasson JF, Chalier C, Rufiange M, Racine J, Joly S, Lachapelle P (2004) Comparing the photopic ERG i-wave in different species. *Vet Ophthalmol 7:189-192.*

Ruiz-Ederra J, Hitchcock PF, Vecino E (2003) Two classes of astrocytes in the adult human and pig retina in terms of their expression of high affinity NGF receptor (TrkA). *Neurosci Lett 337:127-130.*

Ruiz-Ederra J, Garcia M, Hernandez M, Urcola H, Hernandez-Barbachano E, Araiz J, Vecino E (2005) The pig eye as a novel model of glaucoma. *Exp Eye Res 81:561-569.*

Saito T, Kondo H, Toyoda J (1981) Ionic mechanisms of two types of on-center bipolar cells in the carp retina. II. The responses to annular illumination. *J Gen Physiol 78:569-589.*

Seaman AJ, Rullman DR, Lutcher CL, Moffat C (1965) The living extracorporeal eye. *Scand J Clin Lab Invest 17:Suppl 84:101-108.*

Shahidullah M, Wilson WS (1999) Atriopeptin, sodium azide and cyclic GMP reduce secretion of aqueous humour and inhibit intracellular calcium release in bovine cultured ciliary epithelium. *Br J Pharmacol 127:1438-1446.*

Shahidullah M, Yap M, To CH (2005a) Cyclic GMP, sodium nitroprusside and sodium azide reduce aqueous humour formation in the isolated arterially perfused pig eye. *Br J Pharmacol 145:84-92.*

Shahidullah M, Wilson WS, Yap M, To CH (2003) Effects of ion transport and channel-blocking drugs on aqueous humor formation in isolated bovine eye. *Invest Ophthalmol Vis Sci 44:1185-1191.*

Shahidullah M, Chan HH, Yap MK, Liu Q, To CH (2005b) Multifocal electroretinography in isolated arterially perfused bovine eye. *Ophthalmic Physiol Opt 25:27-34.*

Sharpe LT, Stockman A (1999) Rod pathways: the importance of seeing nothing.

Trends Neurosci 22:497-504.

Sheardown MJ, Suzdak PD, Nordholm L (1993) AMPA, but not NMDA, receptor antagonism is neuroprotective in gerbil global ischaemia, even when delayed 24 h. *Eur J Pharmacol 236:347-353.*

Shen Y, Liu XL, Yang XL (2006) N-methyl-D-aspartate receptors in the retina. *Mol Neurobiol 34:163-179.*

Simoens P, De Schaepdrijver L, Lauwers H (1992) Morphologic and clinical study of the retinal circulation in the miniature pig. A: Morphology of the retinal microvasculature. *Exp Eye Res 54:965-973.*

Sladeczek F, Manzoni O, Fagni L, Dumuis A, Pin JP, Sebben M, Bockaert J (1992) The metabotropic glutamate receptor (MGR): pharmacology and subcellular location. *J Physiol Paris 86:47-55.*

Slaughter MM, Miller RF (1981) 2-amino-4-phosphonobutyric acid: a new pharmacological tool for retina research. *Science 211:182-185.*

Slaughter MM, Miller RF (1983) An excitatory amino acid antagonist blocks cone input to sign-conserving second-order retinal neurons. *Science 219:1230-1232.*

Sonner JM, Zhang Y, Stabernack C, Abaigar W, Xing Y, Laster MJ (2003) GABA(A) receptor blockade antagonizes the immobilizing action of propofol but not ketamine or isoflurane in a dose-related manner. *Anesth Analg 96:706-712, table of contents.*

Strettoi E, Mears AJ, Swaroop A (2004) Recruitment of the rod pathway by cones in the absence of rods. *J Neurosci 24:7576-7582.*

Sullivan RK, Woldemussie E, Pow DV (2007) Dendritic and synaptic plasticity of neurons in the human age-related macular degeneration retina. *Invest Ophthalmol Vis Sci 48:2782-2791.*

Sutter EE, Tran D (1992) The field topography of ERG components in man--I. The photopic luminance response. *Vision Res 32:433-446.*

Tazawa Y, Seaman AJ (1972) The electroretinogram of the living extracorporeal bovine eye. The influence of anoxia and hypothermia. *Invest Ophthalmol 11:691-698.*

Thoreson WB, Purple RL (1989) Effects of using the oxygen-carrying fluorocarbon, FC43, on the ERG of the arterially perfused cat eye. *Curr Eye Res 8:487-498.*

Thumann G, Hinton DR (2001) Cell biology of the retinal pigment epithelium. *In: Retina, 3 Edition (Ryan SJ, ed), pp 104-137. St. Louis: Mosby.*

Tian N, Slaughter MM (1995) Correlation of dynamic responses in the ON bipolar neuron and the b-wave of the electroretinogram. *Vision Res 35:1359-1364.*

Tseng MT, Liu KN, Radtke ND (1989) Isolated, perfused bovine eye a model for

acute retinal toxicity screening. *Lens Eye Toxic Res 6:241-251.*

Tseng MT, Liu KN, Boles CB, Radtke ND (1990) Mitochondrial stability in taurine perfused, hypoxic bovine eye. *Prog Clin Biol Res 351:477-480.*

Ueno S, Trudell JR, Eger EI, 2nd, Harris RA (1999) Actions of fluorinated alkanols on GABA(A) receptors: relevance to theories of narcosis. *Anesth Analg 88:877-883.*

Vaajanen A, Vapaatalo H, Oksala O (2007) A modified in vitro method for aqueous humor outflow studies in enucleated porcine eyes. *J Ocul Pharmacol Ther 23:124-131.*

Vardi N, Morigiwa K (1997) ON cone bipolar cells in rat express the metabotropic receptor mGluR6. *Vis Neurosci 14:789-794.*

Vigh J, von Gersdorff H (2005) Prolonged reciprocal signaling via NMDA and GABA receptors at a retinal ribbon synapse. *J Neurosci 25:11412-11423.*

Wachtmeister L (1998) Oscillatory potentials in the retina: what do they reveal. *Prog Retin Eye Res 17:485-521.*

Wang X, Niwa M, Hara A, Matsuno H, Kawase K, Kozawa O, Mow H, Uematsu T (2002) Neuronal degradation in mouse retina after a transient ischemia and protective effect of hypothermia. *Neurol Res 24:730-735.*

Wassle H, Boycott BB (1991) Functional architecture of the mammalian retina. *Physiol Rev 71:447-480.*

Wehrwein E, Thompson SA, Coulibaly SF, Linn DM, Linn CL (2004) Acetylcholine protection of adult pig retinal ganglion cells from glutamate-induced excitotoxicity. *Invest Ophthalmol Vis Sci 45:1531-1543.*

Werblin FS, Dowling JE (1969) Organization of the retina of the mudpuppy, Necturus maculosus. II. Intracellular recording. *J Neurophysiol 32:339-355.*

Woodward WR, Choi D, Grose J, Malmin B, Hurst S, Pang J, Weleber RG, Pillers DA (2007) Isoflurane is an effective alternative to ketamine/xylazine/acepromazine as an anesthetic agent for the mouse electroretinogram. *Doc Ophthalmol 115:187-201.*

Xin D, Bloomfield SA (1999) Comparison of the responses of AII amacrine cells in the dark- and light-adapted rabbit retina. *Vis Neurosci 16:653-665.*

Yang P, Chen L, Zwart R, Kijlstra A (2002) Immune cells in the porcine retina: distribution, characterization and morphological features. *Invest Ophthalmol Vis Sci 43:1488-1492.*

Yang XL (2004) Characterization of receptors for glutamate and GABA in retinal neurons. *Prog Neurobiol 73:127-150.*

Zeevalk GD, Nicklas WJ (1996) Hypothermia and metabolic stress: narrowing the cellular site of early neuroprotection. *Pharmacol Exp Ther* 279:332-339.

Zenisek D, Henry D, Studholme K, Yazulla S, Matthews G (2001) Voltage-dependent sodium channels are expressed in nonspiking retinal bipolar neurons. *J Neurosci 21:4543-4550.*